Contribution à l'étude de la diffusion élastique entre ions lourds - Influence de quelques voies de réaction

H. Doubre

THÈSE

PRESENTEE

AU CENTRE D'ORSAY

UNIVERSITÉ PARIS-SUD

POUR OBTENIR

LE GRADE DE DOCTEUR ES-SCIENCES PHYSIQUES

PAR

Hubert DOUBRE

Sujet : Contribution à l'étude de la diffusion élastique entre ions lourds - Influence de quelques voies de réaction.

Soutenue le **devant la Commission d'examen**

MM. M. RIOU — Président.

J.M. LOISEAUX
J.C. BIZOT
B. FERNANDEZ
A. GOBBI
C. MARTY
— Examinateurs.

INTRODUCTION

Les réactions induites par les ions lourds constituent en physique nucléaire, actuellement, un domaine d'études caractérisé par une grande activité et une croissance rapide. Le développement des accélérateurs a permis d'utiliser des projectiles de masse et d'énergie de plus en plus élevées. Toutefois, la physique des ions lourds diffère suivant la masse des noyaux considérés : ions "lourds-légers" ou "très lourds".

Dans les collisions entre les premiers, l'identification d'un grand nombre de voies de sortie reste réalisable et la définition de l'énergie incidente peut être très bonne (de l'ordre de 10 keV). Une forte dépendance des sections efficaces avec l'énergie a été observée. Elle a suscité beaucoup d'intérêt, et de spéculations. Au voisinage de la barrière coulombienne, la présence [Al 60] de résonances (larges de quelques centaines de keV) dans le système $^{12}C+^{12}C$ a été considérée comme une évidence pour des interactions de type quasi-moléculaire entre les noyaux. A énergie plus élevée, la mise en évidence [Br 77] de nombreux états étroits du système composé a amené une extension du concept de quasi-molécule, incluant des états seuils dont la formation et la nature sont encore mal décrites. Mais surtout, la structure large (de quelques MeV) observée dans les fonctions d'excitation élastiques constitue une donnée essentielle dans l'étude des phénomènes associés à la voie d'entrée. Récemment, il a été proposé [Fe 76] que cette structure est la signature d'états intermédiaires, immédiatement couplés à la voie d'entrée, à l'origine de l'accumulation d'états de spins très voisins à certaines énergies privilégiées dans le système composé. Une compréhension correcte de cette structure large, et plus généralement du comportement de la voie élastique en fonction de l'énergie, s'avère donc nécessaire. C'est à une description et une interprétation des fonctions d'excitation élastiques que s'attache ce travail.

Sur le plan expérimental, une exigence est apparue : des données tronquées (distributions angulaires ou fonctions d'excitation insuffisamment étendues) conduisent presque immanquablement à des conclusions fausses ; au contraire, si elles sont complètes, on est frappé par la grande quantité de phénomènes coexistant entre eux qu'elles révèlent. La surface $\sigma(E,\theta)$ doit donc être explorée avec un pas assez fin : un exemple a été fourni par les mesures extensives [Ma 69] sur le système $^{16}O+^{16}O$ (celui pour lequel les sections efficaces élastiques présentent la structure la plus accusée). Des comparaisons, aussi dépourvues d'ambiguïté que possible, entre différents systèmes sont également susceptibles d'éclairer l'origine de cette structure et de tester les modèles proposés. Le noyau ^{20}Ne est intéressant de ce point de vue, car c'est un noyau à configuration simple $^{16}O+\alpha$; peu de systèmes dans lesquels il intervient ont été étudiés jusqu'ici pour des raisons expérimentales. L'utilisation, pour ce travail, du faisceau de ^{20}Ne fourni par le cyclotron de l'I.S.N. de Grenoble a permis d'étudier les systèmes $^{12}C+^{20}Ne$ et $^{20}Ne+^{20}Ne$. Plus spécifiquement, la comparaison des systèmes $^{12}C+^{20}Ne$ et $^{16}O+^{16}O$ est l'une de celles qui devrait être sans ambiguïté : même cinématique, même noyau composé, mais dans le premier cas, des noyaux facilement excitables, dans le second, des noyaux rigides. Cette comparaison est présentée au chapitre I, ainsi que les résultats sur le système $^{20}Ne+^{20}Ne$.

De telles recherches sur les systèmes d'ions légers s'appuient évidemment sur des modèles. Il est naturel de confronter ceux-ci à d'autres systèmes mettant en jeu des ions beaucoup plus lourds. Ceux-ci donnent lieu à une physique très différente de celle décrite ci-dessus : la résolution expérimentale, généralement moins bonne, et les voies de sortie trop nombreuses conduisent plutôt à des études de type statistique. C'est le cas, en particulier, pour les collisions très inélastiques observées avec ces systèmes et sur lesquelles beaucoup de résultats expérimentaux sont actuellement rassemblés.

D'un intérêt tout particulier est le système $^{40}Ca+^{40}Ca$, sur lequel ont déjà été observées [Co 74] ces réactions très inélastiques (tenues pour caractéristiques des collisions entre ions lourds) dont la section efficace représente une fraction appréciable de la section efficace de réaction. Ce système a été considéré, dans ce travail, comme un système de transition. Il a été étudié, grâce à la présence contiguë à l'I.P.N. d'Orsay de l'accélérateur Alice et du tandem MP, avec les mêmes soucis de bonne définition et résolution que des systèmes d'ions beaucoup plus légers. La première partie du chapitre II décrit les mesures de sections efficaces élastiques qui font apparaître une dépendance monotone avec l'énergie. Deux explications ont pu être proposées de ce résultat. La première est une forte absorption dans le système $^{40}Ca+^{40}Ca$: il a donc été entrepris de dresser expérimentalement un bilan des voies possibles pour ce système, et de suivre l'influence de l'énergie incidente sur ce bilan. Dans la seconde, il est proposé d'étendre au domaine des ions très lourds des modèles associés aux ions légers. Au chapitre III, l'analyse de la structure en énergie des fonctions d'excitation élastiques est donc reformulée, en utilisant une décomposition de l'amplitude de diffusion. Cette méthode permet une description simple et élégante d'un très large ensemble de phénomènes et fournit un cadre à l'étude de la diffraction qui domine toutes les situations abordées expérimentalement dans ce travail.

La majorité des résultats présentés ont été publiés, ou sont en cours de publication. Pour ne pas alourdir cette rédaction, les articles principaux ont été seuls reproduits, à la place que leur assigne le plan ci-dessus. Pour les autres articles, leur référence est indiquée.

CHAPITRE I

LES SYSTÈMES $^{20}Ne+^{12}C$ ET $^{20}Ne+^{20}Ne$

I - RAPPEL.

La mise en évidence, par Siemssen et al. [Ma 69], d'une structure large dans les fonctions d'excitation élastiques du système $^{16}O+^{16}O$ a marqué le début d'une grande activité expérimentale centrée sur l'étude des mécanismes d'interaction entre ions lourds de masse voisine de 16. Les résultats de ces auteurs ont constitué la première étude portant sur un domaine étendu ($B_c \leqslant E_{c.m.} \leqslant 3B_c$ où B_c est la barrière coulombienne), l'énergie incidente variant par pas de 500 keV (lab) ou même 100 keV si nécessaire. Leurs caractéristiques révélaient un comportement inattendu à l'époque. En particulier, les fonctions d'excitation présentent trois types de structure : la plus large, d'environ 3 MeV, est celle que nous étudions dans ce travail ; elle correspond,sans doute possible,à un phénomène spécifique du potentiel qui règne entre les deux ions lourds à grande distance ; la structure fine correspond aux fluctuations statistiques dues au recouvrement des résonances du noyau composé ^{32}S ; enfin une structure intermédiaire ($\sim$ 300 keV) paraît être présente. Ces résultats prouvent donc, dans les réactions entre ions "lourds légers", la coexistence de processus dont les temps caractéristiques diffèrent grandement (entre 10^{-19} et 10^{-22}s). Il allait bientôt être montré que la présence d'une structure large, à grand rapport pic-sur-vallée, sur des sections efficaces élevées est la signature de la transparence du potentiel d'interaction pour les ondes partielles rasantes, à l'origine des collisions périphériques. Ces ondes partielles donnent lieu à la diffusion élastique et aussi aux réactions de transfert directes. Il en résulte que l'étude de réactions où les propriétés de la surface nucléaire sont déterminantes va occuper une large place de la physique des ions lourds ; à côté,les réactions dans lesquelles les ions forment un noyau composé constituent un phénomène beaucoup plus global, où la nature des ions entre de façon moins décisive.

En même temps que des recherches théoriques pour reproduire et comprendre ces résultats, nombre d'expériences ont été réalisées sur des noyaux de masse voisine [Si 71]. La même structure, large de 2 à 3 MeV, s'observe sur presque tous les systèmes. Elle peut quelquefois être noyée sous le bruit de fond que constituent les fluctuations d'Ericson, mais dans ce cas, on la retrouve en moyennant, sur un intervalle d'énergie d'environ 1 MeV, la fonction d'excitation mesurée avec une résolution en énergie bien supérieure [Re 73]. Les valeurs du rapport pic-sur-vallée, de la pente moyenne de la fonction d'excitation, enfin des sections efficaces moyennes, sont sensibles à la nature du système.

Cette structure a souvent été mal interprétée. On peut montrer rapidement qu'en aucun cas une telle structure ne devrait mériter le nom de résonance. La figure I.1 tirée de [Si 67] est à ce sujet suffisamment convaincante : la structure n'est pas invariante avec l'angle ; sa largeur, que l'on définira ici comme la distance (en énergie) entre deux maximums, ou minimums, décroît quand l'angle augmente. Comme il n'est pas possible, avec des ions chargés, de définir une section efficace totale élastique, il est difficile d'avoir une idée globale du comportement du système en fonction de l'énergie. Il faut étudier, et auparavant mesurer, toute la surface $\sigma(E,\theta)$ pour pouvoir l'interpréter correctement.

Il a été reconnu rapidement que ce phénomène de structure dans la fonction d'excitation élastique peut être reproduit par les prédictions du modèle optique. C'est donc qu'il relève d'un potentiel moyen, sur lequel il fournit des informations. La recherche des propriétés nucléaires qui lui donnent lieu s'est donc trouvée ramenée à celle des propriétés du potentiel qui le reproduit. Une certaine coïncidence entre l'énergie des "bosses" de la fonction d'excitation à 90° (considérée, pour les systèmes d'ions identiques, comme la plus représentative, parce que contenant la moindre contribution coulombienne), et les énergies propres des états non liés du puits réel du potentiel optique a d'abord été remarquée. Par analogie avec ce qui se passe pour les nucléons, on parle alors de résonance de forme, ou de résonance à l'intérieur du puits. On notera qu'on a négligé le rôle de la partie imaginaire du potentiel, dont la profondeur n'est faible qu'à la surface du noyau, et admis que la position des états propres ne dépendait pas de cette profondeur.

La comparaison des valeurs des paramètres optiques déterminées sur les différents systèmes de noyaux $A \simeq 16$ a pourtant montré que le comportement des fonctions d'excitation dépend grandement de la partie imaginaire du puits. Ainsi, on oppose généralement les fonctions d'excitation à 90° des deux systèmes $^{16}O+^{16}O$ et $^{18}O+^{18}O$ [Sh 70], ce dernier système étant beaucoup plus absorbant que tous les autres. Elles sont cependant reproduites par des potentiels optiques ayant même partie réelle. C'est donc dans la partie absorptive du potentiel optique que se trouvent introduites les données propres à chaque noyau, comme sa structure, ou encore la plus ou moins grande probabilité des réactions vers les voies ouvertes au système. C'est ce qui fait le modèle d'absorption dépendant du moment angulaire.

II - LE MODELE D'ABSORPTION DEPENDANT DU MOMENT ANGULAIRE.

Ce modèle, d'abord proposé par Robson et al. [Ch 70], repose sur une loi de conservation associée au moment angulaire. Les collisions rasantes, qui jouent un rôle dominant dans la diffusion élastique et les transferts, sont celles dans lesquelles la voie d'entrée amène un moment angulaire :

$$\ell_i \tilde{=} k_i R_i (1 - 2n_i/k_i R_i)^{1/2}$$

où k_i et n_i sont respectivement le nombre d'ondes et le paramètre de Sommerfeld de la voie, et

$$R_i = r_o (A_1^{1/3} + A_2^{1/3})$$

Si une voie de sortie emmène un moment angulaire rasant :

$$\ell_f \tilde{=} k_f R_f (1 - 2n_f/k_f R_f)^{1/2}$$

bien inférieur à ℓ_i, cette voie sera largement défavorisée par ce simple argument cinématique. A ℓ_f doit cependant être ajouté le spin de la voie, si les produits de réaction ont un spin non nul, et on peut aussi remplacer les valeurs de ℓ_i et ℓ_f, données dans les formules précédentes, par les valeurs du moment angulaire ℓ_g dans la voie, défini par :

$$T(\ell_g) = 1 - |S_N(\ell_g)|^2 = 1/2$$

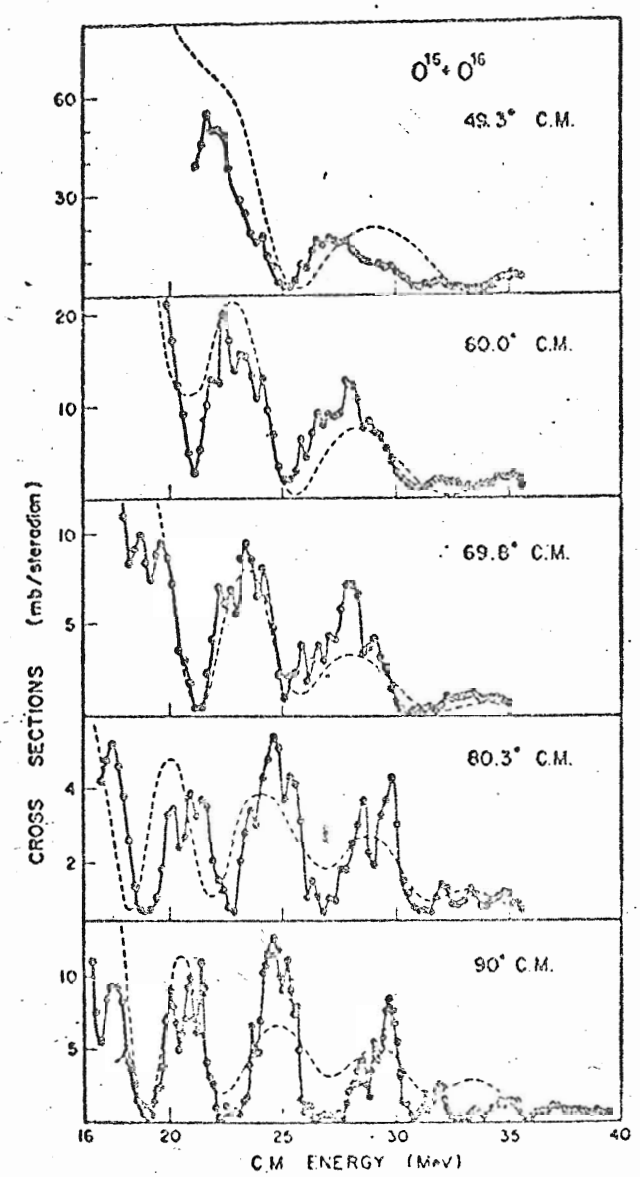

Fig.I.1. Fonctions d'excitation de la diffusion élastique $^{16}O+^{16}O$ à différents angles d'observation. Cette figure est tirée de la référence [Si 67].

où T est le coefficient de transmission pour l'onde ℓ, et $S_N(\ell)$ la partie nucléaire de la matrice S, calculée par le modèle optique.

Ainsi, à énergie donnée, des voies existent certainement qui ne sont pas capables d'emmener le moment angulaire introduit par la voie d'entrée. Ces voies ne jouent qu'un rôle négligeable dans l'absorption.

Ce sont évidemment les chaleurs de réaction (ainsi que le spin des produits) des différentes voies qui déterminent si celles-ci peuvent évacuer le moment angulaire amené dans les collisions rasantes. Les chaleurs de réaction dépendent de la structure des noyaux, via leurs masses. La figure I.2 donne les Q de réaction compris entre -20 et +10 MeV, pour plusieurs systèmes qui sont dans ce travail ; les traits fins correspondent à des réactions procédant vraisemblablement par la formation puis la désintégration du noyau composé ; les traits épais repèrent les réactions dont on pense qu'elles se produisent par un transfert direct.

On comprend le rôle joué par le système $^{16}O+^{16}O$: la grande stabilité de ce noyau se traduit par des Q de réaction très négatifs pour toutes les réactions rasantes, à l'exception du transfert d'un ou deux alphas :

$$^{16}O+^{16}O \rightarrow {}^{12}C+^{20}Ne \quad Q = -2.432 \text{ MeV}$$
$$^{16}O+^{16}O \rightarrow {}^{8}Be+^{24}Mg \quad Q = -0.484 \text{ MeV}$$

Par contre, il existe toujours des voies de réaction ayant $Q > 0$ lorsqu'elles passent par le noyau composé : après ces émissions de protons, neutrons ou alphas, le noyau résiduel peut d'ailleurs être laissé dans un état de spin élevé. Faut-il tenir compte de ces voies pour décrire la dépendance de l'absorption vis à vis du moment angulaire ?

Vandenbosch [Va 71] a donné deux arguments pour ne considérer que les seules voies directes, c'est-à-dire celles qui sont immédiatement couplées à la voie d'entrée. En étudiant comment varie avec l'énergie la coupure effective ℓ_c appliquée [Ch 70] à l'absorption dans le cas $^{16}O+^{16}O$, Vandenbosch trouve (fig.I.3) que cette quantité augmente comme le moment angulaire emmené par les voies directes, et non pas comme celui qu'emporteraient les voies venant d'un noyau composé, auquel la voie d'entrée n'est d'ailleurs que peu couplée (Shaw et al. [Sh 67] ont démontré que la contribution du noyau composé ne dépasse certainement pas 10% de la section efficace élastique, pour $\theta_{c.m.}=90°$). Par contre, dans le cas du système $^{18}O+^{18}O$, la conservation du moment angulaire incident n'interdit pas plusieurs transferts directs (d'un alpha, d'un neutron, diffusion inélastique...).

On explique ainsi les grandes sections efficaces trouvées pour la diffusion élastique $^{16}O+^{16}O$ et la décroissance rapide avec l'énergie dans le cas $^{18}O+^{18}O$.

Le modèle peut certainement être amélioré. Par exemple, la structure dans $^{16}O+^{16}O$ devrait disparaître vers 26 MeV (c.m.) quand le transfert alpha devient une voie de sortie possible. Il se trouve qu'elle s'atténue beaucoup au-delà de 31 MeV quand la voie inélastique s'ouvre. Quelles voies jouent donc un rôle déterminant ? D'autre part, trois grandeurs caractérisent la structure : section efficace moyenne, pente de la fonction d'excitation, rapport pic-sur-vallée. Sont-elles toutes soumises pareillement à ce phénomène d'absorption dépendant du moment angulaire ?

Pour continuer à tester ce modèle, deux systèmes très voisins de ceux cités dans cette introduction ont été étudiés. Le système $^{12}C+^{20}Ne$ fournit évidemment une illustration immédiate du modèle, par ses propriétés vis à vis du système $^{16}O+^{16}O$: il conduit au même noyau composé de ^{32}S, et pour une même énergie d'excitation, ce noyau composé a pratiquement même moment angulaire dans les deux cas (toutefois le système $^{16}O+^{16}O$ ne peuple pas d'états de J impair). Ceci permet de faire porter la comparaison sur les mêmes voies directes ouvertes à l'un et l'autre de ces systèmes. On a vu sur la figure I.2 que la diffusion inélastique vers l'état 2^+ du ^{20}Ne, à 1.63 MeV, le transfert d'un alpha ($Q = 2.432$ MeV) peuvent être des sources d'absorption importantes pour le système $^{12}C+^{20}Ne$.

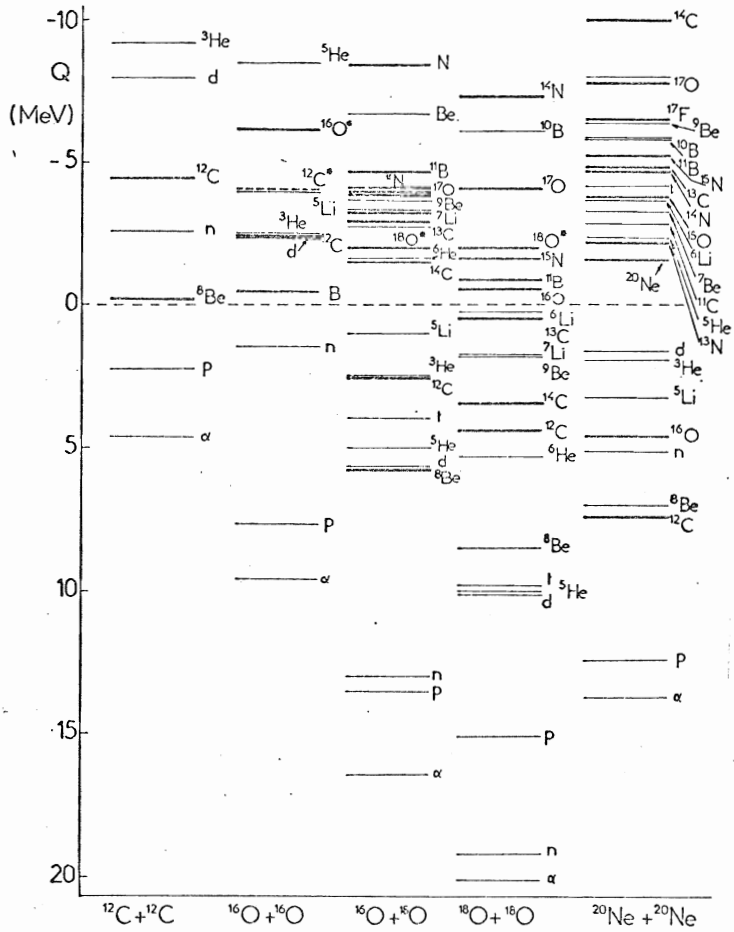

Fig.I.2. Q des réactions à 2 corps pour cinq systèmes d'ions lourds. Les traits épais correspondent à des réactions directes, les traits fins à des réactions passant vraisemblablement par la formation du noyau composé.

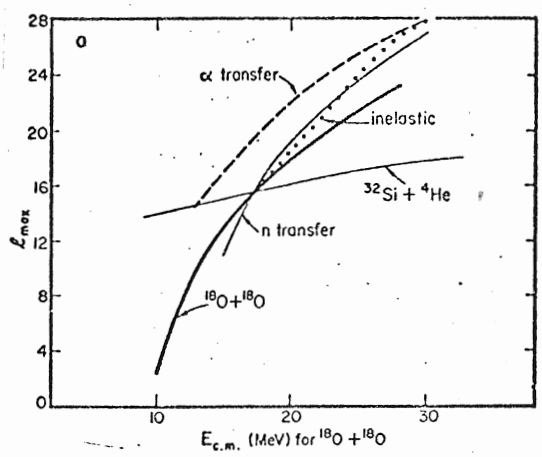

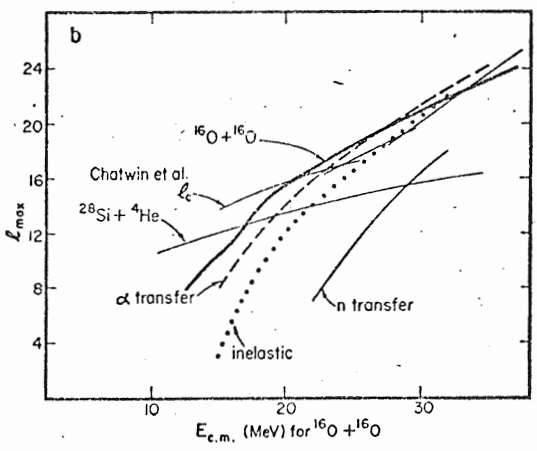

Fig.I.3. Moments angulaires associés aux voies de réaction des systèmes $^{16}O+^{16}O$ (en bas) et $^{18}O+^{18}O$ (en haut). En traits épais : moment angulaire rasant pour les voies indiquées. La courbe notée ℓ_c correspond aux valeurs empiriques de Chatwin et al. [Ch 70]. Cette figure est tirée de la référence [Sh 70].

Avec le système $^{20}Ne+^{20}Ne$, on revient à un système de particules identiques ; des voies directes sont également ouvertes et une comparaison au système $^{18}O+^{18}O$, considéré comme l'exemple de l'absorption forte, est proposée.

III - ETUDE DU SYSTEME $^{12}C+^{20}Ne$.

1. Introduction.

Ce système a déjà été étudié partiellement par Vandenbosch, Webb et Zisman [Va 74]. Ces auteurs ont publié une fonction d'excitation élastique à $\theta_{c.m.} = 70°$ sur le domaine d'énergie $18 \leqslant E_{c.m.} \leqslant 28$ MeV, et comparé les distributions angulaires des systèmes $^{16}O+^{16}O$ et $^{20}Ne+^{12}C$ à 23.3 MeV.

Il a déjà été dit plus haut que cette comparaison apparaissait insuffisante, parce que limitée à un domaine trop étroit d'angles et d'énergies. Les directions de travail suivantes ont donc été fixées :

- Mesure de la fonction d'excitation à $\theta_{c.m.} = 90°$, pour permettre la comparaison à la fonction d'excitation du système $^{16}O+^{16}O$ dans une situation où seules les ondes paires interviennent.

- Mesure de cette fonction à un angle arrière : on espère ainsi, en diminuant la contribution coulombienne, réduire les ambiguïtés habituelles sur le potentiel du modèle optique, et peut-être aussi avoir une indication de ce que "pourrait" être le comportement à l'arrière du système $^{16}O+^{16}O$, sur lequel on a spéculé bien souvent.

- Surtout acquisition de données sur les voies inélastiques et de transfert alpha. Ces mesures permettent, d'une part, des analyses en voies couplées tout à fait dans l'esprit du modèle de Vandenbosch [Va 71], et, d'autre part, donnent une première idée de la façon dont le système se distribue sur les différentes voies de sortie.

L'expérience et ses résultats ont fait l'objet d'une lettre [Do 75a] et d'un article [Do 77a]. Cet article suit immédiatement cette introduction. Auparavant, on peut faire quelques remarques : de telles mesures, effectuées à l'aide d'un cyclotron, ont été rendues encore plus difficiles par les irrégularités trouvées sur les diverses fonctions d'excitation. L'énergie incidente était mesurée par le système d'analyse magnétique du cyclotron de Grenoble, et si sa valeur est entachée d'une incertitude de 200 à 300 keV, ceci correspond à environ 100 keV dans le système du centre de masse. De toute façon, c'est au comportement moyen des fonctions d'excitation que l'on s'intéresse ; la contribution du noyau composé est discutée dans l'article.

Il est mentionné au paragraphe III.C de l'article [Do 77a] l'utilisation de la décomposition de Fuller [Fu 75]. Il s'agit à cet endroit d'une technique puissante qui sera expliquée dans le chapitre III. Cette décomposition a pour point de départ la forme asymptotique des polynômes de Legendre :

$$P_\ell(\cos\theta) \sim \left(\frac{1}{2\pi(\ell+\frac{1}{2})\sin\theta}\right)^{1/2} \cos\left[(\ell+\tfrac{1}{2})\ \theta - \frac{\pi}{4}\right] \sim \left(\frac{1}{\pi(2\ell+1)\sin\theta}\right)^{1/2} \left\{ e^{i\left[(\ell+\frac{1}{2})\,\theta - \frac{\pi}{4}\right]} + e^{-i\left[(\ell+\frac{1}{2})\theta - \frac{\pi}{4}\right]} \right\}$$

qui fait apparaître chaque polynôme comme la somme de deux ondes progressives, contournant le potentiel diffuseur pour atteindre les directions $\pm\theta$. Cette décomposition, valable pour ℓ grand, peut être effectuée de façon exacte si on utilise les fonctions de Legendre de deuxième espèce $\tilde{Q}_\ell^{(\pm)}(\theta)$, dont les formes asymptotiques sont précisément $e^{\pm i\left[(\ell+\frac{1}{2})\theta - \frac{\pi}{4}\right]}$. Le calcul de ces quantités a été programmé et toute amplitude:

$$f(\theta) = \sum_{\ell=0}^{\infty} a_\ell \, P_\ell(\cos\theta)$$

peut ainsi être décomposée suivant $f(\theta) = f^{(+)}(\theta) + f^{(-)}(\theta)$, avec

$$f_\ell^{(\pm)}(\theta) = \sum_{\ell=0}^{\infty} a_\ell \, \tilde{Q}_\ell^{(\pm)}(\cos\theta)$$

Ce sont les modules de ces amplitudes qui sont portés sur les figures 8 et 11 de notre article.

2. Etude expérimentale du système $^{12}C+^{20}Ne$.

Nous reproduisons ici l'article [Do 77a].

EXPERIMENTAL STUDY OF THE $^{20}Ne+^{12}C$ SYSTEM

H.DOUBRE, J.C.ROYNETTE and E.PLAGNOL

Institut de Physique Nucléaire, BP n°1, 91406 Orsay, FRANCE

J.M.LOISEAUX, P.MARTIN and P.deSAINTIGNON

Institut des Sciences Nucléaires, BP n°257, Centre de Tri,
38044 Grenoble Cedex, FRANCE

IPNO-PhN-77-16

Experimental study of the $^{20}Ne + ^{12}C$ system

H. Doubre, J.C. Roynette and E. Plagnol

Institut de Physique Nucléaire, BP n°1, 91406 Orsay, France

and

J.M. Loiseaux, P. Martin and P. de Saintignon

Institut des Sciences Nucléaires, BP n°257, Centre de Tri
38044 Grenoble Cedex, France

Abstract.

Excitation functions for elastic, inelastic and four-particle transfer channels of the $^{12}C+^{20}Ne$ system were measured from 17 to 35 MeV (c.m.). The elastic scattering data (excitation functions and angular distribution at 24.7 MeV) have been analyzed with the optical-model. Elastic and inelastic scattering are also studied in the framework of the coupled-channel Born approximation. The results emphasize the importance of the 2^+ state of ^{20}Ne in the description of the absorption. The comparison with the $^{16}O+^{16}O$ system is discussed.

NUCLEAR REACTIONS $^{12}C(^{20}Ne,^{20}Ne)^{12}C$ measured excitation functions, $E_{c.m.}$ = 17 to 35 MeV, $\sigma(\theta)$ at 24.7 MeV; $^{12}C(^{20}Ne,^{20}Ne^*)^{12}C$ and $^{12}C(^{20}Ne,^{16}O)^{16}O^*$ measured excitation functions, $E_{c.m.}$ = 17 to 35 MeV. Optical-model and coupled channel analysis.

I. Introduction.

The striking difference found when comparing the 90° elastic scattering excitation functions of the $^{16}O+^{16}O$ and $^{18}O+^{18}O$ systems led Shaw, Vandenbosch and Mehta[1] to specify the physical support of the model[2] of angular momentum-dependent absorption. Their interpretation of the experimental data is based upon the strength of the direct reaction channels able to carry away the angular momentum associated with the grazing collisions in the entrance channel. These ideas have been quantitatively checked in an analysis[3] of the elastic and inelastic scattering between ^{16}O and ^{18}O. In this system the additional difficulty due to the presence of elastic (and inelastic) transfer at backward angles arises.

A system which perfectly lends itself to such an analysis is certainly the $^{12}C+^{20}Ne$ one. Several features of this system are of particular interest : the same compound nucleus as in the $^{16}O+^{16}O$ case is formed (with the important difference that only even, positive parity states are populated in the latter case) ; at a given c.m. energy the same angular momenta should be available ; finally, the interference of the elastic transfer (here an 8-particle transfer) can be expected to be negligible.

A first experiment investigation[4] of the $^{12}C+^{20}Ne$ elastic scattering was performed at forward angles ($\theta_{c.m.} \leq 80°$) and its results show the expected similarity with the $^{18}O+^{18}O$ system. Another experimental study[5] over the same energy range, undertaken at about the same time, arrived at a less clearcut conclusion : it was observed that this system behaves in a manner which can be depicted as intermediate between $^{16}O+^{16}O$ and $^{18}O+^{18}O$, and especially that the excitation function pattern depends strongly on the observation angle. Explicitly, the forward-angle data are really reminiscent from the strong-absorption cases, whereas a well-developed structure is observed at larger angles. The aim of this paper is to present the results of a rather extensive study of the elastic and inelastic scattering and of some of the most important transfer reactions induced by the interaction between ^{12}C and ^{20}Ne. Such a set of data allows for a coupled-channel analysis, taking into account the direct reactions, as required by the Vandenbosch model[1]. On the other hand, any comparison between the model calculations reproducing the most important characteristics of the $^{16}O+^{16}O$ and $^{12}C+^{20}Ne$ systems should help to clarify open questions such as compound nucleus

absorption, entrance channel effects and surface-localized reactions. All of them are decisive in stating more accurately the features of absorption in heavy-ion reactions.

II. Experimental method and results.

The experimental method has already been described elsewhere[5] and will only be shortly repeated. Because of the large resulting centre-of-mass velocity, the use of a ^{20}Ne beam allows for standard detection and identification of the reaction products, even at backward angles and for negative Q-value channels. The ^{20}Ne (4^+ and 5^+ charge state) beam from the cyclotron of the Institut des Sciences Nucléaires, Grenoble, bombarded a 100 $\mu g/cm^2$ thick carbon target. The identification of the reaction products was achieved by means of two different systems. Close to 90° (c.m.), the energy and angle for both the outgoing particle and the coincident recoil nucleus were recorded (kinematical coincidence technique). This was obtained using two large-area solid-state detectors, resulting in a solid angle of 2.4 msr. The angular acceptance was ±3° (c.m.). Special care was taken to keep the maximum geometrical efficiency of the system. The energy resolution in the sum spectra (fig.1) depends only on the beam-energy dispersion and the target thickness, and was found to be of the order of 600 keV. At forward angles, a solid-state telescope was used. The thickness of the ΔE-detector was 13 μm and the solid angle was 0.2 msr. The telescope energy resolution was about 1 MeV for the ^{20}Ne ions detected at 25° lab. This telescope was used to identify and to measure the energy of the ^{20}Ne and ^{16}O ions resulting from elastic (or inelastic) scattering and from the four-particle transfer $^{12}C(^{20}Ne,^{16}O)^{16}O$ at forward angles respectively, and to detect the ^{12}C recoil nuclei corresponding to elastic (and inelastic) scattering at backward angles.

Two symmetrically-aligned counters, at 45° relative to the beam direction looked at a gold target located downstream, and were thus used as monitors. Dead-time corrections were taken into account.

Excitation functions were measured at lab energies ranging from 45 to 93 MeV ($16.9 \leqslant E_{c.m.} \leqslant 34.9$ MeV). The cyclotron energy was varied in steps of approximately 7 MeV ; carbon foils of known thicknesses were then used to

15

decrease the beam energy to the desired values. The beam qualities were checked to remain sufficiently good for our purpose.

At 24.7 MeV (c.m.), an angular distribution was measured between 8° and 150° (c.m.), the angular acceptance of the detectors being consequently reduced to ±1° (c.m.).

In fig.2, elastic scattering excitation functions at 70°, 90° and 130° (c.m.) are shown. At 70°, no structure appears and this is in complete agreement with the data obtained by Vandenbosch, Webb and Zisman[4] on the energy range they have studied. It is however interesting to note that the lack of structure seems to persist at higher energy. On the contrary, the excitation functions obtained at 90° and 130° are strongly structured. This confirms our previous measurements[5]. It may be worthwhile to note that the average slope of the excitation functions decreases with increasing angle. The observation that the average cross section levels off between 90° and 150° provides a hint for the occurence of Fraunhofer diffraction. This would not be expected[6] in the presence of a strongly absorbing potential. The same remark can be made when looking at the fig.3 which shows the angular distribution measured at 24.7 MeV (c.m.). Its shape has been shown[5] to be intermediate between the prediction of a transparent[7] optical-model potential fitting the $^{16}O+^{16}O$ elastic scattering and that of the strongly absorbing potential proposed[1,4] by the Seattle group. This shape is also reminiscent of the $^{16}O+^{18}O$ system, the behaviour of which was described as half-way between $^{16}O+^{16}O$ and $^{18}O+^{18}O$.

On fig.4 and 5 are plotted the excitation functions for the inelastic channels : $^{12}C(^{20}Ne,^{20}Ne_{2+})^{12}C$ and $^{12}C(^{20}Ne,^{20}Ne_{4+})^{12}C$, at three different angles. One notices that the latter reaction cannot be experimentally distinguished from the excitation of ^{12}C in the reaction $^{12}C(^{20}Ne,^{20}Ne)^{12}C_{2+}$ (though angular-momentum-matching considerations should considerably damp the latter). These excitation functions also have a structured shape, though not so sharp as for the elastic channel. One can see that the elastic scattering cross sections decrease much more rapidly with energy than the 2^+ channel ones, and that the 4.3 MeV excitation energy channel has a nearly constant cross section over the investigated energy range. This shows that the inelastic channels take a more and more important part in the process as energy increases. Since, at each angle, and even at the lower

AG

energies, the inelastic cross sections are of the same order of magnitude as the elastic ones, it appears that the role of the former channels cannot be ignored in the analysis of the latter one.

The excitation functions for the four-particle transfer reactions leading to the ground state and to the two (unresolved) doublets at 6-7 MeV in ^{16}O are shown in fig.6. The sharp structure of the former maybe due to the only occurence of even partial waves in the reaction amplitude. The inverse reaction $^{16}O(^{16}O,^{12}C)^{20}Ne$ has been extensively studied by Singh et al.[8] and by Rossner et al.[9]. It has been checked that our results are compatible with theirs, through the detailed balance theorem. One should note that the cross sections, nearly constant with energy, are slightly smaller than in inelastic channels, as expected from angular-momentum considerations.

To summarize these results, a noticeable structure is observed in the elastic and inelastic scattering at large angles, quite comparable to what was found in other light systems, as for example $^{16}O+^{14}N$, $^{16}O+^{15}N$ or $^{16}O+^{18}O$ [10]. With respect to $^{16}O+^{16}O$, cross sections are much smaller and the peak-to-valley ratio is strongly damped. With respect to $^{18}O+^{18}O$, large oscillations are still present, both on the excitation functions and the angular distribution.

III. Optical-model analysis.

Over such a range of angles and energies, and with the strong constraints imposed by two sharply different patterns in the forward and backward hemisphere, it was found very difficult to reproduce the experimental results with a single (and simple) optical-model potential. The results obtained with a strongly absorbing one, and with a transparent one, are first presented and compared. Then several modifications based upon physical considerations are discussed.

III.1. Simple optical-model potentials.

The predictions of the optical-model potential (hereafter referred to as potential A - see parameters in table I) proposed[4] by Vandenbosch, Webb and Zisman are compared in fig.2 to the experimental elastic excitation functions. A fairly good agreement is achieved at forward angles. This

17

agreement does not persist at larger angles where the calculated cross sections underestimate the experimental values, and where the predicted pattern does not exhibit the observed gross structure. This can be easily explained: this potential is strongly absorbing (large value of the ratio W/V, identical geometry for the real and the imaginary well). This precludes any forward-angle oscillation, and the diffusivity of the imaginary well is large enough to completely absorb (without any reflection) the lower partial waves. Such a potential reminds of the one suggested[1] for the $^{18}O+^{18}O$ system, but the availability of large-angle data in the case of non-identical particle scattering helps in understanding the scattering process more precisely.

This process cannot be described by what is usually referred to[10] as transparency. The figure 3 compares to the experimental angular distribution the predictions of the potential (labeled potential S, see table I) proposed[10] by Siemssen et al. for the $^{16}O+^{18}O$ elastic scattering. Whereas the average cross section is well obtained over the whole angular range, too large oscillations show up at forward angles ($\simeq 70°$), and these oscillations damp out too rapidly in the backward hemisphere. As will be shown later, this reproduces a typical Fraunhofer diffractive situation, due to the fact that the incoming wave penetrates sufficiently deep into the real well to feel a real nuclear phase shift.

To reproduce the two prominent features of the data, it is thus necessary to suppress any nuclear phase shift (that is, to absorb the surface waves before they enter the real nuclear well) and however to allow for some reflection of the lower partial waves.

III.2. Comparison with the $^{16}O+^{16}O$ potential.

To get these effects, and obtain some primary information on the absorption mechanism, it appears that one could use the comparison with the $^{16}O+^{16}O$ system as a guide. Since the expected difference with $^{20}Ne+^{12}C$ lies in the direct open reactions, which are surface-localized, it is reasonable to keep the $^{16}O+^{16}O$ optical-model potential proposed[7] by Gobbi et al., and to add a surface absorption. The "best" parameters for this surface absorption are given in table I (potential G). The same quadratic energy-dependence as proposed by Gobbi et al. was kept. To suppress the forward oscillations, it was necessary to pull this surface part largely out of the volume absorption. The

period of the large angle oscillations is also in favour of a large radius, which can be due to the nature of the considered reactions and to the deformation of the colliding nuclei. One sees in fig.2 and 3 that most of all the forward structure cannot be damped out without attenuating a large part of the backward one. However this procedure permits to roughly determine the range of the surface absorption, together with its strength, and gives a starting point for coupled-channel calculations.

In their analysis[7] of the $^{16}O+^{16}O$ elastic scattering, Gobbi et al. suggested a search for a general trend in the optical-model potential fitted to heavy-ion elastic scattering. They prescribe to use for the imaginary potential, aside from a surface part describing the direct channels strongly coupled to the entrance one, a volume part having the same geometry as the real well, and the strength of which would be proportional to the compound nucleus density. Accordingly, the surface part above determined was kept, and the Lang formula[11] was used in the level density calculations (the parameters are $a = 3.39$ MeV^{-1} and $r_0 = 1.425$ fm). This potential is labeled potential C and its predictions are reported on fig.2 and 3. It is quite noticeable that in this case the main weakness of the fit is in the too large values obtained at backward angles. This is explained by the strong reflection the low partial waves are submitted to. This reflection is due to the too drastic ℓ-dependence implied by the level density formula, as already pointed out[7] by Gobbi et al. However the merit of this calculation is to clearly exhibit the role of the low partial waves in backward elastic scattering. Specific effects of these waves have been recently discussed[12] in the case of $^{12}C+^{12}C$ elastic scattering. So far, their importance was not clearly recognized when discussing elastic scattering, especially at relatively low energy.

III.3. Reflection coefficients and S-matrix.

The fig.7 shows, from a typical strong absorption case (potential A), how the reflection coefficients η_ℓ are distorded when one uses the other potentials. Potential S gives the now well-known kinks, but here it should rather be characterized by the large reflection the low partial waves are submitted to, as well as by the rapid transition from $\eta_\ell \simeq 0.05$ to $\eta_\ell \simeq 1$. This effect is also found with potential C. On the other hand, one sees that the use of an outer surface part in the imaginary potential favours reflection at low ℓ, whereas the surface waves are more absorbed than with potential A.

A9

Another illustration of the internal and barrier contributions, and of their respective effect in different angular regions is given when one uses the Fuller decomposition[13] of the scattering amplitude. This decomposition is obtained when splitting the Legendre polynomials into their negative- and positive-deflection-angle travelling components. The structure observed is then explained by the interference between the two resulting components of the scattering amplitude. The advantage[6] is one deals with smooth and well-behaved components as a function of angle (and energy), rather than with the complicated total scattering amplitude. In the case of the potential A, the almost total absence of a nuclear phase shift results in a typical smooth cut-off case : both components have the same angular dependence and their interference gives only negligible oscillations whatever the angle is (see fig.8). On the contrary, the transparent potential S is an example of Fraunhofer diffraction, that is interference between two components decreasing exponentially, with different slopes. The obtained pattern has maximum structure when they cross themselves ($\theta_{c.m.} \simeq 75°$), then the structure damps out.

One understands now that, in the $^{20}Ne+^{12}C$ case, one looks for the forward pattern given by the potential A and then the persistent structure resulting from two components of same magnitude, having the same slow angular dependence. A similar situation has already been found[12] in the $^{12}C+^{12}C$ case at high energy. It is obtained with the contribution of low partial waves in the scattering amplitude, as can be seen in fig.8 in the case of the potential C for example.

It is attractive to compare the features of the $^{20}Ne+^{12}C$ data with the angular distribution[14] of $^{16}O+^{28}Si$ elastic scattering at 35 MeV. Both systems certainly have similar properties with respect to absorption (particularly a strong inelastic transition to the first excited 2^+ state). The two angular distributions exhibit the same rapid fall-off, then a strongly oscillatory behaviour at large angles. This led Braun-Munzinger et al.[14] to phenomenologically analyse their data with a strong-absorption S-matrix on which was superimposed a surface Regge-pole. It can be shown[15] that a parametrized Regge-pole has the effect of adding a rather flat contribution to both components of the scattering amplitude, giving rise to an interference spread over the whole backward hemisphere. One thus finds similar features in the two systems. These features are expected to be reproduced in coupled-channel calculations.

To end up with this analysis, and in spite of the only modest agreement found between optical-model predictions and the data, several facts have been explicited. First, the surface waves appear to be correctly described by the potential A, which reproduces the smooth ("barrier") part of the S-matrix. Large-angle data are an evidence for a sizeable contribution of low partial waves. This last point was recently pointed out in several similar analyses, and can certainly be connected with parametrizations as Regge poles, even though the physical existence of a Regge pole is not established. These points have been illustrated, using the Fuller decomposition. This method does not yet give accurate predictions for the optical-model parameters, but it helps to make clearer these physical features which determine the data. The effects which were described above can certainly be also reproduced with coupled-channel calculations. Before to describe the results of the latter technique, some interfering phenomena have to be studied, namely compound nucleus effects and elastic transfer.

IV. Compound nucleus and elastic transfer effects.

The irregularities observed on the excitation functions, the low magnitude of the cross sections and systematics on "alpha" nuclei raise the question of the compound contribution to the elastic cross section.

This point was first studied by Vandenbosch and Bernhardt[17]. Their analysis was applied to the first published part of our data[5] (limited to the energy range $22 \leqslant E_{c.m.} \leqslant 28$ MeV). With reasonable parameters, they calculated the compound-elastic cross section via the Hauser-Feshbach (H.F.) code STATIS[18]. Their conclusion is that this cross section is of the same order of magnitude as the experimental one at 90° and 130°, and that the "direct" elastic scattering can only be observed at c.m. angles smaller than, say, 80°.

After an extension of the code STATIS to a sufficient number of partial waves ($\ell_{max} = 42$), the compound contribution to the channels discussed in this paper was evaluated over the whole energy range investigated. Two extreme sets of parameters already used in Sect.III have been used in the entrance channel to clarify the importance of the transmission coefficients in that channel. Except for the optical-model parameters of the entrance channel, all the other parameters used in that calculation were

taken from ref.[17]. A first result is that the elastic scattering is the only channel in which the H.F. cross sections can be compared to the experimental one (the former is much smaller than the latter in any other channel). The second and important result is the strong dependence of the HF elastic cross section on the used transmission coefficients. This dependence can be read on the fig.9 where one sees that the two predictions differ by about one order of magnitude, even when applying a cut-off to the angular-momentum population of the compound nucleus.

A third point is the total disagreement between the shape of the compound elastic excitation function and the observed pattern, particularly its slope : the predicted 90° cross section as obtained from the strong absorption transmission coefficients is much smaller on the first two bumps (E = 17-22.5 MeV), of comparable order of magnitude on the third one (E = 22.5-27.5 MeV) and larger for E ≥ 28 MeV. This is not due to the fact that only 6 channels are considered in the calculation, since from angular momentum and energy considerations, these channels should[17] provide almost the totality of the HF denominator.

From these calculations it appears that a compound nucleus contribution to the elastic scattering cannot be excluded at backward angle and high incident energy. A similar contamination is found in the 2^+ and 4^+ channels only when using the potential A and no cut-off. Besides the fact that it is extremely difficult to evaluate this contribution, one can observe that the experimental excitation functions exhibit the same pattern over the whole energy range, with regular diffraction oscillations. A possible conclusion is that irregularities due to compound nucleus effects, and for which a correlation can be found at different angles and for different channels, are superimposed on these diffraction oscillations. Evidently, it is only the diffractive structure this paper is concerned with.

Another plausible mechanism interfering with the elastic scattering is elastic transfer. This transfer would involve eight particles and is expected to occur with rather low cross sections. Since the elastic cross sections are also low, one cannot exclude their contribution. The cross sections for the transfer are certainly localized at angles of the order of 150°, the "grazing" angle for elastic scattering being of the order of 30°. This authorizes to attribute the whole of the cross section around 90°

to elastic scattering alone. An evaluation of the transfer contribution at large angles is extremely difficult in the case of a large number of particles transferred between light nuclei ; it would require a full-recoil D.W.B.A. calculation and the absolute value of the cross section still depends on an unknown spectroscopic factor. This contribution cannot be further elucidated. However, one notices that cross sections at 140° do not exceed the ones at 90°, and this is a situation that potential scattering alone can certainly account for.

V. Coupling to the inelastic channels.

It was seen in Sect.II that the inelastic scattering cross sections are of the same order of magnitude or even larger than the elastic ones. Moreover, it has been shown in Sect.III that the data require the same modifications of the S-matrix as obtained when one uses a coupled-channel analysis rather than optical-model calculations. A coupled-channel study therefore appears as a consistent procedure to reproduce these effects.

It is well-known that the distortion of the elastic cross sections becomes less effective when the Q-value of the coupled channel is more negative. Since in the present case, the first excited state to be considered is the 2^+ state ($E_x = 1.63$ MeV) of ^{20}Ne, whereas the following ones are higher by more than 3 MeV, it was thought reasonable (and also extremely time-saving) to limit the coupling to this state in ^{20}Ne. This channel is also the best-matched one from the angular-momentum viewpoint.

It is from this well-matched channel that the surface absorption (or direct-reaction absorption) is expected to originate. Thus the difference between the typically weakly-absorbing $^{16}O+^{16}O$ system and any neighbouring one, as the $^{12}C+^{20}Ne$ one, should come mainly from transitions to this 2^+ state. This assumption was checked in a calculation performed with the coupled-channel code ECIS[19]. A rotational ^{20}Ne nucleus and a complex coupling (that is, where both real and imaginary wells are deformed) are assumed. The collective length $\beta_2 R$ had the realistic[20] value 2 fm. As it is usual in heavy-ion inelastic scattering computations, a special attention had to be paid to the matching radius value (here 50 fm)

and to the number of partial waves taken into account (here 200). The optical-model potential used in the calculation is reported in table I as potential G_2. One observes that, when taking explicitly into account the best-matched channel, the radius of the surface-absorption has to be reduced from 1.45 to 1.35 fm. Thus, the surface-absorption parameters are the same that Gobbi et al. used[7] with a volume-absorption proportional to the level density in ^{32}S to fit the $^{16}O+^{16}O$ data.

The results of this calculation are reported in fig.10 for the excitation function of the ground state channel, and in fig.4 for the first excited state channel. Concerning the elastic scattering, the following remarks can be done : the oscillations at 70° are again insufficiently damped ; the gross structure at 90° and 130° is well reproduced, though, at the latter angle, calculated cross sections are too low. Inelastic scattering at 72° is well described, both in magnitude and in phase. On the contrary, the predictions at 88° are too low at high energy, and they are largely underestimated at 130°. Similarly, in the elastic angular distribution, oscillations at forward angles are satisfactorily damped, though they are not completely rubbed out. At larger angles, the agreement is fairly good.

Similar calculations have been reported[21] by Osterfeld, Hnizdo and Toepffer over a limited range of energy ($22 < E_{c.m.} < 28$ MeV). These authors use the Gobbi potential to describe the entrance and exit channels, but rather than adding a surface absorption, they increase the imaginary range from 1.27 to 1.35 fm. This appears to be a very similar procedure as ours. A fairly good agreement is found with the experimental angular distribution at 23.3 MeV [4] between 30°and 80°c.m. but they argue that the predicted forward-angle oscillations are an evidence for a unsatisfactory description of the physical process. Especially, they observe that an acceptable fit to the data could only be obtained when, in addition to the coupling, the range of the imaginary potential is increased by about 6% as compared to the $^{16}O+^{16}O$ value. Their conclusion is that the coupling to the first excited state in ^{20}Ne is not sufficient to explain all the observed differences between the $^{16}O+^{16}O$ system and the $^{12}C+^{20}Ne$ one. It seems however likely that taking into account more channels in the coupled-channel calculations one could damp the diffractive oscillations at forward angles, as well as increase the inelastic cross sections at backward angles and high energy. The 4^+ state was

therefore introduced in our coupled-channel calculation and the above-mentioned effects were obtained (this is at variance with the results of Osterfeld et al.). Unfortunately, it is not possible to fit parameters on the excitation functions when three states are taken into account, since the amount of computation-time becomes prohibitive. This is the reason why the excitation functions for the inelastic scattering to the 4^+ state in ^{20}Ne are compared to second order D.W.B.A. predictions in the fig.5. The shape of the excitation function is only roughly reproduced, but at least at 77° and 84° c.m. the right order of magnitude is obtained. On the contrary, at 127°c.m., the calculations grossly underestimate the cross sections. The result was similar when the coupled-channel calculation was carried out for the 0^+, 2^+ and 4^+ state at 24.7 MeV.

To make more evident the effect of the coupling on the S-matrix, the Fuller decomposition was applied to the elastic scattering amplitude at 24.7 MeV using the S-matrices resulting from the coupled-channel calculation as well as from the optical model one, with the potential G_2. The results are reported in fig.11. Since the effect of a nuclear phase shift is[15] to decrease the ratio $|f^-/f^+|$ of the two angular components of the scattering amplitude (sect.III.3) when the angle increases, one sees that the net effect of the coupling is a reduction of the nuclear phase shift responsible for forward-angle oscillations, then both travelling components have comparable amplitude in the backward hemisphere, thus resulting in a strong oscillatory pattern. The effect on the reflection coefficients is also given in the box of the fig.11. Once again, the role of the lower partial waves is emphasized. All of these effects were described[16] by Rawitscher, whose predictions are seen to be valid in different physical situations.

Conclusion.

Several channels of the $^{12}C+^{20}Ne$ system have been experimentally studied over a large energy range (from 1.7 to 3.5 times the Coulomb barrier). A rapid decrease of the elastic cross section as a function of energy is observed at 70°c.m., whereas a noticeable structure shows up at 90° and 130°. It has been demonstrated that the forward-angle pattern is the signature of a strong-absorption S-matrix, reproducing the "barrier" part of the actual S-matrix. On the other hand, the structure at larger angles implies a non-negligible contribution from low-ℓ partial waves, an effect which has now been observed on several systems. These features have been reproduced as a whole using the optical-model potential fitted to the typical $^{16}O+^{16}O$ weak-

absorption situation, under the condition of adding a surface imaginary well to simulate the strong coupling of the entrance channel to other direct reactions.

From a coupled-channel analysis, it was found that the same picture, i.e. coupling between the elastic channel and the 2^+ first excited state in ^{20}Ne satisfactorily describes both the elastic and inelastic scattering. This coupled-channel analysis uses the Gobbi potential but a weakest surface absorption term, the location of which has to be pulled in the nuclear well as compared to the first-order optical-model analysis. The conclusion of our analysis, in agreement with the similar investigation[21] by Osterfeld, Hnizdo and Toepffer, is that one cannot describe the $^{12}C+^{20}Ne$ system as differing from the $^{16}O+^{16}O$ one by the only strong coupling to the 2^+ first excited state in ^{20}Ne. This is not a surprising result: the excitation functions which were measured for the inelastic scattering to the 2^+ and 4^+ states in ^{20}Ne, and for the four-particle transfers show that the cross sections for these processes stay at a remarkably constant level over the energy range investigated. This proves their sizeable contribution to the absorption and that, by no means they should be neglected in the balance. Certainly, this makes more difficult a decision concerning the origin of absorption.

Osterfeld, Hnizdo and Toepffer open an interesting field of investigation in suggesting that the absorption in the $^{12}C+^{20}Ne$ system could be governed by the density of precompound states. This was already considered in a calculation[22] by Helling, Scheid and Greiner, in which, unfortunately, these authors had to assume a similar ℓ-dependence for precompound and compound states. Osterfeld, Hnizdo and Toepffer use the two-center shell-model and find more level-crossings when ^{12}C and ^{20}Ne nuclei approach each other than with the $^{16}O+^{16}O$ system. However, these crossings occur[23] at rather small center separations, whereas it has been shown in Sect. III that the surface absorption takes place at much larger distances.

We conclude that an evaluation of the precompound absorption would be extremely useful. It appears difficult to find a situation where the precompound and the direct absorption would have features sufficiently different to firmly establish their coexistence.

Clearly, comparisons between the experimental behaviour of different systems still remain the only help to solve the problem of absorption in heavy-ion scattering.

Acknowledgments.

Many thanks are due to S.M.Lee and C.Marty for discussions on this problem. Three of us (H.D., J.C.R. and E.P.) thank Pr J.Valentin and Pr. Longequeue for the hospitality we found in Grenoble.

References

1) R.W.Shaw, R.Vandenbosch and M.K.Mehta, Phys. Rev. Lett. 25, 457 (1970).

2) R.A.Chatwin, J.S.Eck, D.Robson and A.Richter, Phys. Rev. C1, 795 (1970).

3) R.Vandenbosch, W.N.Reisdorf and P.H.Lau, Nucl. Phys. A230, 59 (1974).

4) R.Vandenbosch, M.P.Webb and M.S.Zisman, Phys. Rev. Lett. 33, 842 (1974).

5) H.Doubre et al., J. Physique (Lett.) 36, L-113 (1975).

6) E.Plagnol, H.Doubre and C.Marty, Phys. Lett. 67B, 377 (1977).

7) A.Gobbi et al., Phys. Rev. C7, 30 (1973).

8) P.P.Singh et al., Phys. Rev. Lett. 28, 1714 (1972).

9) H.H.Rossner, G.Hinderer, A.Weidinger and K.Eberhard, Nucl. Phys. A218, 606 (1972).

10) R.H.Siemssen, H.T.Fortune, A.Richter and J.W.Tippie, Phys. Rev. C5, 1839 (1972).

11) D.W.Lang, Nucl. Phys. 42, 353 (1963).

12) N.Rowley, H.Doubre and C.Marty, Phys. Lett. B (in press).

13) R.C.Fuller, Phys. Rev. C12, 1561 (1975).

14) P.Braun-Munzinger et al., Phys. Rev. Lett. 38, 944 (1977).

15) N.Rowley and C.Marty, Nucl. Phys. A266, 492 (1976) and C.Marty, private communication.

16) G.H.Rawitscher, in Proceedings of the Symposium on heavy ion scattering (Argonne National Laboratory report No ANL 7837, 1971 (unpublished)).

17) R.Vandenbosch and K.G.Bernhardt, J. Physique (Lett.) 37, L-161 (1976).

18) R.G.Stokstad, Wright Nuclear Structure Laboratory, Yale University Internal Report No 51 (1972), unpublished.

19) J.Raynal, D. Ph.T 71-48 preprint (unpublished).

20) P.H.Stelson and L.Grodzins, Nuclear Data A1, 21 (1965).

21) F.Osterfeld, V.Hnizdo and C.Toepffer, Phys. Lett. 68B, 319 (1977) and Contribution to the European Conference on Nuclear Physics with heavy ions Caen (1976), p.10.

22) G.Helling, W.Scheid and W.Greiner, Phys. Lett. 36B, 64 (1971).

23) U.Mosel, J.Maruhn and W.Greiner, Phys. Lett. 34B, 587 (1971).

Table caption

Table I. Parameters used in the optical-model calculations and in the coupled-channel calculations. Potentials are in Mev and lengths in fm.

Figure captions

Fig.1. Spectra in 4 different situations of the kinematical coincidence. The "left" detector is at the indicated angle. The "right" one is at 45°. The peaks labeled a, b, c, and d correspond to the inelastic scattering to the 4^+ and 2^+ state in ^{20}Ne, the elastic scattering, and the transfer to the ground state of ^{16}O respectively.

Fig.2. Excitation functions for the elastic channel at 3 angles. The full line, dot-dashed line and dotted line correspond to the predictions of the potentials A, G and C respectively.

Fig.3. Elastic scattering angular distribution at 24.7 MeV. The full line, dot-dashed line and dashed line correspond to the predictions of the potentials S, G and C respectively.

Fig.4. Excitation functions for the inelastic scattering to the 2^+ state in ^{20}Ne. The curve gives the predictions of the coupled-channel analysis.

Fig.5. Excitation functions for the inelastic scattering to the 4^+ state in ^{20}Ne. The curve gives the predictions of a second order D.W.B.A. calculation.

Fig.6. Excitation functions for the 4-particle transfer.

Fig.7. Reflection coefficients at 24.7 MeV for the optical-model potentials used in the analysis.

Fig.8. Decomposition of the scattering amplitude at 24.7 MeV, according to the Fuller method, in its two travelling components f^+ and f^-.

Fig.9. Compound contributions to the elastic channel. Curves a) and b) are calculated with the transmission coefficients of the potential A, curves c) and d) with the transmission coefficients of the potential S. In the cases b) and d) an angular momentum cut-off was applied in the compound nucleus population.

Fig.10. Results of the coupled-channel analysis for the elastic channel.

Fig.11. Fuller decomposition of the scattering amplitude and reflection coefficients as obtained from the potential G_2 at 24.7 MeV. Full lines refer to the coupled-channel calculation, thin lines to the optical-model one.

Table I

Potential	V	r_{ov}	a_v	W	r_{ow}	a_w	W_d	r_{od}	a_d	Reference
A	17	1.35	0.57	$1 + 0.54\ E_{c.m}$	1.35	0.57				4
S	$12+0.25\ E_{c.m}$	1.35	0.49	$0.4+0.15\ E_{c.m}$	1.35	0.49				10
G	17	1.35	0.49	$0.8+0.2\ E$	1.27	0.15	$-0.31+0.003E^2_{c.m}$	1.45	0.805	7
C	17	1.35	0.49	see text			$-0.31+0.003E^2_{c.m}$	1.45	0.805	7
G_2	17	1.35	0.49	$0.8+0.2\ E$	1.27	0.15	$-0.2+0.002\ E^2_{c.m}$	1.35	0.6	7

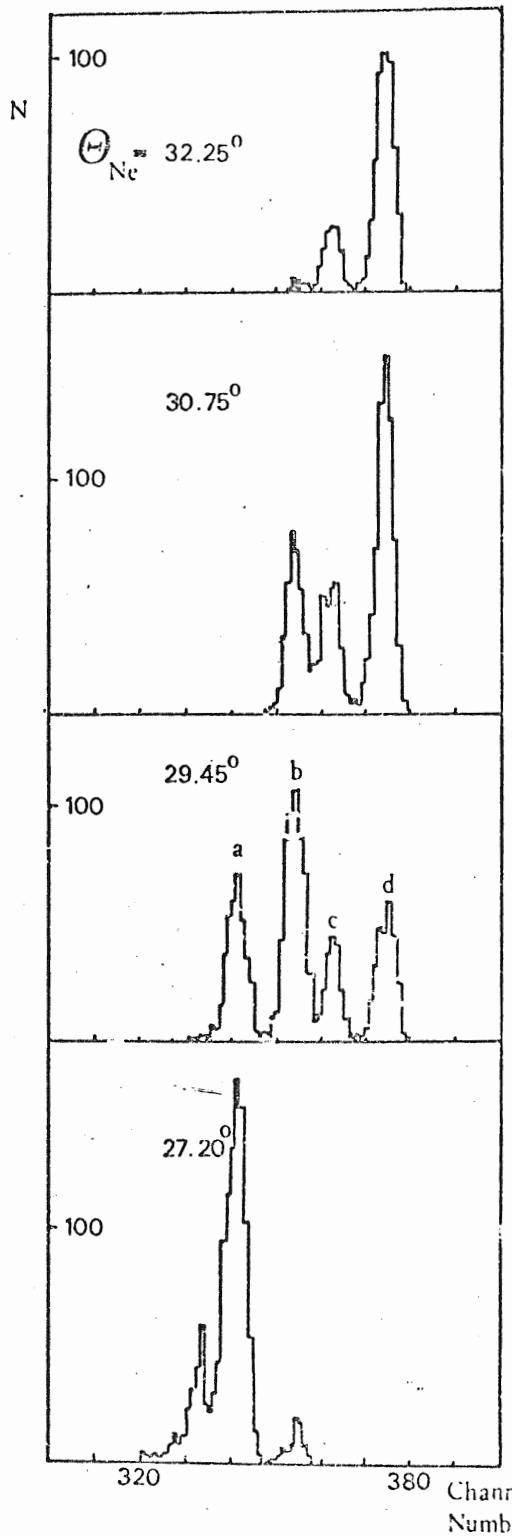
N
100
$\Theta_{Ne^{**}}$ 32.25°
30.75°
100
29.45°
b
100
a
d
c
27.20°
100
320
380
Channel
Number

Fig. 1

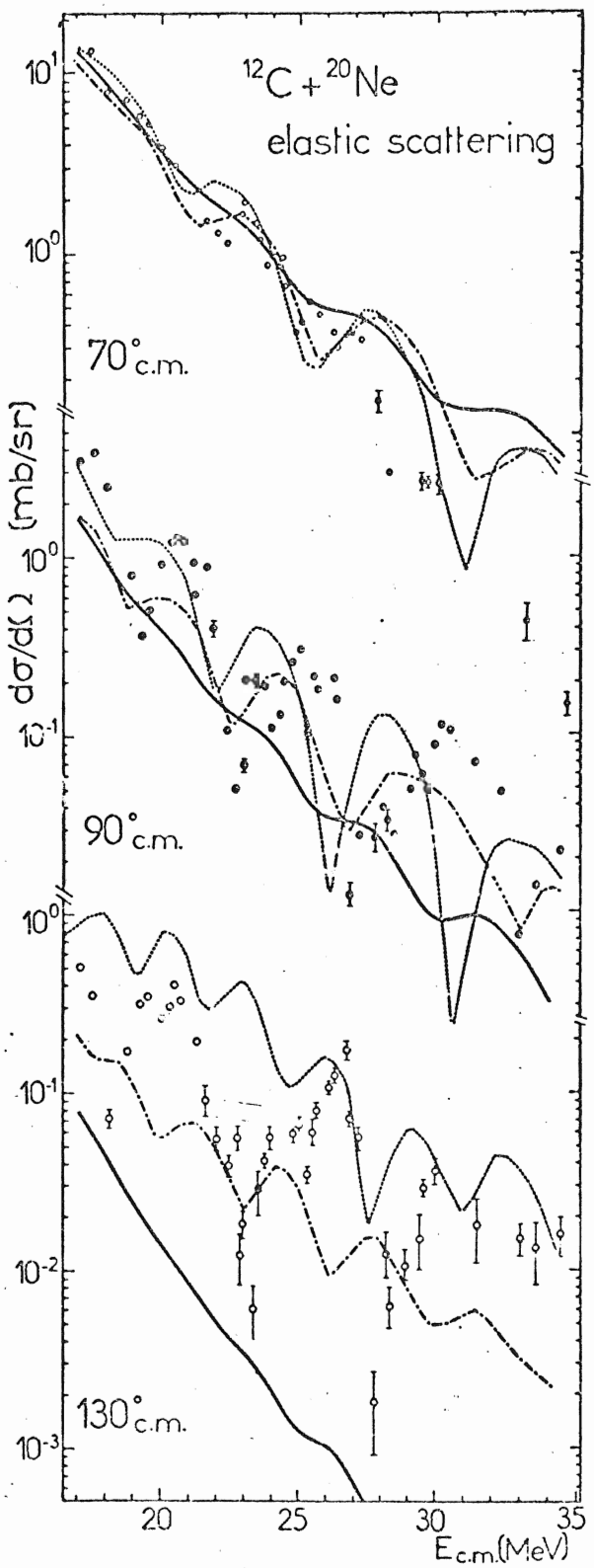
$^{12}C + ^{20}Ne$
elastic scattering
70° c.m.
90° c.m.
130° c.m.
dσ/dΩ (mb/sr)
10^{1}
10^{0}
10^{0}
10^{0}
10^{-1}
10^{-1}
10^{-2}
10^{-3}
20
25
30
35
$E_{c.m.}$(MeV)

Fig. 2

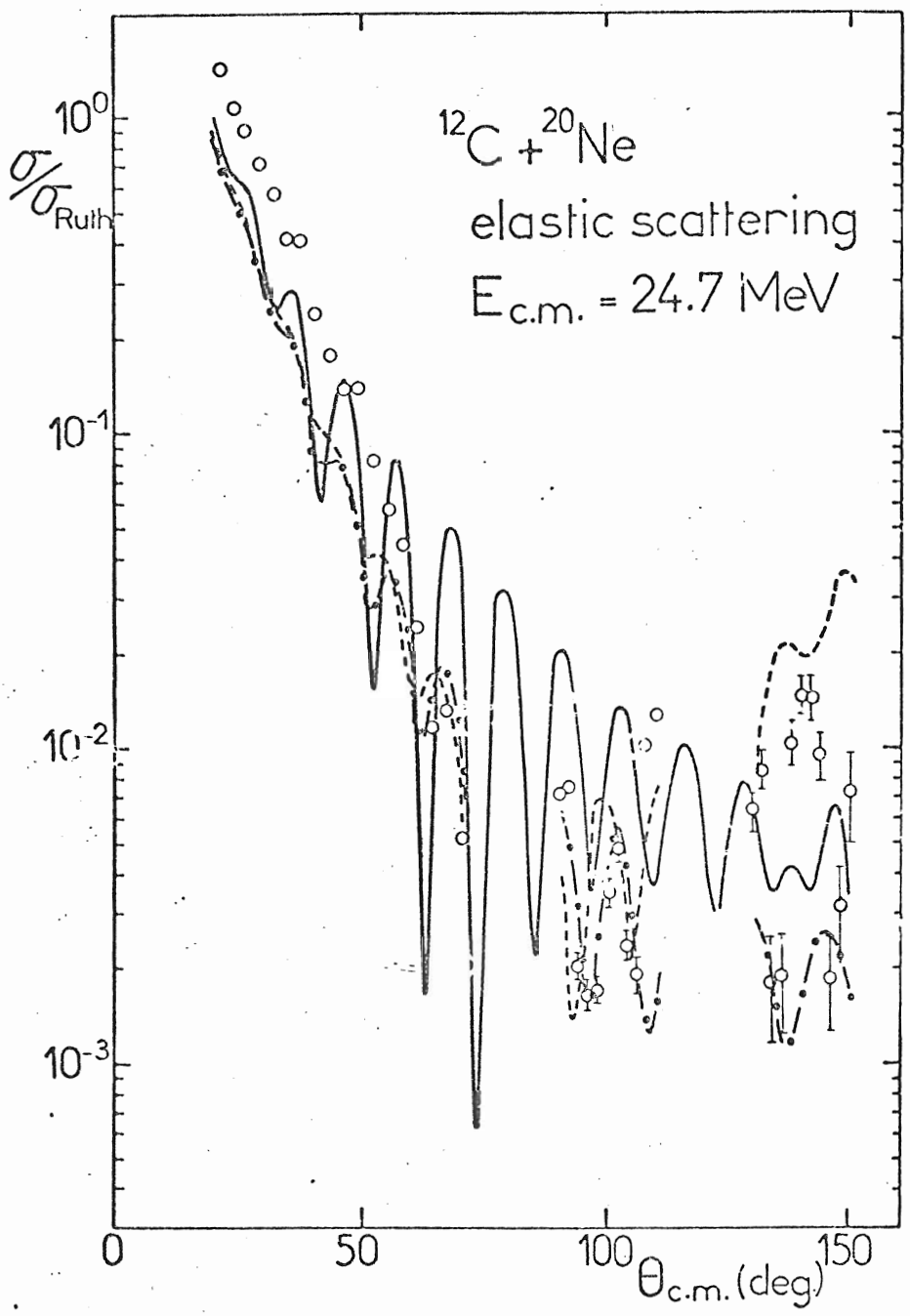
$^{12}C + ^{20}Ne$
elastic scattering
$E_{c.m.} = 24.7$ MeV
σ/σ_{Ruth}
10^0
10^{-1}
10^{-2}
10^{-3}
0
50
100
150
$\theta_{c.m.}$ (deg.)

Fig 3

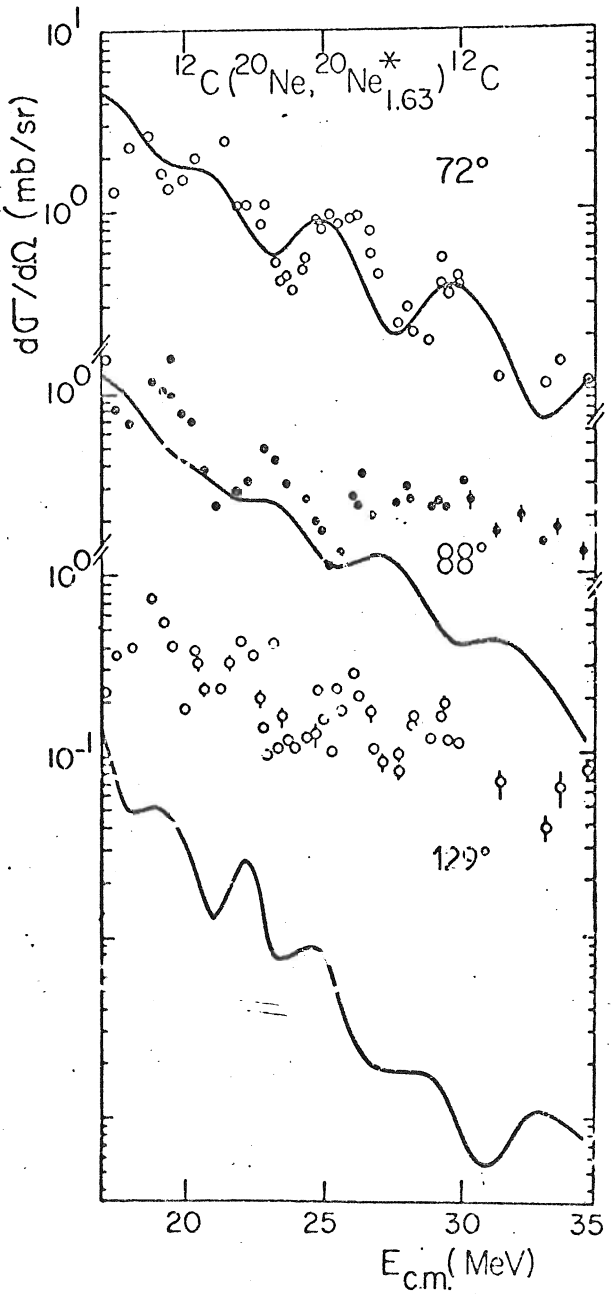
$^{12}C(^{20}Ne,^{20}Ne^{*}_{1.63})^{12}C$
72°
88°
129°
$d\sigma/d\Omega$ (mb/sr)
10^{1}
10^{0}
10^{0}
10^{0}
10^{-1}
20
25
30
35
$E_{c.m.}$ (MeV)

Fig. 4

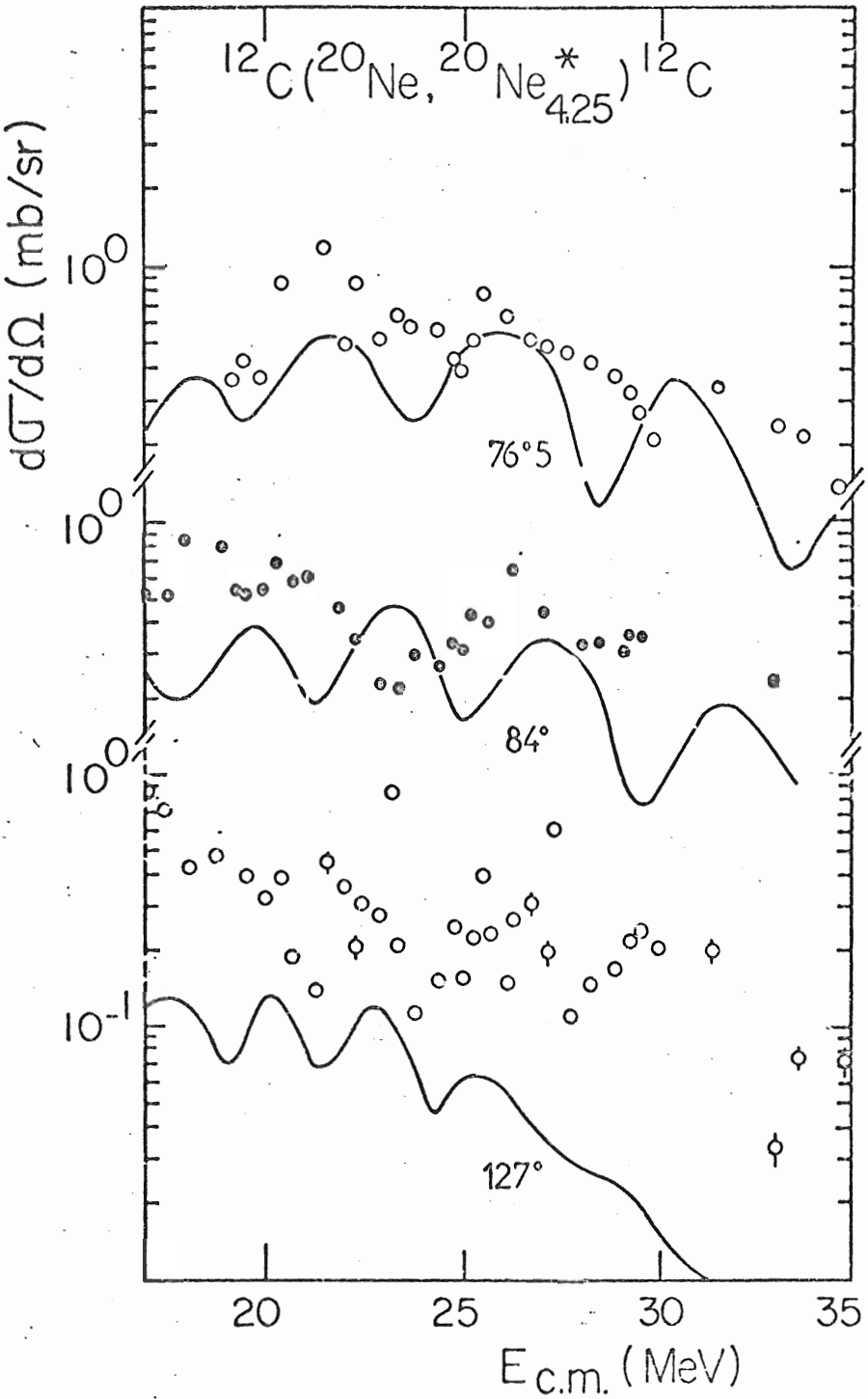
$^{12}C(^{20}Ne, ^{20}Ne^{*}_{4.25})^{12}C$
dσ/dΩ (mb/sr)
10^{0}
10^{0}
10^{0}
10^{-1}
76°5
84°
127°
20
25
30
35
E c.m. (MeV)

Fig. 5

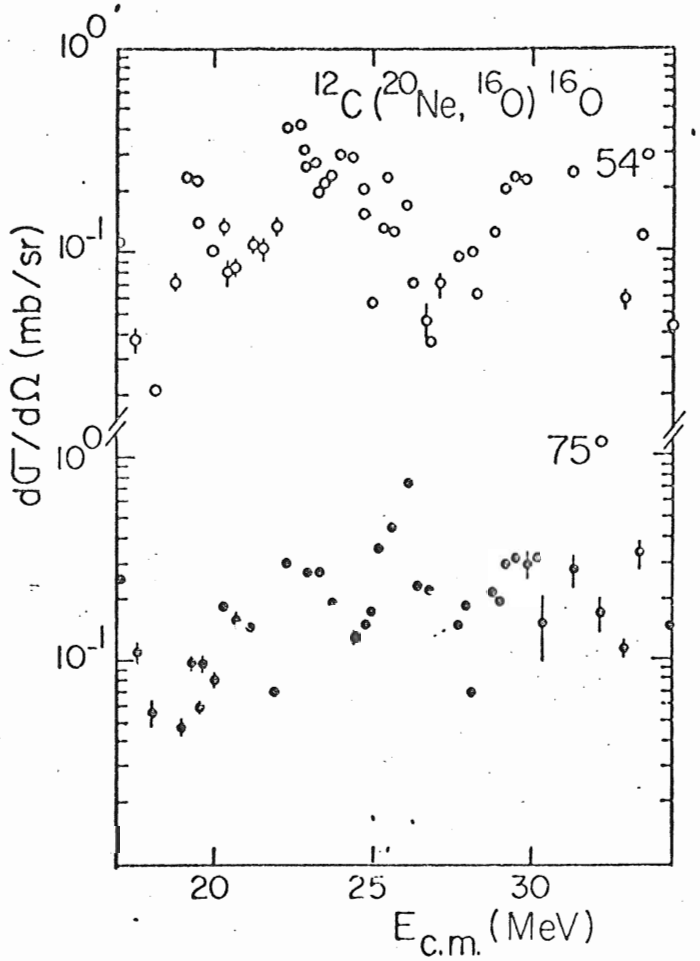
$^{12}C(^{20}Ne, ^{16}O)^{16}O$
54°
75°
10^0
10^{-1}
10^0
10^{-1}
$d\sigma/d\Omega$ (mb/sr)
20
25
30
$E_{c.m.}$ (MeV)

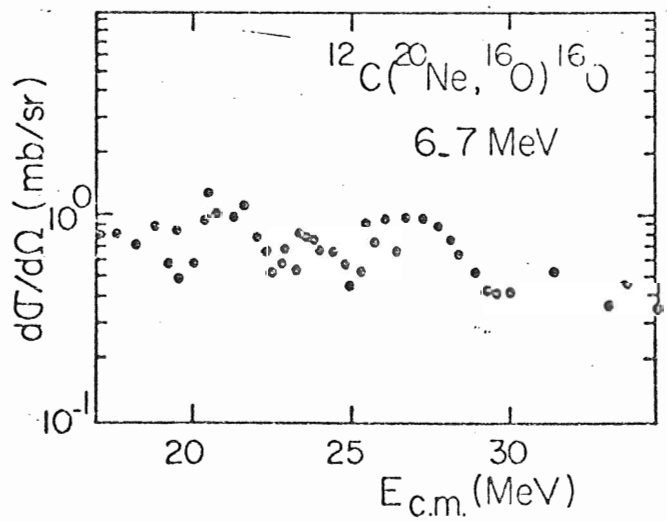
$^{12}C(^{20}Ne, ^{16}O)^{16}O$
6.7 MeV
10^0
10^{-1}
$d\sigma/d\Omega$ (mb/sr)
20
25
30
$E_{c.m.}$ (MeV)

Fig. 6

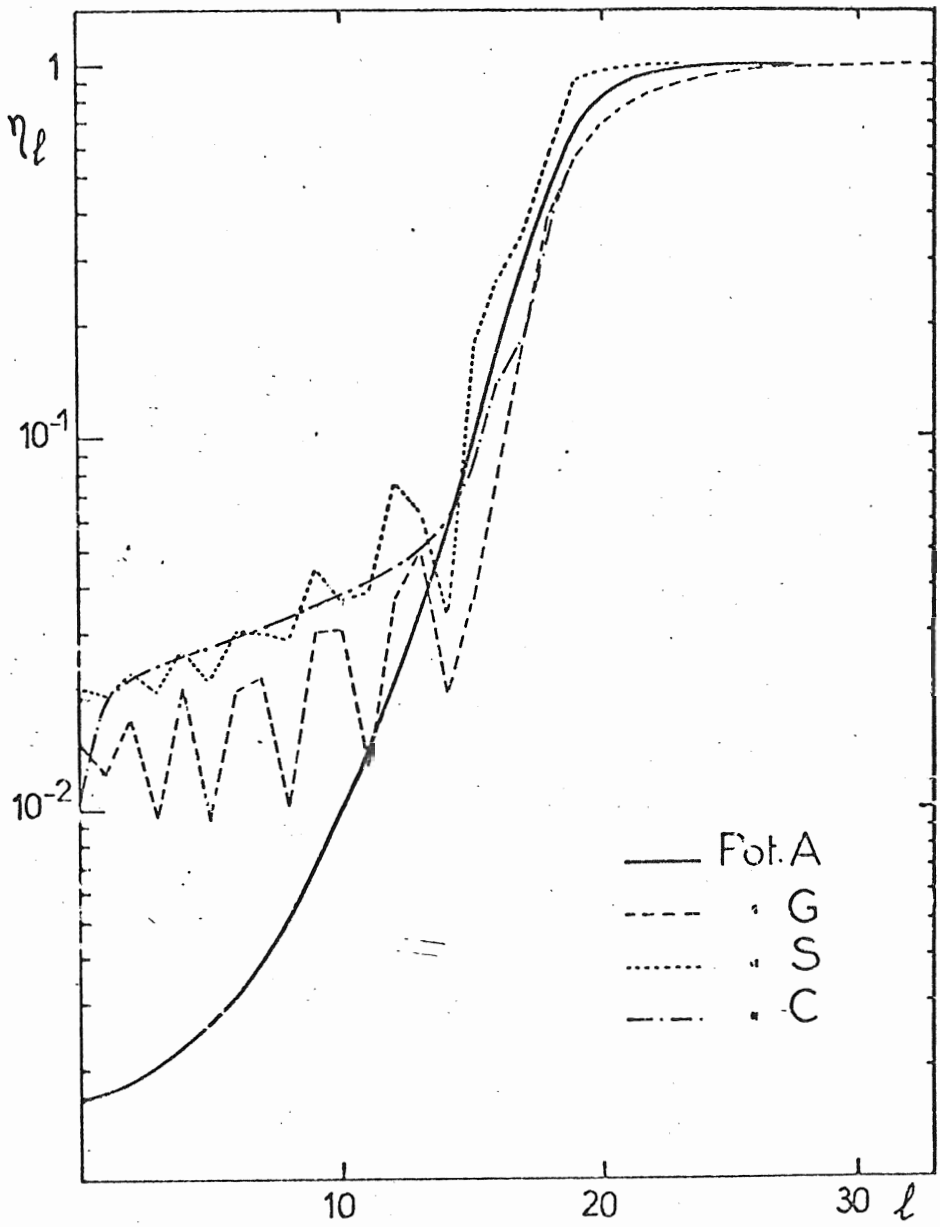

Fig 7

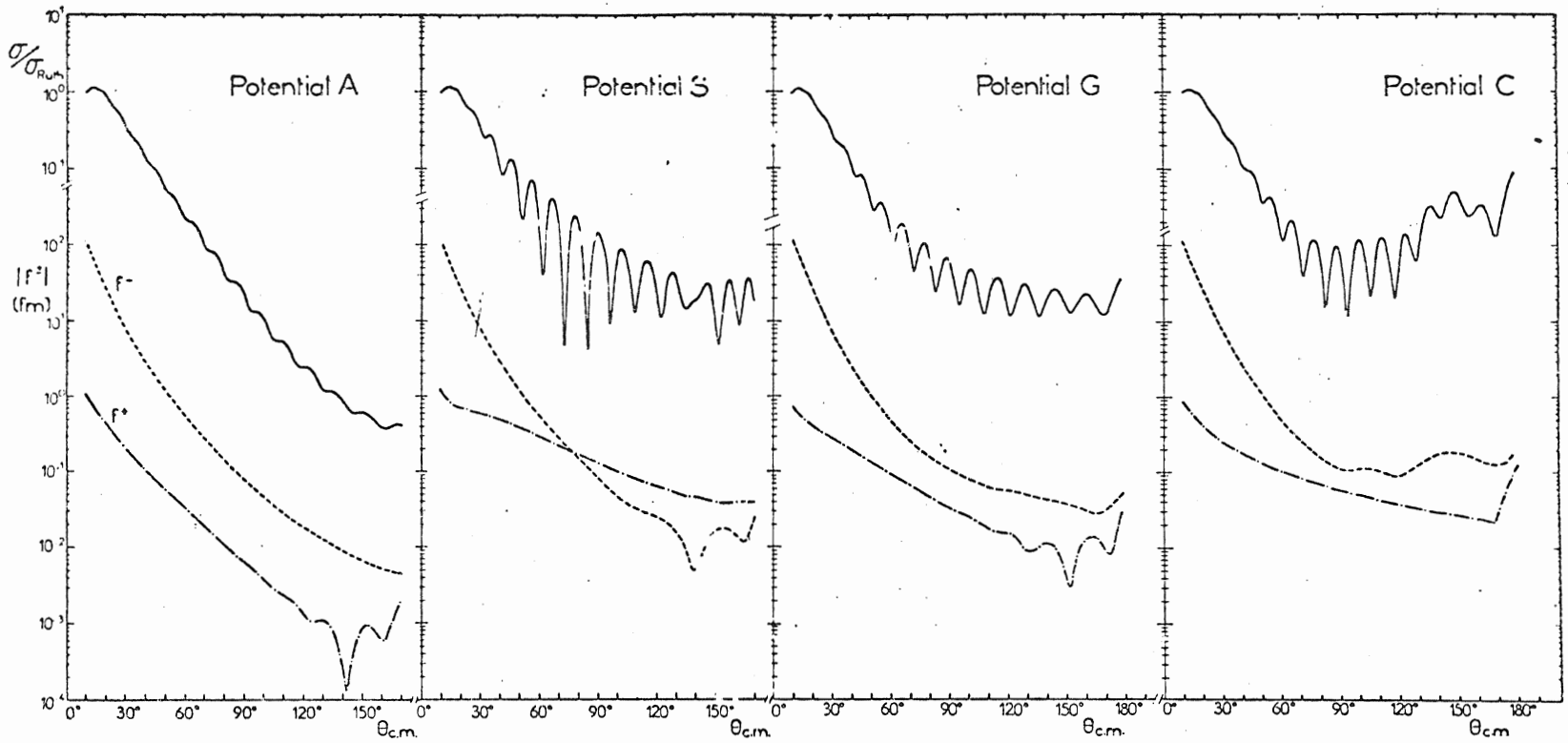
Potential A
Potential S
Potential G
Potential C
σ/σ_Ruth
|f²| (fm)
f⁻
f⁺
θc.m.
0°
30°
60°
90°
120°
150°
180°

Fig. 8

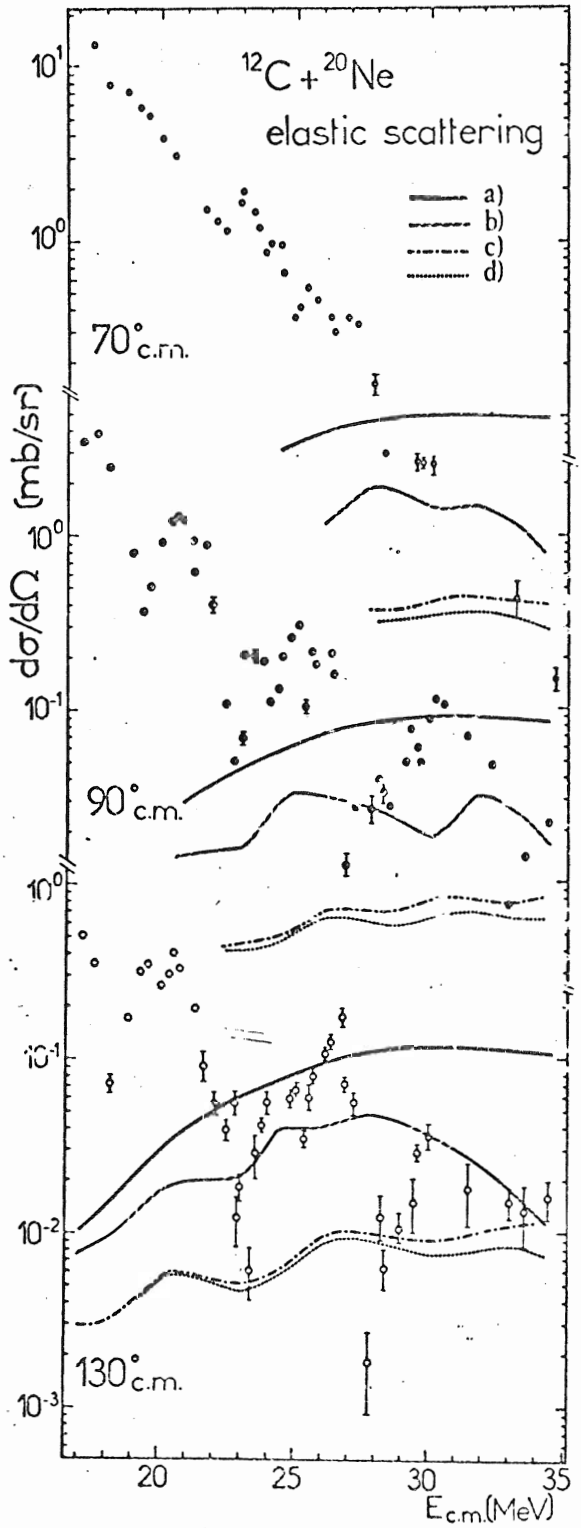
$^{12}C + ^{20}Ne$
elastic scattering
a)
b)
c)
d)
70° c.m.
90° c.m.
130° c.m.
dσ/dΩ (mb/sr)
10^{1}
10^{0}
10^{0}
10^{-1}
10^{0}
10^{-1}
10^{-2}
10^{-3}
20
25
30
35
$E_{c.m.}$(MeV)

Fig. 9

11

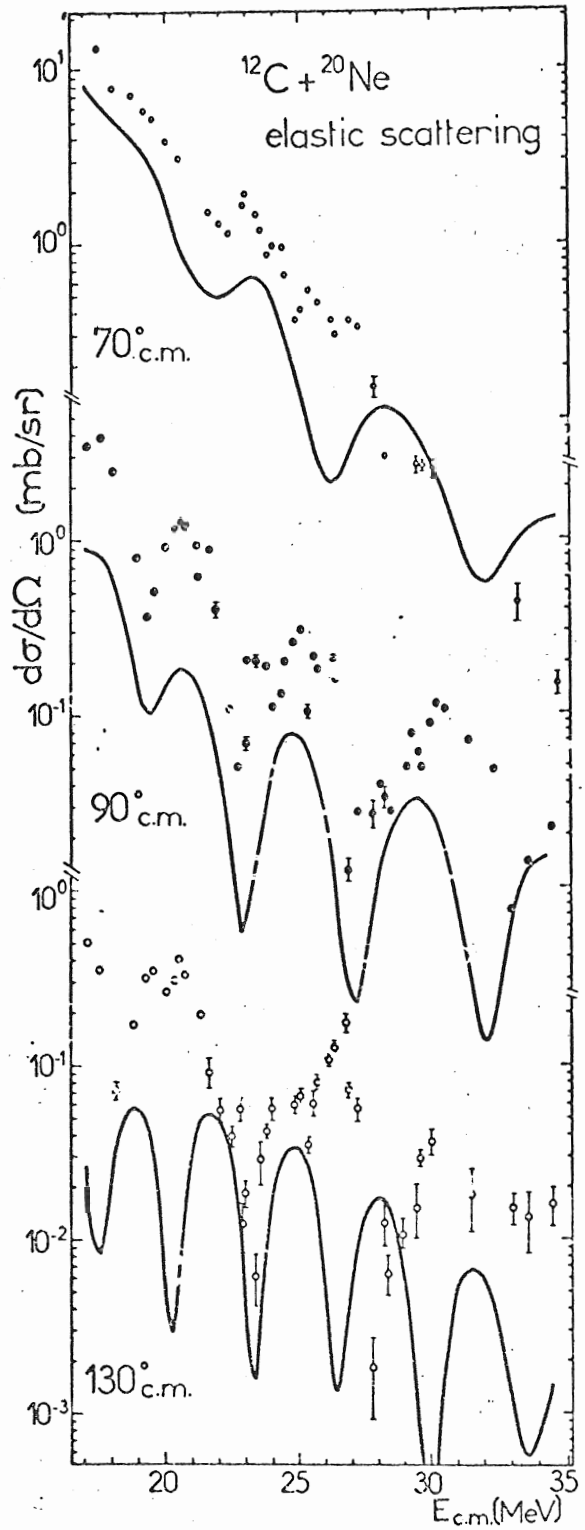
$^{12}C + ^{20}Ne$
elastic scattering
70° c.m.
90° c.m.
130° c.m.
dσ/dΩ (mb/sr)
10^{1}
10^{0}
10^{0}
10^{-1}
10^{0}
10^{-1}
10^{-2}
10^{-3}
20
25
30
35
$E_{c.m.}$(MeV)

Fig. 1a

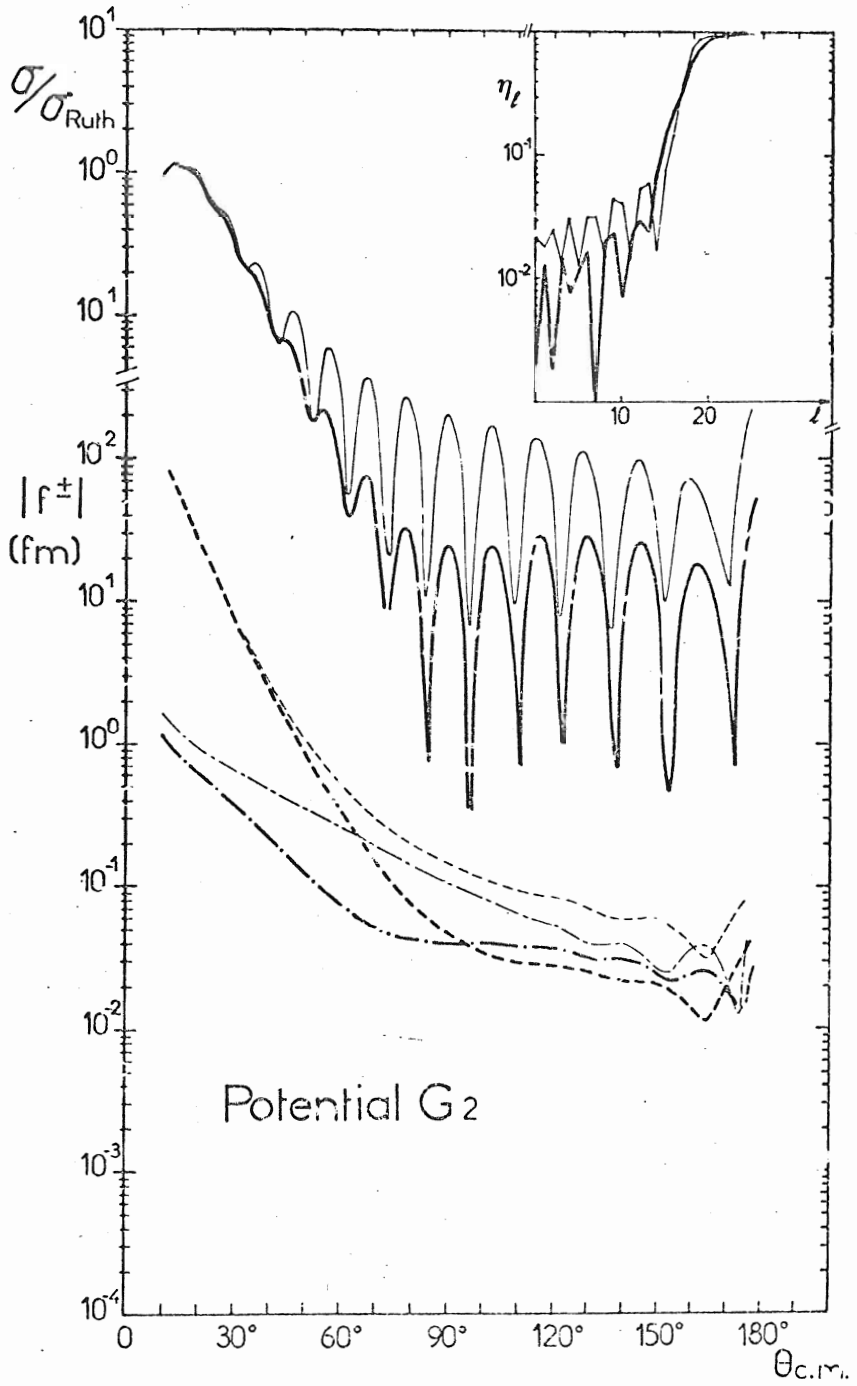
σ/σ_{Ruth}
$|f^{\pm}|$
(fm)
η_l
l
Potential G 2
$\theta_{c.m.}$
0
30°
60°
90°
120°
150°
180°

Fig. 11

3. Conclusion.

Cette étude a été présentée comme un test du modèle d'absorption dépendant du moment angulaire dû à Vandenbosch. On trouve que le couplage au premier état 2^+ du ^{20}Ne permet de reproduire convenablement l'ensemble des résultats, et un calcul unique parce qu'onéreux indique qu'en incluant l'état 4^+ du ^{20}Ne, l'accord peut être amélioré. Ces observations sont tout à fait en faveur du modèle de Vandenbosch.

Par ailleurs, la méthode proposée par Fuller montre que les petites ondes partielles jouent ici un rôle déterminant. Les résultats obtenus aux angles arrière leur sont entièrement dus. On explique leur présence par l'existence de voies directes (essentiellement inélastiques ici) immédiatement couplées à la voie élastique.

Ce rôle des petites ondes partielles est le résultat majeur de cette analyse. Il avait jusqu'ici été tenu pour négligeable dans les réactions entre ions lourds. La contribution de ces ondes partielles est certes de faible amplitude, mais elle est relativement isotrope et vient interférer à grand angle avec celle des ondes partielles rasantes ; le résultat de cette interférence a une influence considérable sur l'allure des distributions angulaires et des fonctions d'excitation.

Au chapitre III seront donnés d'autres exemples de ce rôle des petites ondes partielles.

IV - ETUDE DU SYSTEME $^{20}Ne+^{20}Ne$.

1. Motivations.

En dépit des difficultés expérimentales qu'elle présente, l'étude du système $^{20}Ne+^{20}Ne$ est intéressante à plusieurs points de vue.

Il s'agit d'un système dont les deux noyaux appartiennent à la couche 2s1d ; un seul système qui possède cette propriété, $^{18}O+^{18}O$, avait été étudié auparavant [Sh 70]. A côté de la transition inélastique vers le premier état excité du ^{20}Ne ($E^* = 1.63$ MeV), il existe deux autres voies favorisées du point de vue cinématique, ce sont les voies :

$$^{20}Ne+^{20}Ne \rightarrow {}^{16}O+^{24}Mg \quad Q = +4.585 \text{ MeV}$$
$$^{20}Ne+^{20}Ne \rightarrow {}^{12}C+^{28}Si \quad Q = +7.408 \text{ MeV}$$

La comparaison avec le système $^{12}C+^{20}Ne$, ou $^{16}O+^{18}O$, est tout à fait frappante (fig.I.2). La majorité des transferts se situe à $Q \simeq -5$ MeV, mais parmi eux, seuls quelques uns paraissent probables. On notera surtout que le transfert d'une particule alpha est ici plus exothermique que dans le cas $^{18}O+^{18}O$. Le système $^{20}Ne+^{20}Ne$ paraît donc un bon candidat pour tester le modèle d'absorption dépendant du moment angulaire : les transferts directs devraient être source d'une absorption encore plus forte que dans le système $^{18}O+^{18}O$. Si, en outre, la densité d'états composés ou précomposés joue un rôle dans l'absorption, ces états vont accentuer cet effet car leur densité est plus grande dans ^{40}Ca que dans ^{36}S, à énergie d'excitation donnée. Ce système est aussi un système symétrique, et, étant données les difficultés expérimentales, on peut espérer des informations non ambiguës de la seule fonction d'excitation à 90°. Enfin, c'est un premier pas vers les systèmes lourds, parmi lesquels est étudié ci-dessous le système $^{40}Ca+^{40}Ca$; il est intéressant de voir comment les fonctions d'excitation se modifient quand la charge et la masse augmentent. Ceci est nécessaire quand on compare le grand nombre de résultats déjà acquis au voisinage de l'oxygène 16, ou sur des systèmes comportant au moins un oxygène 16 dans la voie d'entrée, aux données très éparses dont on dispose pour des masses réduites plus élevées.

2. Conditions expérimentales.

Ces expériences ont également été réalisées sur le cyclotron de Grenoble. Il a évidemment été nécessaire de construire une cible gazeuse. Le plan de cette cible apparaît sur la figure I.4. Le faisceau de ^{20}Ne, précédemment collimaté et d'énergie comprise entre 40 et 90 MeV, pénètre et sort de la cible par deux fenêtres de Ni d'épaisseur 0.565 mg/cm^2. La cible a été dessinée pour permettre la seule mesure de la fonction d'excitation élastique à $\theta_{c.m.} = 90°$. Les particules diffusées à ±45° du faisceau sortent par des fenêtres identiques de Ni. On voit cependant sur la figure que la particule incidente traverse également une certaine épaisseur de gaz (0.4 mg/cm^2 à la pression de 150 torrs qui était celle de travail) avant la collision. Mais surtout, une épaisseur comparable (2 × 0.32 mg/cm^2) est traversée avant les fenêtres de sortie ; ceci provoque des pertes d'énergie, dont les fluctuations peuvent être considérables. On donne dans le tableau I.1 quelques chiffres significatifs de la situation expérimentale.

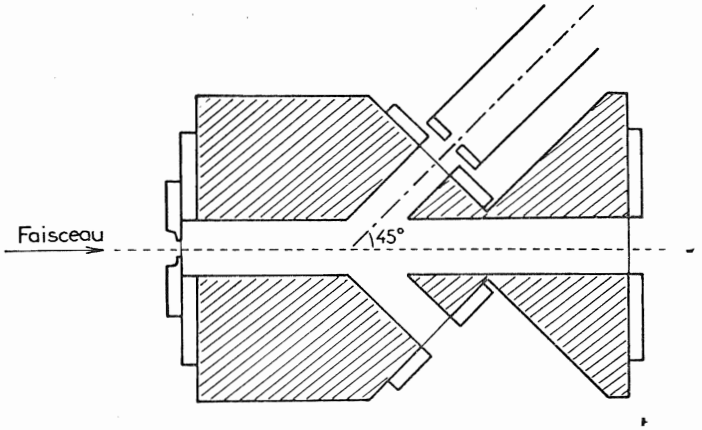

Fig.I.4. Plan de la cible gazeuse utilisée dans l'étude du système $^{20}Ne+^{20}Ne$. L'échelle vaut 2.

Le seul contrôle de l'épaisseur de ^{20}Ne offert aux particules incidentes était fourni par la lecture de la pression dans la cible. Celle-ci était reliée à un large volume de gaz pour amortir des effets dus aux fuites éventuelles. Ce contrôle minimum s'est révélé suffisant car les mesures se sont avérées tout à fait reproductibles (une partie de l'expérience refaite après six mois). Comme pour le système $^{20}Ne+^{12}C$, la mesure utilisait la méthode de la coïncidence cinématique entre deux détecteurs à barrière de surface situés à 12.5 cm du centre de la cible gazeuse. L'un des détecteurs portait un diaphragme de dimensions 2 × 18 mm, l'autre étant largement ouvert pour assurer un rendement de coïncidence maximal. Il est assez remarquable qu'avec un tel dispositif une résolution expérimentale meilleure que le MeV ait été atteinte. Ce problème de résolution en énergie est important, non seulement pour séparer le pic élastique des inélastiques, plus intenses que l'élastique dès que $E_{c.m.} \simeq 2B_c = 37$ MeV, mais aussi du transfert d'une particule alpha. Les niveaux excités du ^{24}Mg peuvent en effet donner lieu à des pics se confondant avec le pic élastique, car la méthode de la coïncidence cinématique, telle qu'elle est utilisée, identifie une voie par son seul Q de réaction. L'identification peut cependant être améliorée en étudiant par exemple le rapport des énergies des particules détectées en coïncidence. Dans ce but, les énergies E_1 et E_2 des deux particules sont enregistrées et on procède hors-ligne à une analyse plus sévère, événement par événement.

Il est apparu qu'une des difficultés de cette expérience était due au problème de diffusion multiple dans les feuilles de Ni à la sortie de la cible gazeuse : à faible énergie incidente, les ions issus de la réaction n'ont plus, après traversée du gaz, qu'une très petite énergie (cf. tableau I.1). Ils sont donc très sensibles à la diffusion multiple qu'introduit la traversée du gaz, et surtout du Ni qui constitue la fenêtre de sortie de la cible. On peut prévoir deux effets : une variation du rendement de coïncidences avec l'énergie, qui peut diminuer la pente de la fonction d'excitation, et surtout un amoindrissement de la résolution angulaire (le résultat de la mesure ne représentant plus qu'une moyenne sur les angles voisins de 90°). A titre indicatif, on trouvera dans le tableau I.1 la racine de l'élargissement carré moyen [Ba 63] résultant de la traversée de la feuille de Ni en fonction de l'énergie.

Tableau I.1.

E_{react} (MeV)	35	50	75	90
E_{inc} (MeV)	41.7	56	80	94.5
E_{diff} (MeV)	17.5	25	37.5	45
E_{det} (MeV)	10	18	31.2	39
$\theta_{1/2}$ (deg)	1.9	1.5	1.	0.6

Tableau I.1. Caractéristiques de l'étude expérimentale du système $^{20}Ne+^{20}Ne$. E_{react} est l'énergie moyenne à laquelle à lieu la réaction. Le faisceau a l'énergie E_{inc}. E_{diff} et E_{det} désignent respectivement l'énergie de chaque ion à l'endroit du choc et à l'arrivée dans le détecteur. $\theta_{1/2}$ est l'élargissement carré moyen dû à la diffusion multiple.

La normalisation relative des sections efficaces a été obtenue à partir des données d'un moniteur visant une feuille de Ni. La normalisation absolue est évidemment autrement compliquée. Comme ni le cyclotron, ni la cible ne permettent de descendre à l'énergie de la barrière coulombienne, les mesures faites aux énergies les plus proches de celle-ci ont été utilisées comme normalisation de la façon suivante : les prédictions des potentiels qui reproduisent les situations de $^{16}O+^{16}O$ et $^{18}O+^{18}O$ (en modifiant seulement les rayons par la loi en $A^{1/3}$) ont été calculées pour $E_{c.m.} < 25$ MeV . Comme, à ces énergies, les résultats ne diffèrent pas par plus de 10%, leur moyenne a été considérée comme la valeur de la section efficace élastique mesurée sur le système $^{20}Ne+^{20}Ne$.

3. Résultats.

La fonction d'excitation obtenue est présentée sur la figure I.5. Elle a été mesurée pour des énergies de réaction comprises entre 20 et 43 MeV (c.m.) alors que la barrière coulombienne est voisine de 18.5 MeV.

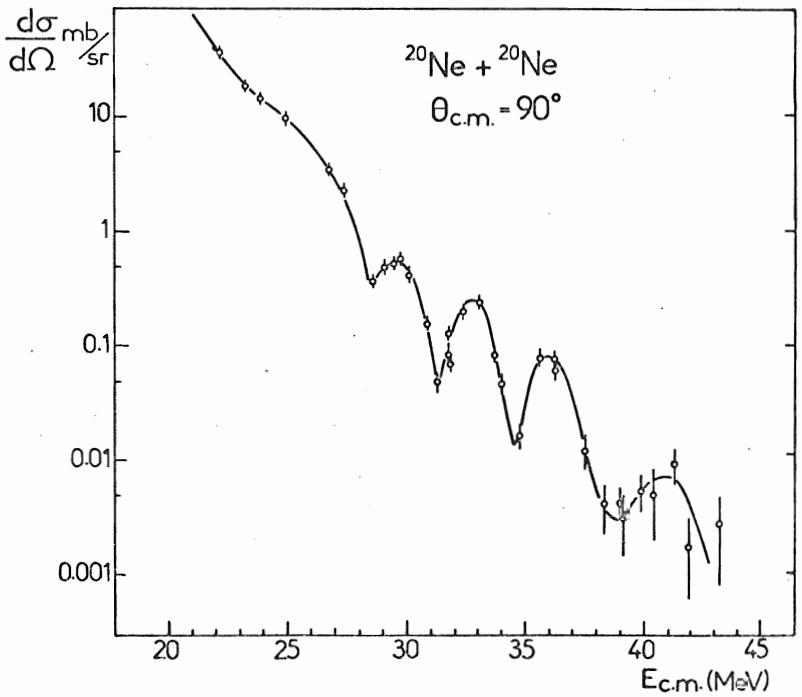

Fig.I.5. Fonction d'excitation de la voie élastique pour le système $^{20}Ne+^{20}Ne$.

Les difficultés dues à la diffusion multiple ont été signalées ci-dessus ; elles impliquent une ouverture angulaire effective, dans le c.m., pouvant atteindre ±3° (c.m.). La forme de la fonction d'excitation expérimentale ne devrait pas s'en trouver fortement distordue. En effet, les calculs optiques auxquels il a été fait allusion ci-dessus indiquent que l'oscillation de la distribution angulaire, centrée à 90°, a une largeur totale de 12° dans le centre de masse (d'un minimum à l'autre). Même si l'ouverture angulaire "effective" a varié avec l'énergie, la présence d'un extremum à 90° nous assure que l'effet de cette variation est resté faible.

La présence d'une structure dans la fonction d'excitation à 90° est indiscutable ; le rapport pic-sur-vallée de cette structure, bien supérieur à ce qu'il est dans le système $^{18}O+^{18}O$, rapproche le système $^{20}Ne+^{20}Ne$ d'autres comme $^{16}O+^{18}O$, ou $^{16}O+^{14,15}N$ [Si 71], moins absorbants. De plus, la section efficace décroît rapidement avec l'énergie. Les oscillations sont obtenues pour une valeur moyenne de $d\sigma/d\Omega = 100$ µb, ce qui est faible. Mais la fonction d'excitation paraît recevoir une moindre contribution du noyau composé que celle observée dans le cas $^{20}Ne+^{12}C$. La période des oscillations est de l'ordre de 3 MeV, ce qui ne diffère pas des systèmes voisins et confirme que la structure observée est bien du même type. On note également que la structure apparaît (par un minimum) à $E_{c.m.} = 28$ MeV ($E_{c.m.}/B_c = 1.52$) c'est-à-dire à un rapport $E_{c.m.}/B_c$ plus petit que dans le système $^{16}O+^{16}O$. Comme on le verra au chapitre III, on s'attendrait plutôt à ce qu'une structure apparaisse à énergie d'autant plus élevée que le système est plus absorbant.

En résumé, les données obtenues pour le système $^{20}Ne+^{20}Ne$ indiquent, dans ce système, une transparence pour les ondes partielles rasantes ($\ell_g \simeq 20$) tout à fait comparable à celle observée sur les systèmes de masse moindre. Il n'apparaît pas non plus sur la forme de la fonction d'excitation de modification radicale due à la plus grande charge ou masse des ions incidents. On peut donc conclure qu'au moins jusqu'à ^{20}Ne, l'observation d'une structure large dans la fonction d'excitation élastique à 90° est un phénomène tout à fait général, et que le système $^{18}O+^{18}O$ apparaît plutôt comme une exception à cette règle.

CHAPITRE II

LE SYSTÈME $^{40}Ca + ^{40}Ca$

I - DIFFUSION ELASTIQUE.

1. Motivations.

Après l'ensemble d'études accomplies concernant des noyaux de masse voisine de 16, à Yale, Argonne et Seattle, il était extrêmement intéressant de passer au système $^{40}Ca+^{40}Ca$ pour y chercher des phénomènes similaires. Plusieurs questions se trouvent en effet posées :

- le modèle d'absorption dépendant du moment angulaire conserve-t-il toute sa validité pour des noyaux incidents beaucoup plus lourds, et beaucoup plus chargés ?

- comment se lit sur la fonction d'excitation la transparence pour les ondes partielles rasantes lorsque les trajectoires sont dominées par la répulsion coulombienne ?

Par ailleurs, même si cette transparence ne se manifestait pas, toute comparaison entre les propriétés de la diffusion élastique à la masse 16 et à la masse 40 peut apporter des renseignements précieux sur le potentiel qui détermine le mouvement des ions, leur degré d'interpénétration, l'état des noyaux lorsqu'ils sont en contact... Ce passage de la masse 16 à la masse 40 va donc fournir des informations nouvelles sur le mécanisme de la diffusion élastique entre ions de masse "moyenne". On peut étudier, en particulier, comment s'opère la transition entre la diffusion de Fraunhofer, typique de la diffusion d'ions légers sur les noyaux et la diffraction de Fresnel, trouvée en diffusion d'ions lourds par des noyaux fortement chargés.

Il a été vu au chapitre I que le système de deux noyaux magiques donne certainement lieu à une absorption relativement faible. On a calculé,pour le système $^{40}Ca+^{40}Ca$, comment

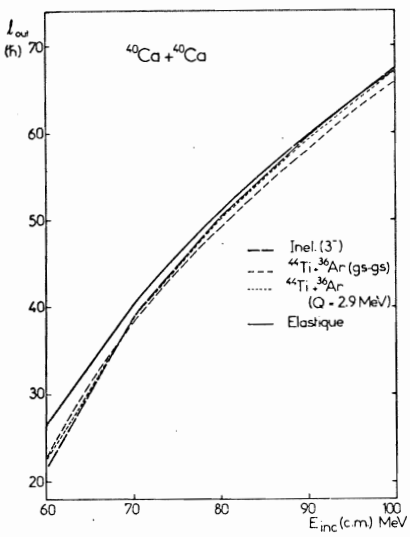

Fig.II.1. Moments angulaires totaux associés à diverses voies de sortie pour des collisions rasantes entre ions ^{40}Ca.

varie le moment angulaire total emmené par différentes voies de sortie avec de l'énergie incidente. C'est ce qu'indique la figure II.1 pour les voies élastique, inélastique (état 3^- du ^{40}Ca à $E^* = 3.74$ MeV), et transferts alpha vers les noyaux d'^{36}Ar et de ^{44}Ti (la transition conduisant aux fondamentaux de ces noyaux ayant $Q = -1.92$ MeV). On note à quel point ces courbes sont proches les unes des autres. Il faut en outre tenir compte de la distribution des moments angulaires autour de ces courbes. La figure II.1 montre donc d'emblée que le système $^{40}Ca+^{40}Ca$ est moins favorable à l'observation d'une structure -ou plutôt, pourrait bien être moins transparent pour les ondes superficielles- que le système $^{16}O+^{16}O$. Toutefois, si on traçait les figures correspondantes pour des systèmes voisins de ce dernier (comme $^{16}O+^{15}N$, $^{16}O+^{18}O$...) on pourrait prédire des situations aussi défavorables, et pourtant une structure large a été observée.

On voit que l'expérience avait à répondre à bon nombre de questions.

2. Accélération d'ions Ca.

Ces expériences ont pu être effectuées essentiellement grâce aux possibilités expérimentales existant au laboratoire. Les deux accélérateurs du laboratoire ont été utilisés : le CEV-Alice et le tandem M.P. On pouvait prévoir que ce dernier fournirait des ions d'énergie allant de 100 à environ 170 MeV, tandis que le système Alice le ferait sur un domaine allant de 175 à 400 MeV. Sur ce dernier les ions Ca sont couramment accélérés. La source d'ions utilisée est du type P.I.G. Une vapeur de Ca naturel provenant d'un four participe au plasma initié par un gaz-support (CO_2 ou Xe). On obtient des intensités comprises entre 50 et 100 µA à l'entrée de l'accélérateur linéaire. Environ 1/10 de cette intensité va être injectée dans le cyclotron. Après stripping, les ions accélérés ont une charge allant de 10^+ à 13^+.

Sur le tandem M.P., l'accélération d'ions ^{40}Ca à ces énergies était réalisée pour la première fois. C'était aussi la première fois que des courants non négligeables étaient obtenus à partir d'une source d'ions Ca négatifs. La source utilisée avec le plus de succès est une adaptation [Du 74] de la source Penning. Il y a production d'ions négatifs par pulvérisation du matériau de la cathode, la décharge étant réalisée dans un mélange de 90% d'H_2 et 10% d'Ar. A l'entrée du tandem, on injecte environ 100 nA. On obtient sur la cible environ 50 nA de Ca de charge 10^+.

3. Expérience.

L'expérience est décrite dans la référence [Do 77b] reproduite ci-après. Un compte-rendu préliminaire de cette expérience avait été donné dans la référence [Do 75b].

ELASTIC SCATTERING OF ^{40}Ca BY ^{40}Ca

H.DOUBRE, J.C.JACMART, E.PLAGNOL, N.POFFE, M.RIOU and J.C.ROYNETTE

Institut de Physique Nucléaire, BP n°1, 91406 Orsay, FRANCE

Elastic scattering of ^{40}Ca by ^{40}Ca

H. Doubre, J. C. Jacmart, E. Plagnol,* N. Poffé, M. Riou, and J. C. Roynette
Institut de Physique Nucléaire, BP No. 1, 91406 Orsay, France
(Received 19 July 1976)

Angular distributions for the elastic scattering of ^{40}Ca by ^{40}Ca at $E_{c.m.}$ = 64.8, 71.8, 88, 93, 112.5, and 120 MeV and excitation functions at 60°, 70°, and 90° (c.m.) over the c.m. energy range 55–120 MeV have been measured. Strong-absorption-model and optical-model analyses are presented. The predictions of several theoretical interaction potentials are compared with the data. The absence of structure in the excitation functions is studied and explained by the large mass and charge of the colliding nuclei.

[NUCLEAR REACTIONS ^{40}Ca(^{40}Ca, ^{40}Ca), $55 \leq E_{c.m.} \leq 120$ MeV; measured $\sigma(\theta, E)$; parametrized S-matrix and optical-model analyses; semiquantal interpretation of excitation functions.]

I. INTRODUCTION

With the observation of a new strongly damped reaction mechanism between heavy ions, it has become crucial to have good estimates of the total reaction cross sections. These are usually obtained from elastic scattering data, since optical-model transmission coefficients give rather unambiguous predictions. Thus, elastic scattering measurements have found a new motivation, since a knowledge of the distribution of the incident flux between the reaction channels is of fundamental importance in heavy-ion studies. Data have been recently published[1] on elastic scattering of very heavy projectiles from heavy targets. These measurements also give primary information on the interaction potential between the nuclei at large distances.

In a program to study the interaction between ^{40}Ca nuclei, data have been collected on the elastic scattering of ^{40}Ca by ^{40}Ca. The theoretical analysis of a systematic experimental investigation of the channels fed by this system might be simplified by the closed-shell nature of this nucleus and the symmetry of the entrance channel. Recent papers have proposed a microscopic description of the dynamics of collisions between identical nuclei.[2] In our case, static and dynamic deformation effects are expected to play a less important role than with any other nucleus, and the large angular momenta involved in the scattering allow for recently developed semiclassical treatments. The ^{40}Ca + ^{40}Ca system is also a challenging test for the calculation of interaction potentials. Moreover, evidence[3] for deep-inelastic transfers at high incident energy in the ^{40}Ca + ^{40}Ca system has been presented and it would be interesting to observe the coupling of these channels to the elastic one. Finally, the experimental difficulties in heavy-ion elastic scattering are somewhat alleviated by the high (>3 MeV) energy of excited states in ^{40}Ca. This nucleus is the heaviest one for which such a situation occurs.

Aside from several angular distributions, excitation functions of the ^{40}Ca + ^{40}Ca elastic scattering are also presented. Such measurements were prompted by the observation[4] of a dramatic structure in the ^{16}O + ^{16}O elastic scattering excitation functions. The analysis[5] which was given of these data and the criteria[6] proposed for the observation of any structure in heavy-ion elastic scattering indicate that the ^{40}Ca + ^{40}Ca system could offer some analogies with the ^{16}O + ^{16}O one: (i) The identity of the incident particles reduces the number of involved partial waves which contribute at a given energy, and (ii) due to the negative Q values of all reaction channels, only the elastic one is able to carry away the initial angular momentum. From these facts, a structure can be expected in the elastic scattering excitation functions. This would be an evidence for a transparent potential where individual grazing partial waves manifest themselves. Up to now, such a transparency was only reported for nuclei close to ^{16}O. For a heavier system, as ^{28}Si + ^{28}Si, no structure was observed.[7] As far as the criteria reported above might be applied to the ^{40}Ca + ^{40}Ca system, this could be the heaviest one where a "quasi-molecular" behavior or, at least, any transparency in the interaction potential could be observed. The present study of the ^{40}Ca + ^{40}Ca elastic scattering extends from 55 to 120 MeV(c.m.); this could be a sufficient range to observe any peculiar behavior as a function of energy. In Sec. VI some implications of the nonobservation of any structure in ^{40}Ca + ^{40}Ca are considered.

Transfer data have also been collected on the same energy range and are to be published.

II. EXPERIMENTAL PROCEDURE

With heavy ions, the requirement of an unambiguous identification of elastic events leads to experimental difficulties. Two of them seem quite crucial when the masses of the colliding nuclei are large. Depending on the incident energy and on specific Q values, the discrimination between elastic scattering and few-nucleon transfer products can become very critical. Furthermore, inelastic scattering strongly excites low-lying states and, at large angles, can be much more likely than elastic scattering. As already mentioned, the $^{40}Ca + ^{40}Ca$ system is the heaviest one in which their separation is possible, and special attention was given to achieve this aim experimentally.

The Institut de Physique Nucléaire, Orsay, has the facilities to accelerate calcium ions over a very large range of incident energies: (i) Below 170 MeV (lab) with the upgraded M.P. tandem: The intrinsic beam qualities are well within the experimental requirements of such a study. The negative ion source is of the Penning type, and has been described elsewhere.[8] (ii) Above 175 MeV (lab) with the Alice accelerator: Although the qualities of the beam are not as good, the larger intensity permits extension of the tandem results over a large energy range.

With both accelerators, a similar experimental technique (Fig. 1) was used. The apparatus consisted of two solid-state detectors, in which the energies E_1 and E_2 of two kinematically associated particles were measured. Together with a time-difference signal between the detectors, the energy signals were recorded on tape for off-line analysis. Using large-area detectors (50×10 mm^2), positioned 15 cm from the target, the effective solid angle was about 3 msr, whereas the horizontal opening could be kept as small as 0.75°. These values were determined by the use of a specially shaped (elliptic) slit in front of one of the detectors, the second one having a sufficiently large aperture to ensure the maximum coincidence efficiency.

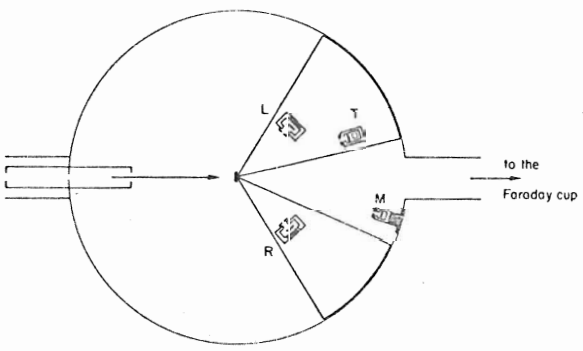

FIG. 1. The scattering chamber and arrangement of the detectors. L and R are the associated detectors, T the ΔE-E telescope, and M a monitor.

Such a method was thought to be more convenient and efficient for the following reasons: (i) The large solid angle allows for the measurement of the small cross sections which are observed around 90° (c.m.). (ii) The kinematical coincidence method is well fitted to a case where the measured energies in each detector are close to each other. (iii) Due to the identity of the incident particles, large oscillations are observed around 90° and the small horizontal opening permits a rather precise determination of the angular distribution. This is crucial in the measurement of the 90° excitation function, where the observation angle has to be known with good accuracy. To achieve this accuracy, the angular distribution was measured over a small angular range at each incident energy. Since the Q values for all reaction channels are negative, the identification of the elastic channel will depend upon the energy resolution of each detector. The resolution of the detectors is found to be 1.1 MeV for the elastic scattering of Ca on Au. This is largely worse than obtained with lighter projectiles, even ^{32}S, and probably due to the larger density of charges created by heavier ions. Two reaction channels might not be separated from the elastic one: (i) the four-particle transfer $^{40}Ca(^{40}Ca, ^{36}Ar_{g.s.})^{44}Ti_{g.s.}$ with a Q value of -1.92 MeV (however, it can be eliminated by analyzing the individual energies in each detector); (ii) the inelastic scattering $^{40}Ca(^{40}Ca, ^{40}Ca)^{40}Ca^*$ to the 3^- state at 3.74 MeV excitation energy in ^{40}Ca.

For the tandem experiment, the target thickness gives the largest contribution to the (E_1+E_2) spectrum width. The overall resolution was found to be about 2.5 MeV. Therefore it can be asserted that, at incident energies smaller than 83 MeV (c.m.) the measured elastic cross sections contain no contribution from any nonelastic channel. At Alice, the overall resolution read on the (E_1+E_2) spectrum is 4 MeV, because of the target thickness and, especially, the beam energy dispersion, and the inelastic transition can give some contamination to the elastic cross sections. At most, the actual elastic cross sections can only be smaller than the values presented. This will be of importance in the discussion on the shape of the excitation functions.

The detectors looked at a 60 μg/cm^2 natural calcium target, evaporated on a 10 μg/cm^2 carbon backing and a gold layer of about 3 μg/cm^2. Due to this target thickness, the uncertainty on the c.m. energy at which the reaction occurs is less than 0.5 MeV though the (E_1+E_2) spectrum resolu-

tion is 2.5 MeV. This 0.5 MeV value was used as the energy step in the measurement of the excitation functions.

At small angles, a ΔE-E telescope was used (where ΔE was obtained from a solid-state detector, the thickness of which was either 8.6 μm or 13.6 μm). This telescope gives the elastic cross section values at small angles ($\theta_{lab} \lesssim 30°$) but it is also convenient to evaluate the population of the different reaction channels at a close-to-grazing angle. The identification was always good enough to separate adjacent elements for $Z \lesssim 25$.

When measuring the elastic scattering over a large range of angles and incident energies, the determination of absolute cross sections is a delicate problem. At very low energies (close to the Coulomb barrier) cross sections oscillate very rapidly, so that accuracy is difficult to obtain. The consistency over the whole set of data was checked, using the 60° and the 70° Mott cross sections at low energy, and the forward cross sections at higher energy where angular distributions do not oscillate. The absolute cross sections over the entire energy range are given within 30%.

III. ANGULAR DISTRIBUTIONS

Five angular distributions are presented in Fig. 2. Two of them are measured with the tandem accelerator ($E_{c.m.} = 64.8$ and 71.8 MeV), two others with the accelerator Alice ($E_{c.m.} = 88$ and 93 MeV). The fifth one is taken from the data of Henning *et al.*[9] at $E_{c.m.} = 55.4$ MeV. At this energy, Coulomb phenomena are still so important that the interference pattern due to the identity of the colliding particles covers the whole angular range. At higher energies, this interference only shows up within a region of about 10° around 90° c.m.

Such a limitation suggests another presentation of the data. As the identity of the particles is found to play only a minor role in the shape of the angular distributions, it appears more meaningful to plot the ratios of the experimental cross sections to the Rutherford cross sections (i.e., to the *non*symmetrized Coulomb cross sections). These ratios are reported in Fig. 3 for six bombarding energies. Except for the lowest incident energy, these curves follow the usual Fresnel pattern.[10]

It has been noticed[11] that the observed large enhancement over the Rutherford cross section value could give information on the influence of the real nuclear potential on the scattering trajectories. Frahn and Venter[12] have shown that the amplitude of this rise increases with the real nuclear phase shift, from the sharp cutoff value:

$$1 + \frac{2}{\pi\sqrt{3}}\left[1 - \left(\frac{3\pi}{4\eta}\right)^{1/2}\right]^{3/2} = 1.23$$

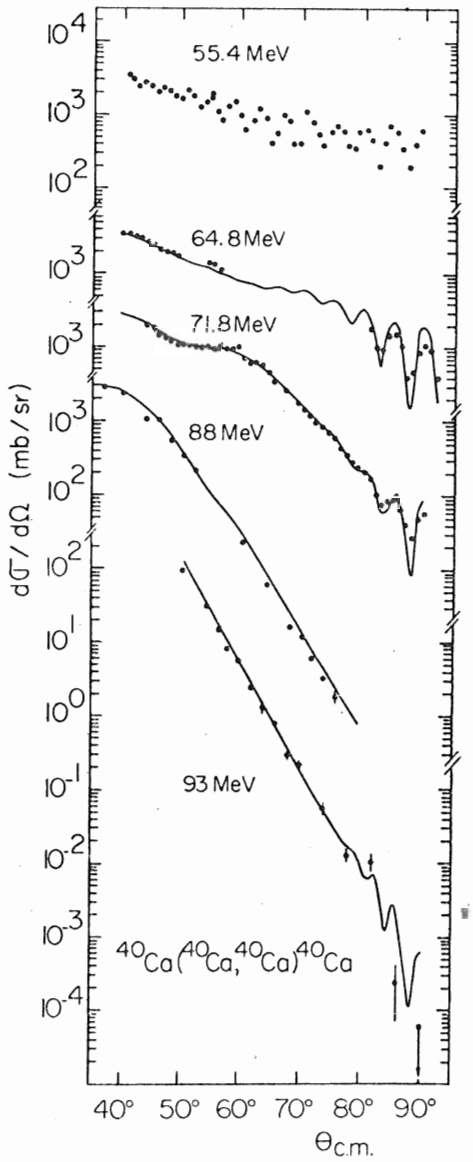

FIG. 2. Angular distributions for the elastic scattering of ^{40}Ca from ^{40}Ca. The solid lines are optical-model predictions. The angular distribution at 55.45 MeV is from Ref. 9.

for $E_{c.m.} = 71.8$ MeV. A smooth cutoff in angular momentum space counteracts the effect of the nuclear attraction. As the data show that this rise is close to 1.23, the "quarter-point recipe"[13] (i.e., the sharp cutoff approximation) can be used to obtain a rough estimate of the distance where nuclear interaction begins to occur. The Fresnel interaction radius and the reaction cross sections as a function of energy are given in Table I, as deduced from the sharp cutoff model from five angular distributions of the Fig. 3. The "quarter-point angular momentum" is obtained from the equation

55

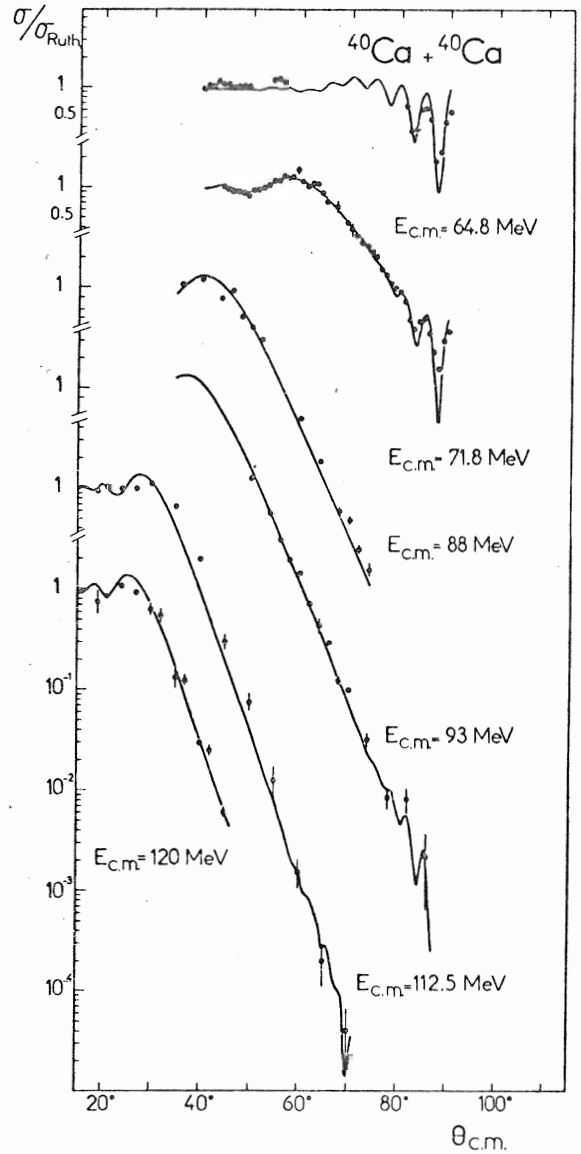

FIG. 3. Ratios of the experimental elastic scattering cross section to the nonsymmetrized Rutherford cross section, as a function of the scattering angle. The solid lines are optical-model predictions.

$$L_{1/4} = \eta \cot(\theta_{1/4}/2) ,$$

where η is the Sommerfeld parameter, and the reaction cross section is given by

$$\sigma_R^{\text{sco}} = \pi\lambda^2 (L_{1/4}+1)^2 .$$

These values will be compared in Sec. V with those predicted by an optical-model analysis.

The Fresnel interaction radius can be reliably taken as:

$$R = 10.63 \pm 0.13 \text{ fm}; \quad r_0 = 1.55 \pm 02 \text{ fm} .$$

This can be compared with the prediction of

TABLE I. Parameters of the ^{40}Ca + ^{40}Ca elastic scattering. Grazing angular momenta, strong interaction radii, and reaction cross sections as deduced from the sharp cutoff model.

E (MeV)	k (fm^{-1})	η	$L_{1/4}$	R (fm)	σ_R^{sco} (mb)
71.8	8.29	33.25	44.9	10.75	960
88	9.18	30.04	60.9	10.67	1430
93	9.43	29.22	65.6	10.72	1570
112.5	10.4	26.57	77.2	10.42	1780
120	10.7	25.73	84.2	10.61	1980

Huizenga[14] which is

$$R = (2C + 3.2) = 10.47 \text{ fm}; \quad r_0 = 1.53 \text{ fm} ,$$

where C is the half-density matter radius.[15] Since this prediction results from a compilation over a large number of systems, one sees that the ^{40}Ca + ^{40}Ca system does not differ from others from the above viewpoint. Such an interaction distance means that nuclear interactions are at play as soon as one nucleus overlaps the other by about 5% of the central density.

It is more difficult, without referring to an optical-model analysis (as it will be done in Sec. VI), to derive additional information about the absorption in the ^{40}Ca + ^{40}Ca system from the shapes of the angular distribution. Fraunhofer oscillations, if any were to be present, would show up in the backward hemisphere, which in this case cannot be observed because of the symmetry of the entrance channel. On the contrary, the oscillations around 90° in the angular distributions come from that symmetry. No conclusion can be safely drawn from the fact that they are only present over a small angular region, as explained below.

A small reduction of the absorption has two consequences: (i) an increase of the critical angle value and (ii) an enhancement of the forward angle oscillations. Quantitatively, the angular shift is very small, so that the resulting effect is a steeper slope for the angular distribution and thus a narrower angular range for the oscillations. This results in the paradoxical situation where smaller cross sections around 90° are due to a smaller absorption. Thus, the range over which the interference oscillations are present cannot be a very significant test of the importance of the absorption.

IV. EXCITATION FUNCTIONS

In Fig. 4 are presented three excitation functions, measured at 60°, 70°, and 90° (c.m.) from 55 MeV (close to the Coulomb barrier) to 120 MeV (c.m.) incident energy. The parts of these excitation functions corresponding to energies smaller than 83 MeV were obtained at the tandem, and there-

fore, as pointed out in Sec. II, are free of inelastic scattering contaminations. At higher energies, such a contamination cannot be ruled out, due to a poorer resolution, in spite of a careful energy calibration. It results from such a situation that the slopes of these excitation functions, in their high-energy part, could only be steeper. It is clear that these excitation functions, in the reasonably large energy range studied here do not exhibit any gross structure. Had the energy resolution been too bad to observe a structure, a break in the excitation function slopes could have been the energy-average result of some transparency in the interaction potential. These data, up to 120 MeV (c.m.) incident energy, and down to 1 μb/sr cross sections do not indicate such a feature. It can also be noticed that, for the low-energy part of these curves, the 0.5 MeV energy step is thought to be small enough for disclosing any irregularity in the excitation functions. Such irregularities are not found.

To conclude, from the shapes of the excitation functions and angular distributions it appears that, in contradiction to what could have been expected, the elastic scattering behavior of the system studied does not depart from the most commonly used strong-absorption model. This point will be strengthened more quantitatively in the following sections.

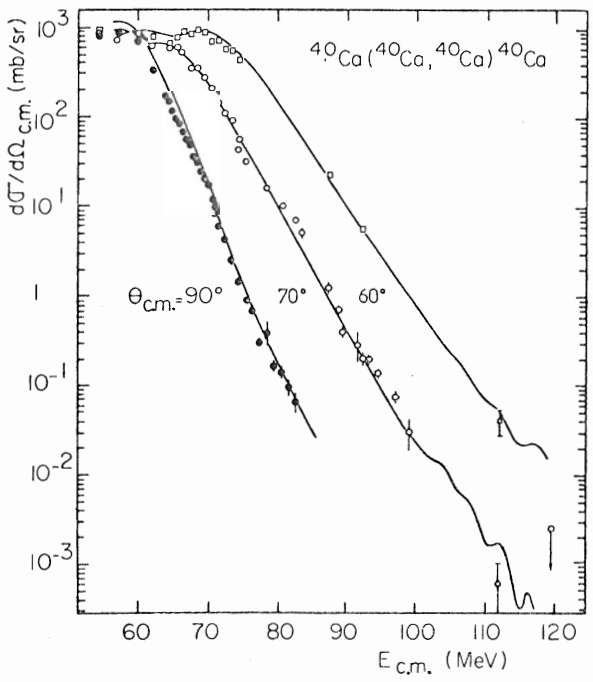

FIG. 4. Excitation functions for the elastic scattering of ^{40}Ca from ^{40}Ca at 60°, 70°, and 90° (c.m.). The solid lines are optical-model predictions.

V. OPTICAL-MODEL ANALYSIS

For such an analysis, a set of data collected over a very large energy range composes a very severe constraint, as first pointed out in the analysis of the ^{16}O + ^{16}O data.[4] Several searches were carried out, from different initial parameter values. By no means should the present result be taken as unique, but it represents an average result which fits the data fairly well. With a four-parameter optical-model potential

$$V_{\text{opt}}(r) = \frac{V + iW}{1 + \exp(r - R)/a} + V_{\text{Coul}}(r) ,$$

where

$$R = 2r_0(40)^{1/3} ,$$

the following parameter values have been obtained:

$$\begin{aligned} V &= 35 \text{ MeV} , \\ W &= 12.13 \text{ MeV} , \\ r_0 &= r_c = 1.35 \text{ fm} , \\ a &= 0.43 \text{ fm} . \end{aligned} \tag{1}$$

The predictions of this optical-model potential are given by the curves of the Figs. 2–4.

The Igo ambiguity was also observed when checking that all the real potential having the same slope and the same depth at the strong interaction radius (as determined in Sec. III), essentially give the same results. This indicates that only the tail region of the potential is of importance. As can also be deduced from the geometry of the real and imaginary potentials, the W/V ratio is a constant equal to 0.4 which is a smaller value than was formerly proposed.[16] It should be noticed that it has been possible to fit the data without any energy or angular momentum dependence of the imaginary potential. Moreover, the reflection coefficients have the typical behavior (i.e., do not present any "kink") of strong absorption for grazing partial waves. This is illustrated in Fig. 5.

From the computed transmission coefficients, one can compare the predicted total reaction cross section with the one deduced from the strong-absorption model. Such a comparison, as reported in Table II, shows how good the predictions of the latter are; the differences never exceed 5%.

The comparison between the $L_{1/4}$ value as given by the strong-absorption model, and the value L_{opt} for which the reflection coefficient is equal to 0.5, also gives agreement within 5%.

From the classical expression

$$L(L+1) = 2\mu R^2(E - E_B)/\hbar^2 ,$$

where L can be taken as the quantity L_{opt} defined above, the six energies for which angular distri-

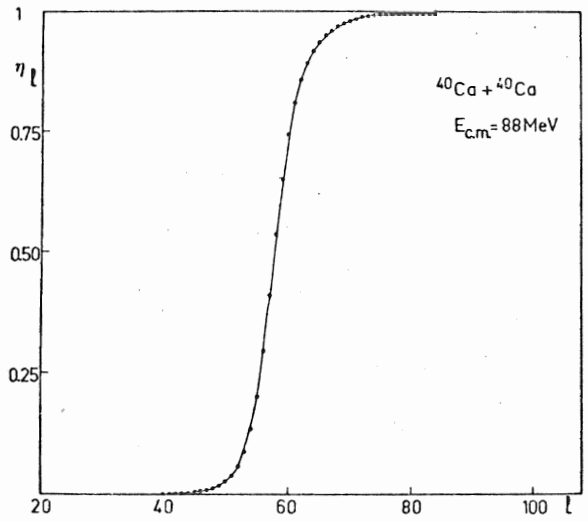

FIG. 5. Plot of the reflection coefficient $\eta(l) = |S(l)|$ as a function of l at 88 MeV (c.m.).

butions were obtained allow for a determination of R and E_B, or rather a check of the consistency of our results. The quantity $L_{\rm opt}(L_{\rm opt}+1)$ is found to be a linear function of E, giving the values

$$r_0 = 1.46 \text{ fm} ,$$

$$E_B = 52.69 \text{ MeV} .$$

In Table II are also reported the values of the quantities Δ and d, defined as follows: Δ represents the width of the transition region on which the reflection coefficients vary from 0 to 1, when fitted by the expression

$$\eta(l) = \{1 + \exp[(L_{\rm opt} - l)/\Delta]\}^{-1} .$$

Classical arguments have been used[17] to show that the energy dependence of Δ could be reproduced by

$$\Delta = kd\left(1 - \frac{\eta}{kR}\right)\Big/\left(1 - \frac{2\eta}{kR}\right)^{1/2} .$$

Here, the value of d, as deduced from this expression, and using the optical-model reflection coefficients, is approximately independent of energy and equal to 0.21 fm. We shall return to this point in Sec. VI.

Several theoretical attempts have been made to estimate the real part of the $^{40}Ca + ^{40}Ca$ interaction potential. Figure 6 shows the predictions of these potentials. First, a folded potential with an effective interaction

$$V_{\rm eff}(r) = \left(6315\,\frac{e^{-4r}}{4r} - 1961\,\frac{e^{-2.5r}}{2.5r}\right) \text{ MeV}$$

was proposed by Satchler.[18] The imaginary part of the optical potential is taken to have the same

TABLE II. Comparison between optical-model predictions and sharp cutoff theory. Δ is the width of the reflection coefficient function in the angular momentum space, and d is the associated thickness at the surface of the nucleus (see text).

E (MeV)	$L_{1/4}$	$L_{\rm opt}$	$\sigma_R^{\rm sco}$ (mb)	$\sigma_R^{\rm OM}$ (mb)	$\Delta_{\rm QM}$	d (fm)
64.8		32.9		669	2.67	0.20
71.8	44.9	42.1	960	939	2.42	0.22
88	60.9	57.7	1430	1390	2.24	0.21
93	65.6	61.7	1570	1495	2.20	0.21
112.5	77.2	75	1780	1808	2.24	0.20
120	84.2	79.4	1980	1900	2.34	0.21

geometry as the real one:

$$V_{\rm opt}(r) = (1 + 0.7i)\,V_{\rm fold}(r) .$$

The satisfactory fit at low energy becomes worse with increasing energy.

The data are also compared with the predictions of two potentials, calculated from the "sudden approximation": Ngô *et al.*[19] have used the Brueckner energy density formalism, while Stancu and Brink[20] derive the interaction potential from the energy functional of the Skyrme interaction. These two potentials give rather similar results. On the other hand, following a procedure already used by Huizenga,[14] and deduced from the liquid-drop theory, the depth and diffuseness of the potential can be determined from the relations:

$$\left(\frac{dV_N}{dr}\right)_{r=2C} = \frac{V_0}{4a} = 2\gamma C$$

with

$$\gamma = 0.9517 \text{ MeV fm}^{-2} .$$

In that case the nuclear potential is taken to have the right value at the strong interaction radius, but the slope differs from the empirically determined one. For these last three potentials, the imaginary part parameters are those given in Eqs. (1).

In Fig. 7 the radial dependence of all of these potentials has been compared. One sees that the theoretical potentials seem to be systematically more shallow than the empirical one at the strong interaction radius.

From these interaction potentials, it has been shown[21] that one can obtain predictions for fusion cross sections. It is remarkable that all these potentials give about the same predictions. These predictions, reported in Fig. 8 have been obtained from the model of Glas and Mosel.[22] One can see that a determination of the nuclear potential depth at the "critical radius,"[21] here taken as

$$R_{\rm crit} = 2(40)^{1/3} \text{ fm}$$

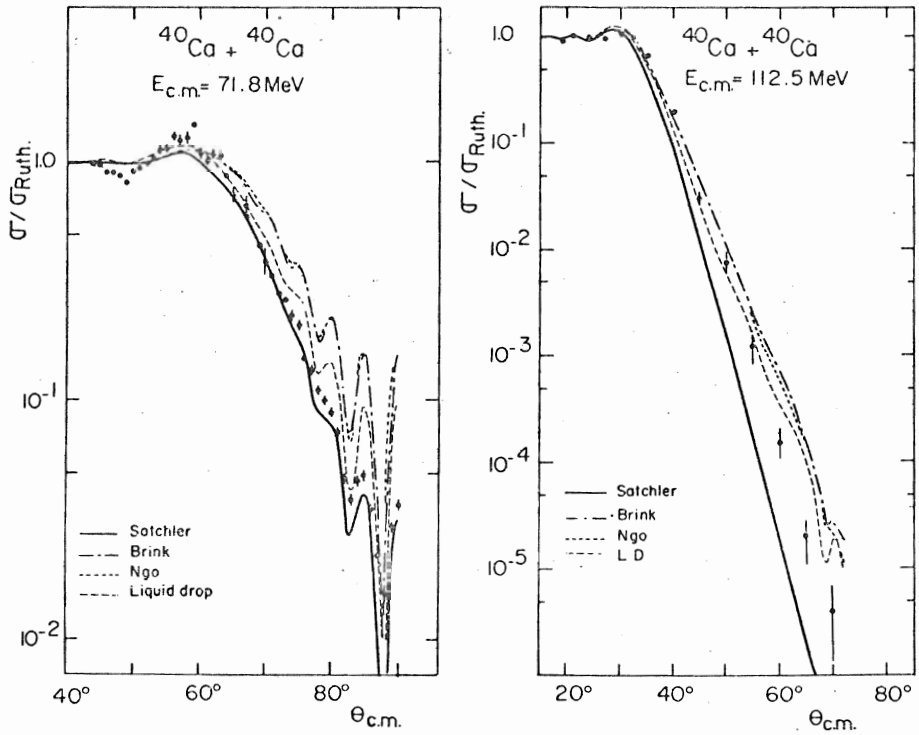

FIG. 6. A comparison between the predictions of several interaction potentials at two incident energies.

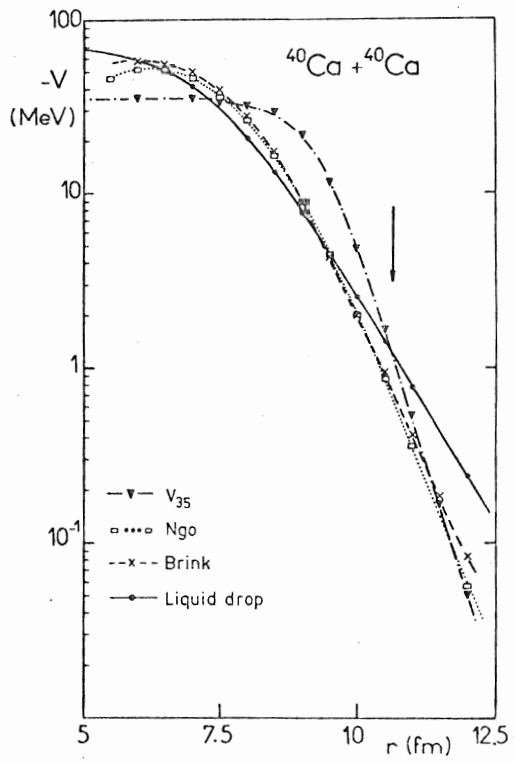

FIG. 7. Comparison of the radial dependence of the real potentials used in optical-model fits. The arrow indicates the strong interaction radius.

could be possible from fusion cross sections, as the predictions from two interaction potentials relevant to the Igo ambiguity but with very different depths are extremely different at high energy.

Thus, a rather good description of the interaction potential for a large separation distance between the ^{40}Ca ions has been obtained. For smaller distances, fusion cross section measurements could help to solve the usual ambiguities.

VI. DISCUSSION OF THE RESULTS

In this section, we wish to compare the $^{40}Ca + ^{40}Ca$ elastic scattering with that of other heavy-ion systems. It was shown in the preceding sections that the $^{40}Ca + ^{40}Ca$ elastic scattering does not seem to differ from elastic scattering of neighboring systems. However, one of the motivations of this study was the similarity between the structure of the ^{16}O and ^{40}Ca nuclei. In a comparison between the experimental data, it can immediately be seen that the $^{40}Ca + ^{40}Ca$ angular distributions and excitation functions exhibit the Fresnel pattern, while the $^{16}O + ^{16}O$ scattering shows a behavior close to Fraunhofer diffraction.

For nuclei of mass close to 16, the excitation functions are characterized by the presence of comparable gross structure. For $^{28}Si + ^{28}Si$ or $^{40}Ca + ^{40}Ca$, the elastic scattering excitation func-

59

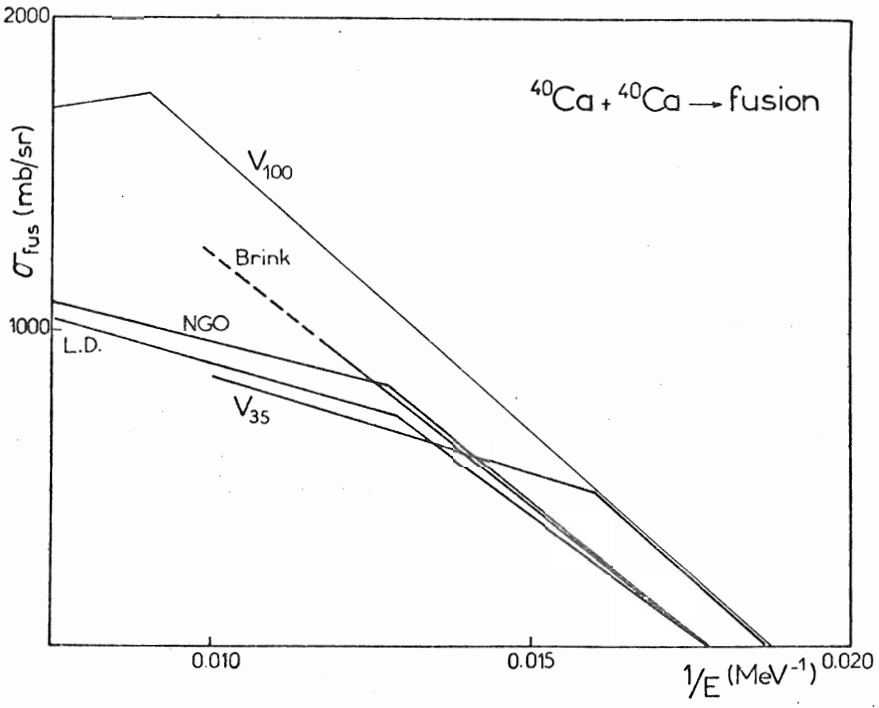

FIG. 8. Glas and Mosel predictions of the fusion cross sections as a function of energy, for several interaction potentials. V_{35} is the potential used in the optical-model analysis. V_{100} and V_{35} satisfy the same Igo criterion $V \exp(R/a) = \text{const}$.

tions are monotonically decreasing. Thus, it appears that maybe the consequence of the larger mass and charge has to be analyzed when comparing data.

At this point, it may be worthwhile to recall the interpretation of the structure observed in excitation functions for masses close to 16. This structure is considered to be evidence for some transparency of the interaction potential for the grazing partial waves. At a given energy, only a single partial wave gives the leading contribution to the scattering amplitude, the others being either absorbed or reflected, and therefore the observed structure appears to be due to the succession of the leading partial waves when the incident energy is increased.[23] As shown by Siemssen,[24] the degree of transparency of the effective potential can be read on the distribution of the reflection coefficients as a function of the angular momentum. In a strong-absorption case, this distribution goes smoothly from 0 to 1, and a rather large number of partial waves give a limited contribution to the elastic scattering amplitude. On the contrary, in the $^{16}O + ^{16}O$ and other weak-absorption cases, this transition occurs within a narrow range of angular momenta.

The structures have been reproduced by optical-model calculations either by reducing[23] the range of the imaginary well as compared to the real one, or through an explicit l dependence of the imaginary well depth.[5] The introduction of this l cutoff in the absorption mechanism leads to enumeration of the exit channels which are able to carry out the entrance angular momentum. Transparency is then observed when such channels do not exist at the incident energy considered. Comparing the $^{16}O + ^{16}O$ and $^{18}O + ^{18}O$ data, Shaw, Vandenbosch, and Mehta[6] proposed that only the direct channels are to be taken into account in such an enumeration. Thus, a structure can be expected when no direct channel is able to carry away the incident angular momentum. This should be the case for $^{40}Ca + ^{40}Ca$, on the basis of Q values for direct transfers.

However, in spite of its large experimental support, such an analysis presents some shortcomings. For instance, as one is interested in the role of the energy in the observation of a gross structure, one could predict from the above criterion that the structure observed in $^{16}O + ^{16}O$ elastic scattering should disappear with increasing energy for $E_{c.m.} \gtrsim 25$ MeV, since several direct channels can then carry away the entrance angular momentum. This is at variance with experimental data,[25] at least if the structure observed in the excitation function is considered to be relevant to the same physical phenomenon. On the other hand, such a structure was only observed for nuclei of

mass close to 16, and in the $^{18}O+^{18}O$ case used as an example of strong absorption by Shaw *et al.*,[6] some bumps still show up in the excitation function. This is not even the case for $^{40}Ca+^{40}Ca$. Finally, as mentioned in Sec. II, the importance of transfer reactions has been estimated. Their cross sections are found to be extremely low up to $E_{c.m.}=75$ MeV, and then slowly increasing with energy. Thus, it has been verified experimentally that the conditions necessary for a structure are fulfilled.

A major difference between the ^{16}O and the ^{40}Ca systems is the much stronger Coulomb repulsion in the latter and it will be attempted to show how this can explain the gradual disappearance of the gross structure going from ^{16}O to ^{40}Ca.

To obtain further insight into this problem, it is convenient to split the scattering amplitude into two terms, using the asymptotic expansion of the Legendre polynomials

$$P_l(\cos\theta)\simeq\left(\frac{2}{\pi(l+\frac{1}{2})\sin\theta}\right)^{1/2}\cos[(l+\tfrac{1}{2})\theta-\tfrac{1}{4}\pi]$$

valid for $l\gg1$ and $\theta\gg l^{-1}$.

Assuming a smooth variation of both the reflection coefficients $\eta(l)$ and the nuclear phase shifts $\delta^N(l)$ over a range Δ of l values around a central value L, we can use the semiclassical approximation of the scattering amplitude:

$$f(\theta)=-\frac{i}{k}\left(\frac{1}{2\pi\sin\theta}\right)^{1/2}\int_0^\infty d\lambda\,\lambda^{1/2}\eta(\lambda)e^{2i\delta(\lambda)}[e^{i(\lambda\theta-\pi/4)}+e^{-i(\lambda\theta-\pi/4)}]$$
$$=f_+(\theta)+f_-(\theta)$$

with $\lambda=l+0.5$.

For large angles (i.e., beyond a "critical" value θ_c) and under the condition that the deflection function has no rainbow, Frahn[26] obtains the following closed expression:

$$f(\theta)=f_-(\theta)+f_+(\theta)=\frac{1}{k}\left(\frac{1}{2\pi\sin\theta}\right)^{1/2}e^{2i\delta(\Lambda)}\{e^{-i(\Lambda\theta-\pi/4)}A(\theta-\theta_c)F[\Delta(\theta-\theta_c)]+e^{i(\Lambda\theta-\pi/4)}F[\Delta(\theta+\theta_c)]/(\theta+\theta_c)\}\ , \quad (2)$$

where $\Lambda=L+0.5$.

To examine the outcome of such a separation, we have to use an analytic approximation for the scattering S matrix. Following Frahn, we use the McIntyre[27] parametrization:

$$S(\lambda)=\eta(\lambda)e^{2i\delta(\lambda)}\ ,$$
$$\eta(\lambda)=\left[1+\exp\left(\frac{\Lambda-\lambda}{\Delta}\right)\right]^{-1}\ ,$$
$$\delta(\lambda)=\sigma(\lambda)+\delta_0\left[1+\exp\left(\frac{\lambda-\Lambda'}{\Delta'}\right)\right]^{-1}\ .$$

It is understood that this parametrization does not fit exactly every feature of the optical-model S matrix, especially as far as the real nuclear phase shifts are concerned. However, it is considered as sufficiently reliable to reproduce the main characteristics of the cross section. Then

$$F[\Delta x]\equiv\int_{-\infty}^{+\infty}d\lambda\,\frac{d}{d\lambda}\,\eta(\lambda)e^{-i(\lambda-\Lambda)x}=\frac{\pi\Delta x}{\sinh(\pi\Delta x)}\ .$$

It should be noted that the expression of $f_+(\theta)$ does not depend upon the condition of no rainbow in the deflection function, but only on the linear expansion of the phase about $\lambda=\Lambda$. Thus, whatever the S matrix is, $f_+(\theta)$ can always be calculated, and substracted from the full $f(\theta)$ obtained by the partial wave summation to obtain $f_-(\theta)$.

To further simplify Eq. (2), we assume that

$$A(\theta-\theta_c)\cong-1/(\theta-\theta_c)\ . \quad (3)$$

It can be shown that for "ordinary cases," this approximation is of no consequence.

As we are interested in the energy dependence of $f(\theta)$, one has to assume some variation of the parameters with energy. Frahn has used the following:

$$\Lambda=kR(1-2\eta/kR)^{1/2}\ ,$$
$$\Delta=kd(1-\eta/kR)/(1-2\eta/kR)^{1/2}\ , \quad (4)$$
$$\delta_0=\alpha/k$$

with

$$R=r_0(A^{1/3}{}_1+A^{1/3}{}_2)$$

and Λ' and Δ' introduce two more parameters r_0' and d' through similar relations.

Within this framework, we will examine the elastic scattering of $^{16}O+^{16}O$ and $^{40}Ca+^{40}Ca$.

A. $^{40}Ca+^{40}Ca$

Frahn and Rehm[28] have been able to fit the $^{40}Ca+^{40}Ca$ data presented in this paper, with the following parameter set: $r_0=1.584$ fm, $r_0'=1.438$ fm, $\alpha=154^\circ$ fm^{-1}, $d=0.286$ fm, $d'=0.58$ fm. The quantities r_0 and d can be compared with those de-

61

termined in the optical-model analysis (Sec. V). It can be observed that d is close to one-half of the optical-model diffuseness a [28] and that the phase does not give rise to a rainbow.

With these values, both components $|f_+(\theta)|$ and $|f_-(\theta)|$ are monotonically varying with energy. Over the whole energy range studied, $|f_+|$ is several orders of magnitude less than $|f_-(\theta)|$, and does not give any significant contribution to the cross section. Obviously no interference pattern can be observed. This conclusion is found to be unaffected by reasonable variations of the parameters.

B. $^{16}O + ^{16}O$

For this system, it has not been possible to obtain an accurate fit of the excitation functions. This is attributed to the limitations introduced by the McIntyre parametrization. The structure phenomenon can be reproduced, particularly its periodicity and the location of the maxima, with the following parameter set: $r_0 = 1.45$ fm, $r_0' = 1.438$ fm, $\alpha = 100°\ \text{fm}^{-1}$, $d = 0.06$ fm, $d' = 0.58$ fm. However, the peak-to-valley ratio is poorly accounted for. As in $^{40}Ca + ^{40}Ca$, it is found that $|f_+|$ and $|f_-|$ vary monotonically with angle and with energy. The main difference between the two systems is that in $^{16}O + ^{16}O$, $|f_+|$, although somewhat smaller than $|f_-|$, is sufficiently large to give rise to interference effects. The relative phase between both interfering amplitudes is close to $e^{i(2\Lambda\theta+\pi)}$. Thus one finds that the maxima of the 90° excitation function correspond to odd integer values of Λ. The 60° excitation function should present maxima with a period 1.5 times larger than at 90°. This is precisely observed in Fig. 9, where the predictions of the optical-model potential proposed by Gobbi *et al.*[23] for the $^{16}O + ^{16}O$ elastic scattering excitation functions at 60° and 90°, and the Λ values deduced from the reflection coefficients are reported [as will be said later, the reflection coefficient function $\eta(l)$ is far from following the Fermi function considered above, but the central value should not be doubtful]. The fact that this behavior is satisfactorily reproduced is considered a good test of the reliability of the approximations introduced above.

C. Influence of the mass on the occurrence of a gross structure

The obvious conclusion of the study of these two systems is that the gross structure seen in the elastic scattering excitation function for light nuclei finds its origin in the interference between $f_+(\theta)$ and $f_-(\theta)$. It is therefore crucial to study the ratio

$$R = \left|\frac{f_+}{f_-}\right|$$

of these two quantities, as the value of this ratio will determine the strength of the interference effect. Within the McIntyre parametrization this ratio is given by

$$R \simeq \frac{\sinh[\pi\Delta(\theta-\theta_c)]}{\sinh[\pi\Delta(\theta+\theta_c)]} \simeq e^{-2\pi\Delta\theta_c} . \tag{5}$$

At the same reduced energy

$$h = \frac{E}{B_C} ,$$

where B_C is the Coulomb barrier and θ_c is the same. Thus one finds that R exponentially depends

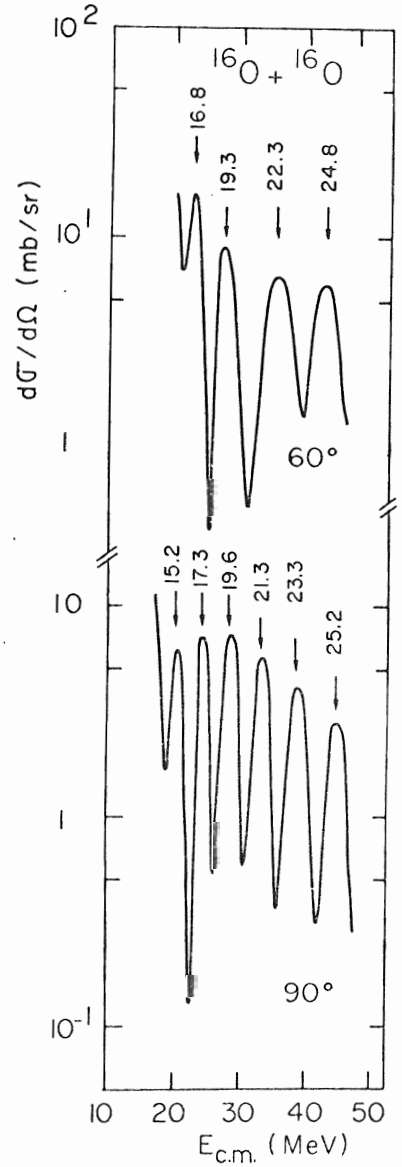

FIG. 9. $^{16}O + ^{16}O$ excitation functions at 60° and 90° as predicted by the Gobbi potential. The numbers indicated at the maxima of the cross section denote the values of Λ for the corresponding energies.

on Δ. This quantity as given by Eqs. (4) can be written for $A = 2Z$ nuclei:

$$\Delta = 3.3\times10^{-2}\frac{d(2h-1)}{[r_0(h-1)]^{1/2}}A^{4/3}. \quad (6)$$

In Fig. 10 the ratio R is plotted as a function of h, for the three systems ^{16}O + ^{16}O, ^{28}Si + ^{28}Si, and ^{40}Ca + ^{40}Ca. The curves have been obtained using the same set of parameters, to point out the mass dependence. The values of d and r_0 which have been used are mean values of those fitting the ^{16}O + ^{16}O and the ^{40}Ca + ^{40}Ca excitation functions.

Equations (5) and (6) show the exponential dependence of R on the mass (or charge) of the colliding nuclei. This explains the differences in behavior observed in Fig. 10. Within the framework of this parametrization, it is immediately clear that for light nuclei, a large interference can be expected, so that structure in the cross sections is easily observed, even at low energies, whereas for heavier mass systems a similar phenomenon can only be obtained at very high energy. The above discussion was based on the dependence of Δ on A; however, Eq. (6) shows that Δ varies linearly with d, which is closely related to the absorptive part of the interaction. This explains the differences between ^{16}O + ^{16}O and the neighboring systems.[6]

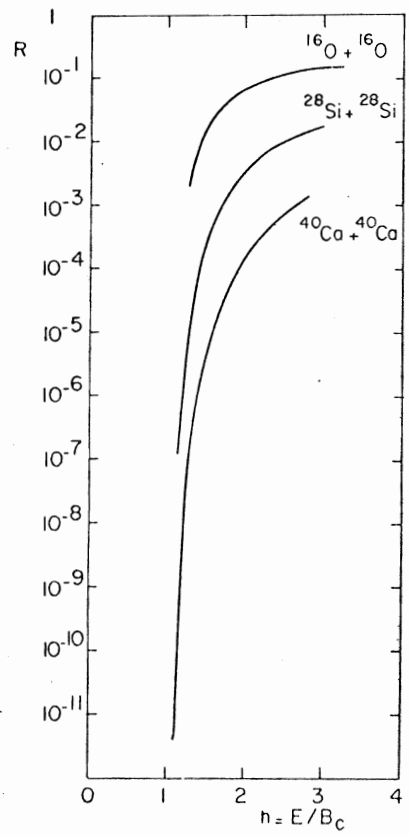

FIG. 10. Plot of the ratio $R = |f_+/f_-|$ (see text) which determines the magnitude of a structure in the excitation functions for three systems of identical nuclei. The parameters used are the following: $r_0 = 1.584$ fm, $d = 0.2$ fm, $r_0' = 1.438$ fm, $d' = 0.58$ fm, $\alpha = 60°$ fm^{-1}.

All these observations seem to be based upon the McIntyre parametrization. However, as shown in Eq. (5), the quantity R only depends on the Fourier transform of the "absorptive shape functions," and also on the value of θ_c. The latter is connected to the shape of the deflection function, and the former to the slope of the function $\eta(l)$. This point has been particularly analyzed by Siemssen *et al.* in their study[29] of the ^{16}O + ^{18}O elastic scattering, as they point out the presence of "kinks" in the function $\eta(l)$, which should affect the Fourier transform $F(\Delta x)$. Another presentation of the same analysis is the introduction[30] of Regge poles in the S matrix to produce these kinks. A quantitative analysis of this situation will be the subject of a separate study.[31] Whatever the importance of these two points for the elastic scattering of light nuclei is, it does not seem that their effects should modify the qualitative conclusions which result from the interpretation in terms of interference.

The purpose of this discussion is to point out that, beyond the specific behavior of each heavy-ion (the signature of which is the possibility of rainbows, kinks ...), there exists, as one goes from ^{12}C to ^{16}O to ^{28}Si and ^{40}Ca, a very strong effect which damps the interference between the two terms of the amplitude. Frahn has shown[10] that this effect, essentially due to the Coulomb repulsion, is similar to the one of a diverging lens.

Thus, even though a parametrization is difficult to find in the ^{16}O + ^{16}O case, which means that this nucleus has a very specific interest, it remains that the main conclusions of the Frahn model can be used to predict the occurrence of a structure. For instance, it is readily understood how oscillations have been observed in the ^{13}C + ^{40}Ca elastic scattering angular distributions by the Brookhaven group,[32] and how the peak-to-valley ratio decreases strongly in the elastic scattering excitation functions when one goes from ^{16}O + ^{16}O to ^{16}O + ^{28}Si.[33]

VII. CONCLUSION

The elastic scattering of ^{40}Ca by ^{40}Ca has been studied over a large range of incident energies, and six angular distributions have been presented. A sharp cutoff model analysis has given an interaction distance of $r_0 = 1.55$ fm (corresponding to overlap for densities equal to 5% of the central density). The optical-model potential which was found to fit the data has a W/V ratio equal to 0.4, considerably smaller than had been found former-

ly. This potential has neither energy nor angular momentum dependence, and the geometries for both wells are identical.

From these results, it appears that the magic of ^{40}Ca does not seem to play an important role in the elastic scattering. No evident transparency shows up, and three excitation functions, measured from the Coulomb barrier to twice this value with a sufficiently small energy step, are monotonically decreasing over this range of incident energies.

Thus, the analogy with the $^{16}O+^{16}O$ system which was looked for is not found. However, it has been possible to show that the larger mass and charge in the ^{40}Ca case would make the observation of such a structure unlikely, even if the studied system had presented some transparency for the grazing partial waves. A specific behavior of the ^{40}Ca nucleus would have to be searched for with a lighter projectile or in a comparison with other systems, as for example $^{40}Ar+^{40}Ca$ or $^{40}Ca+^{44}Ca$.

ACKNOWLEDGMENTS

We would like to express our gratitude to Dr. C. Marty for many enlightening discussions. We thank Professor W. E. Frahn for the interest he has shown for this experiment, and for kindly sending us his results prior to publication. We are also grateful to Dr. G. R. Satchler for allowing us to present the predictions of the folded potential. We would like to thank P. Martin and P. De Saintignon for the part they took in this experiment. We are greatly indebted to M. Dumail and her group for the qualities of the negative Ca ion source. We thank the operating crews of the tandem and Alice accelerators for their assistance, and L. Stab and his group for providing us with the large area detectors.

*Present address: D PhN/BE, CEN Saclay, BP No. 2, 91190 Gif/Yvette, France.

[1]J. R. Birkelund, J. R. Huizenga, H. Freisleben, K. L. Wolf, J. P. Unik, and V. E. Viola Jr., Phys. Rev. C 13, 133 (1976); R. Vandenbosch, M. P. Webb, T. D. Thomas, S. W. Yates, and A. M. Friedman, *ibid.* 13, 1893 (1976).

[2]P. Bonche, S. Koonin, and J. W. Negele, Phys. Rev. C 13, 1226 (1976); S. Koonin, Phys. Lett. 61B, 227 (1976); R. Y. Cusson, R. K. Smith, and J. A. Maruhn, Phys. Rev. Lett. 36, 1166 (1976).

[3]P. Colombani, N. Frascaria, J. C. Jacmart, M. Riou, C. Stéphan, H. Doubre, N. Poffé, and J. C. Roynette, Phys. Lett. 55B, 45 (1975).

[4]J. V. Maher, M. W. Sachs, R. H. Siemssen, A. Weidinger, and D. A. Bromley, Phys. Rev. 188, 1665 (1969).

[5]R. A. Chatwin, J. S. Eck, D. Robson, and A. Richter, Phys. Rev. C 1, 795 (1970).

[6]R. W. Shaw, R. Vandenbosch, and M. K. Mehta, Phys. Rev. Lett. 25, 457 (1970).

[7]A. J. R. Ferguson, in Proceedings of the Symposium on heavy-ion scattering [Argonne National Laboratory Report No. ANL 7837, 1971 (unpublished)], p. 187.

[8]M. Dumail and J. P. Mouffron, Nucl. Instrum. Methods 127, 157 (1975).

[9]W. Henning, P. Müller, M. Richter, H. P. Rother, K. E. Rehm, H. Schaller, and H. Spieler, University of Munich Annual Report, 1972 (unpublished), p. 24.

[10]W. E. Frahn, Ann. Phys. (N.Y.) 72, 524 (1972).

[11]N. Rowley, Nucl. Phys. A239, 134 (1975).

[12]W. E. Frahn and R. H. Venter, Ann. Phys. (N.Y.) 24, 243 (1963).

[13]J. S. Blair, Phys. Rev. 95, 1218 (1954).

[14]J. R. Huizenga, in Proceedings of the Symposium on macroscopic features of heavy-ion collisions [Argonne National Laboratory Report No. ANL/Phy. 76-2, 1976 (unpublished)], p. 1.

[15]W. D. Myers, Nucl. Phys. A204, 465 (1969).

[16]H. Doubre, J. C. Roynette, J. C. Jacmart, N. Poffé, M. Riou, E. Plagnol, and P. De Saintignon, Phys. Rev. Lett. 35, 508 (1975).

[17]J. S. Blair, in *Lectures in Theoretical Physics*, edited by P. D. Kunz and W. E. Brittin (Univ. of Colorado Press, Boulder, Colorado, 1966), Vol. VIIIC, p. 343.

[18]G. R. Satchler (private communication).

[19]C. Ngô, B. Tamain, J. Galin, M. Beiner, and R. J. Lombard, Nucl. Phys. A240, 353 (1975).

[20]F. Stancu and D. M. Brink, Nucl. Phys. A270, 236 (1976).

[21]J. Galin, D. Guerreau, M. Lefort, and X. Tarrago, Phys. Rev. C 9, 1018 (1974).

[22]D. Glas and U. Mosel, Nucl. Phys. A237, 429 (1975).

[23]A. Gobbi, R. Wieland, L. Chua, D. Shapira, and D. A. Bromley, Phys. Rev. C 7, 30 (1973).

[24]R. H. Siemssen, in *Nuclear Spectroscopy and Reactions*, edited by J. Cerny (Academic, New York, 1973), Part B, p. 233.

[25]M. L. Halbert, C. B. Fulmer, S. Raman, M. J. Saltmarsh, A. H. Snell, and P. H. Stelson, Phys. Lett. 51B, 341 (1974).

[26]W. E. Frahn, in *Heavy Ion, High Spin States and Nuclear Structure* (IAEA, Vienna, 1975), p. 157.

[27]J. A. McIntyre, K. H. Wang, and L. C. Becker, Phys. Rev. 117, 1337 (1960).

[28]W. E. Frahn and K. E. Rehm (unpublished) and private communication.

[29]R. H. Siemssen, H. T. Fortune, A. Richter, and J. W. Tippie, Phys. Rev. C 5, 1839 (1972).

[30]K. W. McVoy, Phys. Rev. C 3, 1104 (1971).

[31]E. Plagnol, H. Doubre, and C. Marty (unpublished).

[32]P. D. Bond, J. D. Garrett, O. Hansen, S. Kahana, M. J. Levine, and A. Z. Schwarzschild, Phys. Lett. B47, 231 (1973).

[33]R. H. Siemssen, in Proceedings of the Symposium on heavy-ion scattering [Argonne National Laboratory, Report No. ANL 7837, 1971 (unpublished)], p. 145.

4. Conclusion.

Le plus frappant des résultats obtenus est évidemment la décroissance extrêmement rapide des sections efficaces avec l'énergie et l'angle. Ainsi, on observe sur la fonction d'excitation une variation de la section efficace sur 6 ordres de grandeur. A $E_{c.m.} = 112.5$ MeV, le rapport σ/σ_R a décru jusqu'à 10^{-5} sur un intervalle angulaire $30° \leqslant \theta_{c.m.} \leqslant 70°$.

Ces résultats montrent assez, compte tenu des performances actuelles des sources d'ions et des accélérateurs, que les limites des possibilités expérimentales sont atteintes et que des études sur des ions plus lourds nécessiteront des systèmes de comptage autrement plus performants. Il reste d'ailleurs à montrer que pareilles études peuvent conduire à des résultats non ambigus. Frahn a fait remarquer [Fr77a] qu'à la limite des grands paramètres de Sommerfeld :

$$n = \mu \frac{Z_1 Z_2 e^2}{\hbar^2 k} = 0.1575\ Z_1 Z_2 \sqrt{\frac{\mu}{E}}$$

les distributions angulaires et fonctions d'excitation prennent toutes des formes classiques. Par exemple, l'angle du point-un quart ($\sigma/\sigma_R = 1/4$) ne diffère de l'angle critique que par une quantité d'ordre $n^{-1/2}$. Pour des systèmes fortement chargés, la forme de "diffraction de Fresnel" est souvent parfaitement reproduite. C'est déjà le cas pour le système $^{40}Ca+^{40}Ca$.

Un deuxième résultat important concerne la position de la barrière. Il a été montré dans [Do 77b] que le rayon obtenu pour la barrière est en bon accord avec celui qu'on peut attendre de la systématique sur la diffusion élastique entre ions lourds [Hu 76]. On ne trouve pas ici d'influence de la magicité du noyau ^{40}Ca sur la position de la barrière.

A cause du rôle prédominant joué par l'interaction coulombienne, toute information caractéristique d'un système particulier ne peut plus apparaître que comme une déviation à ce comportement moyen, d'où l'intérêt de l'analyse en modèle optique.

Au chapitre III, on montre que l'influence de la charge est telle que tout effet dû à la transparence pour les ondes rasantes ne peut apparaître avant une énergie $\gtrsim$ 100 MeV (c.m.), lorsque les sections efficaces, très faibles, sont difficilement mesurables.

Auparavant, cette vue d'ensemble sur les réactions induites par le système $^{40}Ca+^{40}Ca$ va être poursuivie en précisant le rôle joué par l'énergie incidente dans ce bilan.

II - REACTIONS TRES INELASTIQUES ENTRE NOYAUX DE ^{40}Ca.

1. Motivations.

Les résultats de la diffusion élastique $^{40}Ca+^{40}Ca$ montrent que l'influence de la fermeture des couches dans le ^{40}Ca ne peut être appréciée avant que les sections efficaces deviennent très faibles. Cette constatation a orienté ce travail dans deux directions.

La première a été une nouvelle formulation de l'analyse de la diffusion élastique, qui est donnée au chapitre III.

La seconde concerne la distribution du flux incident entre les différentes voies, et principalement la présence de réactions très inélastiques, qui a déjà été signalée [Co 74] auparavant sur le même système. Il y a là évidemment une source d'absorption extrêmement importante, puisque sa section efficace est une fraction non négligeable de la section efficace totale. D'autre part, les études portant sur des systèmes plus lourds ont montré qu'il s'agit de processus relativement prompts, qu'on présume être fortement couplés à la voie d'entrée.

Dans les réactions très inélastiques entre noyaux de ^{40}Ca, la symétrie de la voie d'entrée offre l'avantage de permettre d'évaluer la proportion de processus à trois corps, ou de désintégrations séquentielles, puisque les réactions à deux corps dans la voie de sortie doivent avoir un rendement symétrique autour de Z = 20. Cette simplification est compensée par la difficulté à distinguer les produits résultant de la fission du noyau composé de ceux dus à des réactions très inélastiques.

Il était essentiel, pour le bilan qu'on cherche à dresser, de faire cette distinction.

2. Distinction entre fission et processus très relaxés dans le cas d'une voie d'entrée symétrique.

Nous reproduisons ici une lettre [Ro 77b] qui explique comment nous avons procédé.

ON THE TIME SCALE OF $^{40}Ca+^{40}Ca$ STRONGLY DAMPED REACTIONS

J.C.ROYNETTE, H.DOUBRE, N.FRASCARIA, J.C.JACMART, N.POFFE and M.RIOU

Institut de Physique Nucléaire, BP n°1, 91406 Orsay, FRANCE

ON THE TIME SCALE OF $^{40}Ca + ^{40}Ca$ STRONGLY DAMPED REACTIONS

J.C. ROYNETTE, H. DOUBRE, N. FRASCARIA, J.C. JACMART, N. POFFE and M. RIOU
Institut de Physique Nucléaire, B.P. No. 1, 91 406, Orsay, France

Received 22 February 1977

The time dependence of $^{40}Ca + ^{40}Ca$ deep inelastic collisions is studied by means of the fragment charge and mass distributions. Two time components are unfolded. The "fast" one exhibits all features of "quasi-fission". The characteristics of the "slow" component cannot be distinguished from compound nucleus fission.

The observation of "strongly-damped" heavy-ion reactions has prompted many experimental studies. The main features of these reactions are now well established [1, 2]. It has been shown [2, 3] how the so-called "deep inelastic collisions" (D.I.C.) and "quasi-fission" essentially result from the same physical process but manifest themselves differently, according to the relative importance of the Coulomb repulsion. Although quasi-fission exhibits features which rule out any confusion with compound nucleus fission, the situation is not so clearcut in the D.I.C. case where broad Z-distributions and a $(\sin\theta)^{-1}$ dependence of the angular distributions at backward angles are observed for large mass and charge transfers. For products closer to the projectile, the forward peaked angular distributions and the narrow Z-distributions can be considered as evidence for a non-compound mechanism.

An earlier experiment [4] has shown that the main characteristics of the $^{40}Ca + ^{40}Ca$ D.I.C. remain in good agreement with the general trends mentioned above. This letter reports on some new data on the same system. In discussing the observed angular and charge distributions, we attempt to discriminate between the "fast" and "slow" reaction mechanisms.

The mass and charge symmetry of the chosen system ($^{40}Ca + ^{40}Ca$) significantly simplifies an interpretation of the results because the entrance-channel symmetry leads to symmetry in the exit channel as far as binary processes are considered. Therefore, even an inclusive experiment for such a symmetric system may provide information on the emission of light particles from the reaction products. Moreover, studying the D.I.C. in a symmetric system one can easily determine the diffusion parameter [2, 5] entering the Fokker–Planck equation, because the drift coefficient must be equal to zero in case of the mass and charge symmetry. Among other symmetric systems the $^{40}Ca + ^{40}Ca$ combination seems to be especially interesting because the closed-shell structure of ^{40}Ca is very suitable for microscopic calculations of the reaction dynamics [6]. It is important also that the elastic [7] and fusion [8] channels are well known for this particular reaction.

In this paper we discuss some aspects of the reaction mechanism using part of the data on the $^{40}Ca + ^{40}Ca$ reaction obtained previously [9–10], together with new data obtained at $E_{lab} = 256$ MeV for many Z-values of the reaction products ($Z = 5 - 28$) detected in a wide angular range ($\theta_{lab} = 7.5° - 50°$) using the $\Delta E - E$ telescope technique [11].

The measured energy spectra were transformed to the center-of-mass energy spectra $d^2\sigma/d\theta_{c.m.}dQ$ assuming two-body kinematics. All the spectra exhibit the deep inelastic component. (The quasi-elastic component which is present only for $Z \approx 20$ is not discussed in this letter). The most probable c.m. energy corresponding to the deep-inelastic maximum is plotted in fig. 1 as a function of Z and compared with the energy of the Coulomb repulsion calculated for two touching spheres. It is seen from fig. 1 that heavy products ($Z > 20$) have significantly lower energies than the calculated Coulomb energy. This may suggest that the heavy fragments evaporate more nucleons that the light ones. It is worth emphasizing that the average c.m. energies for Z-values close to 20 largely exceed the energy of the Coulomb repulsion (especially at forward angles). This means that these products do not undergo complete relaxation of the kinetic energy.

Strongly-relaxed ($Q = -110 - -30$ MeV) cross sections, when plotted as a function of Z for different c.m.

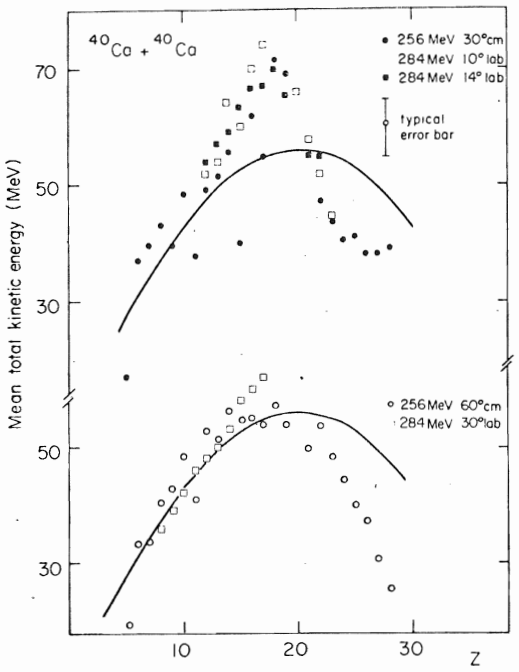

Fig. 1. Average c.m. total kinetic energy of the deep inelastic part of the energy spectra as a function of Z for various angles. The kinetic energies resulting from the Coulomb repulsion of two spherical fragments, $B_C = Z_1 Z_2 e^2/1.225\ (A_1^{1/3} + A_2^{1/3} + 2)$ are also shown (full line).

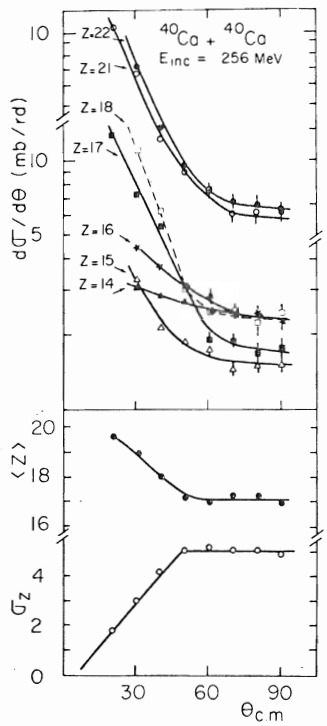

Fig. 2. Characteristics of deep inelastic processes in the $^{40}Ca + ^{40}Ca$ reaction at 256 MeV, as a function of angle: (a) angular distributions $d\sigma/d\theta$ for various elements close to $Z = 20$; (b) average Z-value; and (c) variance σ_Z of Z distributions.

angles exhibit two distinct features. At $\theta_{c.m.} = 20°$ the Z distribution is narrow and peaks close to $Z = 20$; with increasing angle the maximum of this distribution shifts towards smaller Z-values and its width increases. The first two moments of this distribution, $\bar{Z}$ and $\sigma_z^2 = \overline{(Z - \bar{Z})^2}$, are shown in fig. 2 as a function of angle. Both curves exhibit a rapid variation from 20° to 40° (c.m.) and become flat at larger angles. It was checked that these characteristics remain the same if the analysis is performed for a much narrower range of Q values ($Q = -80$- -70 MeV). This is consistent with our previous study of the isotopic distributions in the $^{40}Ca + ^{40}Ca$ reaction at $E_{lab} = 284$ MeV [10]. It was found that the whole (Z, N) distribution shifts when $\theta_{c.m.}$ increases. Its maximum goes from $(Z, N) = (19, 20)$ for $\theta_{c.m.} = 15°$ to $(17, 18)$ for $\theta_{c.m.} = 30°$. It is thus confirmed that light particle emission is not a dominating mode of deexcitation of the fragments emitted at forward angles.

It appears very attractive to relate the variations of $\bar{Z}$ and σ_z and the shape of the differential cross section (fig. 2) to the existence of an incompletely relaxed component in the energy spectra observed at forward angles. To shed some light on this problem, we have split the relaxed cross section into two components. This was achieved in attributing the whole of the cross section at 90° (c.m.) to a "slow component", with a $(\sin\theta)^{-1}$ angular distribution. For this component, a broad Z-distribution is then obtained, the mean value of which is close to 17. This component is thus observed after a sizeable amount of evaporation (a noticeable odd-even pattern is observed which fits well into this frame). Substracting this component, one is faced with a fast process characterized by exponentially decreasing angular distributions and very narrow, angle-independent, Z-distributions ($\bar{Z} = 19$ and $\sigma_Z = 3$) as shown in fig. 3. The resulting spectra are peaked approximately 20 MeV above the exit channel Coulomb barrier. By these properties which are characteristic of a short interaction time, this "fast component" behaves in all respects as the so-called "quasi-fission". As pointed out above, the number of evaporated particles from the reaction products corre-

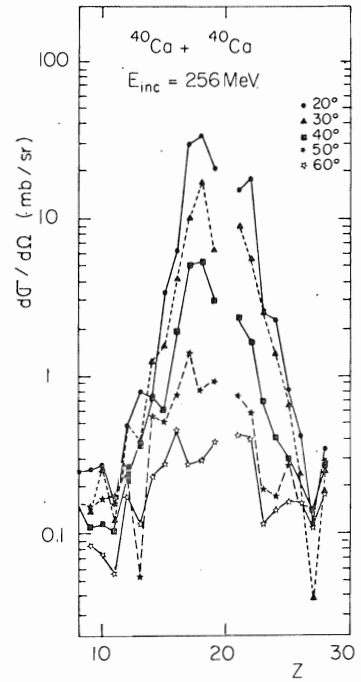

Fig. 3. Z-distributions of the "fast deep inelastic component" at various c.m. angles.

sponding to the "fast component" is very small, in spite of the high excitation energy. One can suppose, therefore, that the excitation energy is shared mostly among collective models.

Before further discussion, attention should be paid to the effects of the entrance channel symmetry. Events occuring at $\pi - \theta$ cannot be distinguished from those at θ. The deep inelastic processes at backward angles are expected to be completely relaxed and to have angular distributions nearly like $(\sin\theta)^{-1}$. In case of the symmetric system, they must contribute to the "slow component" at forward angles.

There is no doubt that the "slow component" includes compound nucleus fission which, in this particular system, cannot be distinguished from two-body completely-relaxed reactions. The total cross section of the "slow component" is found to be 280 mb. This agrees with predictions of the fusion-fission cross section based on the liquid drop model [12]. It should be mentioned that a similar ambiguity seems to appear in experimental data on non-symmetric systems where broad Z-distributions are observed.

The "fast component" exhibits an angle-focusing which immediately calls for a rainbow effect usually associated with less damped collisions. It should be noted that the grazing angle for the $^{40}Ca + ^{40}Ca$ collisions at $E_{lab} = 256$ MeV is quite small $(\theta_{gr})_{c.m.} = 30°$). The observation of the "fast component" up to $50°_{c.m.}$ shows that the relaxed ($Q \leqslant -30$ MeV) $^{40}Ca + ^{40}Ca$ collisions feeding this component can be ascribed to trajectories which cross the beam direction. The cross section for this process becomes negligible with respect to the "slow component" cross section at angles larger than $50°_{c.m.}$.

Maybe our arbitrary way of removing the fission part from the D.I.C. can lead us to too sharp a discrimination between fast processes (similar to "quasi-fission") and slow decays of the "composite system". However, it must be emphasized that removing the "slow component", one obtains a completely different time scale of the remaining part of the D.I.C. as compared with usual analyses in the frame of diffusion models [2, 5]. Moretto and Sventek found [2] that the characteristic diffusion time is comparable with the rotational period of a colliding system. However, the fusion-fission cross section was not substracted in the analysis [2]. It seems very probable that the diffusion time scale is much closer to the energy damping time scale than that reported in ref. [2].

The diffusion model formalism must now be applied to the only "fast" non-compound part of the cross section. However, the variance is found to be constant, whereas Nörenberg [5] predicts a linear dependence with angle. One possible explanation of the discrepancy may be attributed to the fact that the $^{40}Ca + ^{40}Ca$ collisions do not fulfil very well the requirements for a classical description, and therefore the classical correspondence between time and scattering angle is not valid.

To summarize, it is proposed that one can understand the D.I.C. as resulting from two coexisting phenomena: a slow one, indistinguishable from fission and a much faster one, showing all the characteristic features of the so-called "quasi-fission". Only the "fast component" of the cross section can be related to the diffusion mechanism, but the time scale of the diffusion is quite short, comparable with the time scale of the energy damping. This mechanism leads to high excitation energies, but Z-distributions of the reaction products remain narrow. Only a small part of the excitation energy is dissipated in particle emission. This indicates that collective modes are excited predominantly.

We acknowledge the contribution of Dr. C. Stéphan and Dr. P. Colombani in the first part of this experiment. We are grateful to Dr. Wilczynski for enlightening discussions and very careful reading of the manuscript. It is a pleasure to thank Dr. D.H.E. Gross for his interest in this experiment.

References

[1] J. Galin, J. de Phys. 37 (1976) C5-83, and references therein.
[2] L.G. Moretto and R. Schmitt, J. de Phys. 37 (1976) C5-109, and references therein.
[3] B. Tamain et al., Phys. Rev. Lett. 36 (1976) 18.
[4] P. Colombani et al., Phys. Lett. 55B (1975) 45.
[5] W. Norenberg, J. de Phys. 37 (1976) C5-141.
[6] S.E. Koonin et al., preprint (1976).
[7] H. Doubre et al., to be published in Phys. Rev. C.
[8] H. Doubre et al., to be published.
[9] J.C. Jacmart et al., J. de Phys. 36 (1975) C5-107.
[10] N. Frascaria et al., Proc. of the Caen Conf. p. 166 (unpublished) and to be published.
[11] J.C. Roynette et al., to be published.
[12] S. Cohen, F. Plasil and W.J. Swiatecki, Ann. of Phys. 82 (1974) 557.

3. Conclusion.

Bien que l'échelle des temps caractéristiques pour ces réactions soit très vraisemblablement continue, on peut schématiser la situation dans $^{40}Ca+^{40}Ca$ de la façon suivante : à côté d'une composante "lente" qui, ici, ne peut être distinguée de la fission, la composante "rapide" présente des caractéristiques, en particulier une focalisation en angle et en Z, analogues à celles que Moretto et Schmitt [Mo 76] attribuent au phénomène de "quasi fission". Au-dessous de 90 MeV (c.m.) ce phénomène est seul présent, d'où la très faible section efficace pour des produits à numéro atomique un peu éloigné de 20 (disons $|Z-Z_o| > 3$) ; au-delà de 100 MeV, la voie fission est ouverte et tous les numéros atomiques sont peuplés.

Le bilan des voies de sortie du système $^{40}Ca+^{40}Ca$, en fonction de l'énergie incidente, sera donné après que les résultats sur la fusion aient été présentés.

III - LA FUSION ENTRE NOYAUX DE ^{40}Ca.

La mesure des sections efficaces des produits d'évaporation a été la méthode choisie pour évaluer la proportion de la section efficace totale qui va en fusion. Cette expérience est décrite dans la lettre [Do 77c].

EVAPORATION-RESIDUE CROSS SECTIONS IN THE $^{40}Ca+^{40}Ca$ SYSTEM

H.DOUBRE, A.GAMP, J.C.JACMART, N.POFFE and J.C.ROYNETTE

Institut de Physique Nucléaire, BP n°1, 91406 Orsay, FRANCE

and

J.WILCZYŃSKI

Institute of Nuclear Physics, Cracow, POLAND

EVAPORATION-RESIDUE CROSS SECTIONS IN THE $^{40}Ca+^{40}Ca$ SYSTEM

H.Doubre, A.Gamp, J.C.Jacmart, N.Poffé and J.C.Roynette,

Institut de Physique Nucléaire, BP n°1, 91406 Orsay (France)

and

J.Wilczyński

Institute of Nuclear Physics, Cracow (Poland)

Evaporation-residue cross sections for the $^{40}Ca+^{40}Ca$ system have been measured with a position-sensitive E-ΔE telescope. From the deduced values of the barrier and critical radii, it does not appear that the shell-closure in ^{40}Ca has any influence on the fusion phenomenon.

97

Studying fusion excitation functions at the energies close to the Coulomb barrier one can deduce a valuable information about an effective nucleus-nucleus potential. (This information is complementary to the information available from the analysis of the elastic scattering data). At higher energies the fusion data allow to determine such useful parameters as the critical radius and the critical potential [1], which roughly summarize our knowledge of the system at small separation distances.

At low energies and for not very heavy systems the fusion cross section is identical with the evaporation-residue cross section. Only at relatively high energies the fusion-fission process becomes competitive with deexcitation of the compound nucleus through emission of light particles. Therefore for all light and medium compound systems the evaporation cross sections at low energies can be analyzed as the fusion excitation function.

As a part of a study of the $^{40}Ca+^{40}Ca$ system, we have measured evaporation-residue cross sections at incident energies between one and three times the Coulomb barrier. The reasons to study this particular system have been explained elsewhere [2]. As it was mentioned above, these measurements provide an additional test of the optical-model potential determined from our elastic scattering measurements [2]. On the other hand, the fusion cross section of a magic system can be seen as average or "macroscopic" for this mass region and, as recently pointed out by Stokstad [3], a comparison with corresponding values in neighboring, open-shell systems could give some indication on the role of individual nucleons in the fusion process. Accordingly with Glas and Mosel [4], one can expect that the tightness of the system, associated with shell effects, may manifest itself in decreasing the radius parameters as compared with neighboring systems. Finally, recent microscopic calculations [5] have

78

been done for collisions between closed-shell nuclei. In particular, fully three-dimensional time-dependent Hartree-Fock calculations [6] are now available for the $^{40}Ca+^{40}Ca$ system.

The experimental data were taken between 107 and 195 MeV incident energy (lab) in steps of about 5 MeV at the M.P. tandem, and at 300 MeV at the accelerator Alice of the Institut de Physique Nucléaire, Orsay. A 60 $\mu g/cm^2$ natural Ca target evaporated onto a 5 $\mu g/cm^2$ carbon backing was used. The beam was collimated to reduce both the angular dispersion and the beam-spot size on the target. A ΔE-E telescope, at a distance of 57 cm from the target was used. The E detector was a 14×50 mm^2 solid-state detector situated inside the gas volume of a ΔE ionisation chamber. A 33 $\mu g/cm^2$ formvar foil was used as an entrance window of the ionisation chamber. With low energy ($\lesssim E_{inc}/2 = 1.4$ MeV per nucleon) evaporation-residues ($Z \gtrsim 33$), the ΔE-E technique does not allow to determine the individual atomic number of the products but the identification of the whole group of the evaporation-residues was absolutely unambiguous. Besides, it was checked that the carbon backing introduced no contamination to the area of the ΔE-E spectrum where the evaporation residues were observed.

An accurate and continuous control of the beam direction during the entire experiment is very essential in the measurements of the evaporation-residue cross section. Apart from the usual left-right checks, we used a multi-slit entrance window of the ionization chamber, each slit having a width of 0.5°, separated from each other by 1°. From the time difference between the E and ΔE signals, a localisation information is obtained allowing for simultaneous measurements at 5 scattering angles. This increased detection power of our ΔE-E telescope was extremely useful for reliable and accurate determination of the beam direction in each

particular run. This was obtained by comparing the numbers of counts in the elastic scattering peak for all 5 neighboring angles. (The slope of the elastic scattering angular distribution has sufficient angular dependence to obtain the correct position (±0.1°) of the counter with respect to the beam direction). We have thus measured (for each energy) the angular distribution of the compound-residue nuclei. The total cross section for a given energy was obtained from the integration of the angular distribution, normalized to the lab elastic scattering cross section. The main uncertainty in such a procedure is introduced by the extrapolation of the compound-residue angular distribution to very forward angles. This extrapolation was performed by fitting the angular distributions with an analytic expression containing 3 parameters varying smoothly with energy. The total compound-residue cross section (together with some other useful quantities) determined as described above are listed in table I.

Several features of the measured excitation function have to be noted. First, the value of the fusion barrier is found to be : $V_B = 51.5 \pm 0.5$ MeV. This is only slightly lower than the value $V_B = 52.7$ MeV determined from our earlier elastic scattering measurements [2]. Fig.1 shows the evaporation residue cross sections in comparison with the total reaction cross section calculated using the optical-model potential that fits the elastic scattering data over a large energy range [2]. It can be observed that the agreement is rather good at low energies (i.e. up to 70 MeV c.m.). It has been experimentally observed [2] at these energies, that the inelastic scattering to the 3^- excited state of ^{40}Ca is the only reaction channel which is open with a non-negligible cross section. The more transparent potential determined by Richter et al.[7] from elastic scattering data taken at $50 \lesssim E_{c.m.} \lesssim 65$ MeV predicts (fig.1) a reaction cross

80

section lower by about 120 mb than the evaporation-residue cross section.

It appears that at energies above 75 MeV, a number of different channels open, since the evaporation-residue cross section saturates at about 1000 mb and does not follow any longer the increasing reaction cross section. Evidently, this set of channels is related to the so-called strongly-relaxed processes which have been studied separately in the same reaction, $^{40}Ca+^{40}Ca$. Results of these experiments will be published in a forthcoming paper [9]. A good agreement has been found between the threshold energy for strongly-relaxed reactions and the energy at which evaporation residue cross section becomes definitely lower than the total reaction cross section.

It is not excluded that another process can also compete with evaporation, namely the fissioning of the compound nucleus which would yield reaction products of mass numbers close to 40. An evaluation of the fusion-fission cross section in the framework of the charged liquid-drop model [10] requires a good knowledge of the masses in the vicinity of the compound nucleus ^{80}Zr. This condition is not yet fulfilled. However, a reasonable evaluation using the method of ref.[10], as well as results from the code ALICE [11] make clear that fission is negligible at the C.M. energies below 100 MeV. This is also in agreement with the recently proposed analysis [12] of the $^{40}Ca+^{40}Ca$ strongly-relaxed collisions at $E_{c.m.} = 130$ MeV. Specifically, it has been shown that at this energy one observes fast reactions (strongly focused in mass and angle distributions) accompanied by much slower processes, which are undistinguishable from fission because of their broad mass distribution and isotropic $d\sigma/d\theta$ angular distribution. Data have been collected at 90, 100, 115, 130 and 145 MeV c.m. incident energy, and the latter component is not present at the two lowest energies. Therefore it is very likely that

81

the difference observed (fig.2) between the cross section (720 mb) at 150 MeV, and the expected value of the fusion cross section (1100 mb -see below-) is due to the compound-nucleus fission, whereas this latter process can be neglected at lower energies. It is worthwhile to note that the "fission-like" [12] process cross section at 130 MeV was determined to be 320 mb.

Predictions for the $^{40}Ca+^{40}Ca$ fusion cross sections were given [4] by Glas and Mosel, who have used the concepts of critical radius and critical potential. In that framework, the fusion cross section is expected to linearly depend on the quantity E^{-1}, with different slope in the energy ranges below and above the critical energy E_c :

$$\sigma = \pi R_B^2 \left(1 - \frac{V_B}{E}\right) \qquad \text{when } E \leqslant E_c$$

$$\sigma = \pi R_c^2 \left(1 - \frac{V_c}{E}\right) \qquad \text{when } E \geqslant E_c$$

where R_B and R_c are the barrier and critical radii respectively, and V_B and V_c the corresponding values of the ion-ion potential. On fig.2, the evaporation-residue cross section is plotted as a function of E^{-1}. The experimental data are compared to the best fit to the model of Glas and Mosel. The following average parameters have been obtained:

$V_B = 51.4$ MeV $\quad R_B = 10.22$ fm $\quad r_{oB} = 1.49$ fm

$V_c = 24.$ MeV $\quad R_c = 6.65$ fm $\quad r_{oc} = 0.97$ fm

It is interesting to note that Glas and Mosel predict correctly a positive value for the critical potential. This classifies the considered system definitely among "heavy" ones (light systems have negative value of the critical potential). However, the value of the fusionbarrier suggested

82

in ref.[4] is too large, as already noticed [2] and the predictions consequently underestimate the evaporation-residue cross sections. One can also notice a good agreement between the reduced critical radius and the value systematically used since the work by Galin et al.[1].

One can then ask whether the fusion of the $^{40}Ca+^{40}Ca$ system gives an evidence for the closed-shell structure of the colliding nuclei. The answer is clearly negative. Our analysis of the data in the framework of the Glas and Mosel model shows that both the critical radius and the barrier radius for the $^{40}Ca+^{40}Ca$ system do not show any deviation from the values obtained from other (non-magic) systems. Similar conclusion is drawn from recent analysis [13] of the near-to-barrier fusion excitation functions for many different systems, including the $^{40}Ca+^{40}Ca$ data : the effective nucleus-nucleus potential required to reproduce these data follows the macroscopic systematics of a numerous set of different colliding systems. This conclusion is especially important in the light of the well-known idea of Glas and Mosel [4] which relate the critical radius with the position of the first level-crossing in the configuration-energy levels calculated with the two-center shell model. Since the analysis of the $^{40}Ca+^{40}Ca$ fusion data does not confirm this hypothesis (see two variants of the Glas and Mosel predictions in fig.2), one can suppose that the level-crossing concept, based on adiabatic calculations, is not sufficient to deduce the microscopic phenomena which are responsible for dissipative processes in heavy-ion reactions. Perhaps some fast collective and single-particle excitations, in the nucleus-nucleus collision, provide the first step in overcoming the shell gap before adiabatic effects (such as level-crossings) could play a role.

These remarks are also valid in connection with the results of

83

Bonche et al. [6] who deduced the fusion cross sections as a function of energy from a full three-dimensional time-dependent Hartree-Fock calculation. Even if they fairly well reproduce the shape of the excitation function, they find the fusion barrier located at too high energy. They attribute this discrepancy to two reasons : i) the force used in the calculations and ii) mainly the fourfold symmetry kept, (i.e., 4 particles occupy the same spatial orbit). As a result, only 4 particle-4 hole excitations are available, making this system much stiffer than it is.

It should be noticed that all the microscopic calculations which take into account the shell-structure of ^{40}Ca yield too high the interaction barrier of the system as compared with our experimental result. Such a result is obtained from sudden [14] as well as from adiabatic [15] calculations, from the momentum-space folding model [16] and from time-dependent Hartree-Fock [5] evaluations, even when transverse degrees of freedom are taken into account [6]. On the contrary, macroscopic estimates [17,18] in which the shell-structure of ^{40}Ca is neglected are much more satisfying. These latter estimates have been reported in fig.2.

To summarize, the measurement of the evaporation-residue cross sections for the $^{40}Ca+^{40}Ca$ system, in the energy range up to three times the Coulomb barrier, is presented and a very efficient experimental method described. No evidence for a specific behavior of the system associated with the shell closure of ^{40}Ca was found. On the contrary, the data indicate that the excitation processes (usually referred to as friction) are sufficiently strong to destroy the specific structure of the colliding nuclei already in the first stages of the collision.

We would like to thank Prof. D.H.E.Gross for several stimulating discussions and for communication of his results prior to publication.

References

[1] J.Galin, D.Guerreau, M.Lefort and X.Tarrago, Phys. Rev. C9 (1974) 1018.

[2] H.Doubre et al., Phys. Rev. C15 (1977) 693.

[3] R.G.Stokstad, Proc. Fall Creek Falls Meeting on Heavy-Ion Collisions, (1977) to be published.

[4] D.Glas and U.Mosel, Nucl. Phys. A237 (1975) 429 and Phys. Lett. 49B (1974) 301.

[5] S.E.Koonin et al., Phys. Rev. C15 (1977) 1359.

[6] P.Bonche, B.Grammaticos and S.E.Koonin, to be published.

[7] M.Richter et al., Nucl. Phys. A278 (1977) 163.

[8] L.G.Moretto and R.Schmitt, J. de Physique, Suppl., 11 C.5 (1976) 109.

[9] J.C.Roynette et al., to be published.

[10] S.Cohen, F.Plasil and W.J.Swiatecki, Ann. Phys. (N.Y.) 82 (1974) 557.

[11] F.Plasil and M.Blann, Phys. Rev. C11 (1975) 508.

[12] J.C.Roynette et al., Phys. Lett. 67B (1977) 395.

[13] K.Siwek-Wilczyńska and J.Wilczyński, to be published.

[14] C.Ngô et al., Nucl. Phys. A252 (1975) 237.

[15] H.Flocard, private communication.

[16] D.A.Saloner, C.Toepffer and B.Fink, Nucl. Phys. A283 (1977) 131.

[17] D.H.E.Gross and H.Kalinowski, private communication.

[18] J.Wilczyński, private communication.

85

Table I

$E_{c.m.}$ (MeV)	53.5	55.	57.5	60	62.5	65	67.5	71.	73.5	77.	81.	85.	87.5	91.1	97.5	150.
σ_{tot} (mb)	103	278	377	511	548	600	663	862	894	902	977	1045	950	982	1024	720
$\Delta\sigma$ (mb)	25	50	40	30	50	45	70	50	50	40	50	70	70	75	100	50
σ_{meas} (%)	15	40	25	60	25	70	22	65	40	55	57	67	62	64	40	70
θ_{max}	1°5	1°5	1°3	1°6	1°9	2°1	2°1	2°	2°2	2°5	2°5	2°4	2°7	2°9	3°	4°1

Table caption

Total evaporation residue cross sections as a function of energy.

$\sigma_{meas.}$ gives the percentage of the total cross section which was actually measured.

$\theta_{max.}$ gives the angle at which the differential cross section $\frac{d\sigma}{d\theta}$ is maximum. This quantity was derived from a fit to the measured angular distribution, as explained in the text.

Figure captions

Figure 1. Comparison of the evaporation-residue cross section with the predictions of an absorbing potential (full line - ref.[2]) and of a much more transparent one (dashed line - ref.[7]).

Figure 2. Evaporation-residue cross section as a function of $E_{c.m.}^{-1}$. The predictions of Glas and Mosel (ref.[4]) are given by the thin line and the dashed line, for an "average" and a "magic" system respectively. The dashed-dotted line gives the predictions of Wilczyński (ref.[17]) and the long-dashed line gives those of Gross (ref.[16]). The thick full line results from a fit using the Glas and Mosel formula.

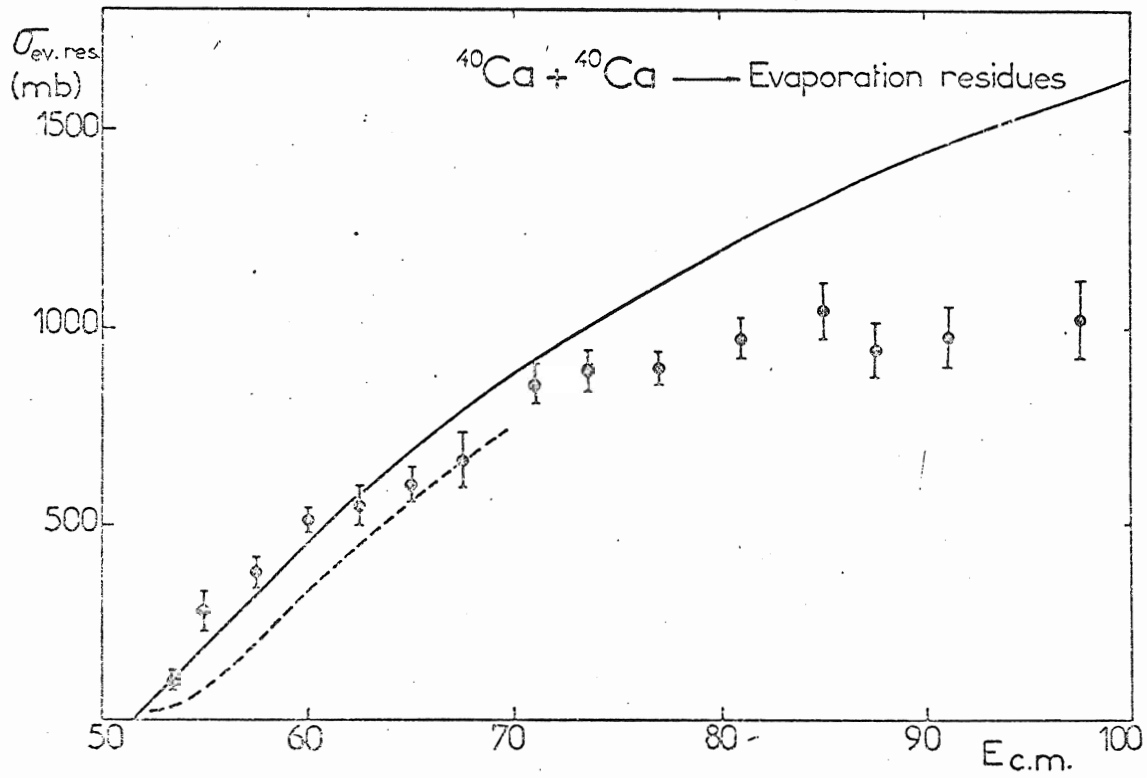
$\sigma_{ev.res.}$
(mb)
1500
1000
500
$^{40}Ca + ^{40}Ca$ —— Evaporation residues
50
60
70
80
90
100
E c.m.

Fig. 1

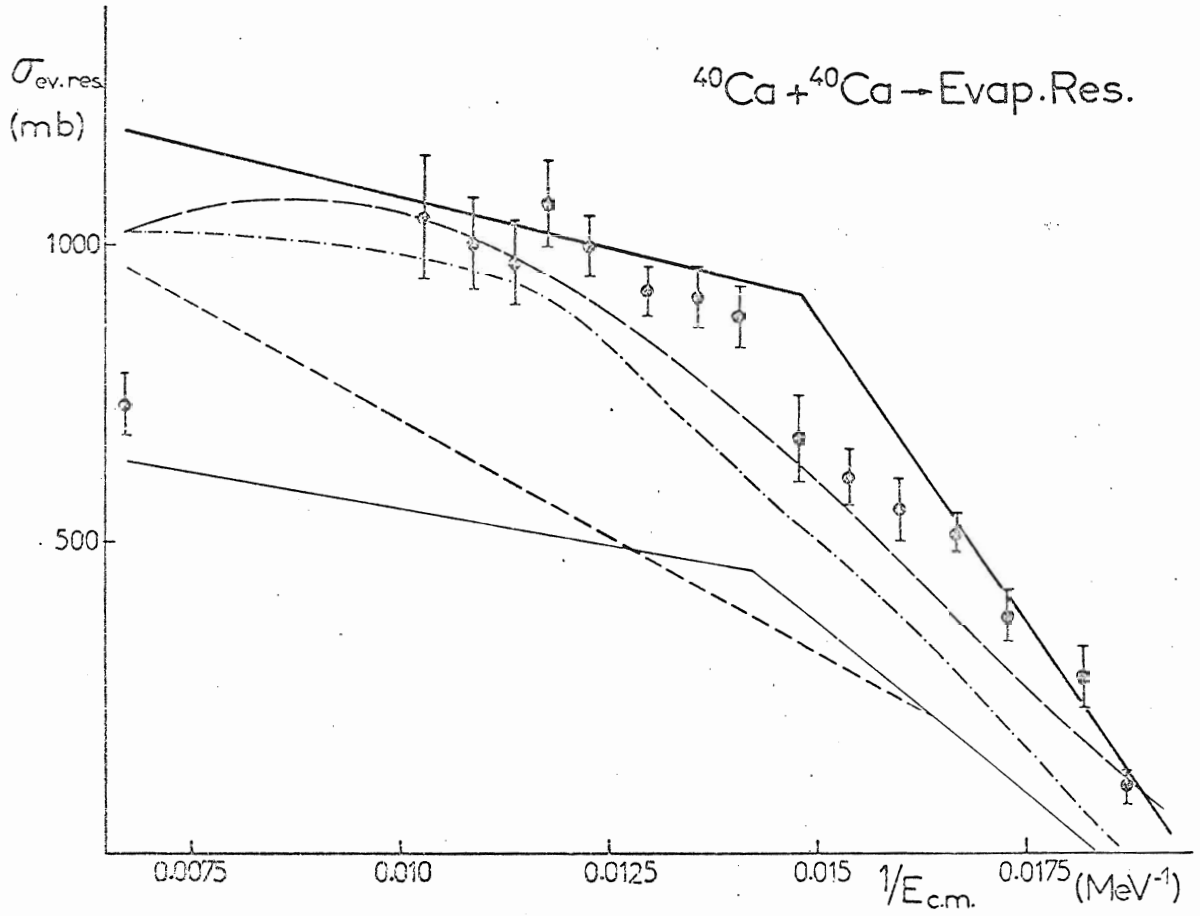
$\sigma_{ev.res.}$
(mb)
$^{40}Ca + ^{40}Ca \rightarrow$ Evap.Res.
1000
500
0.0075
0.010
0.0125
0.015
0.0175
$1/E_{c.m.}$ (MeV^{-1})

cb

Les résultats sont cohérents avec ce qui précède : la magicité des noyaux de ^{40}Ca n'apparaît pas plus sur le comportement des sections efficaces de fusion avec l'énergie. Les calculs microscopiques de Bonche et al. [Bo 77] montrent également combien il est difficile de reproduire des sections efficaces relativement élevées, inattendues pour ce système. A la lettre [Do 77c], qui décrit la mesure et donne les résultats de la fusion $^{40}Ca+^{40}Ca$, nous ajoutons la figure II.2 tirée de [Bo 77]. Cette figure montre quelles améliorations sont à apporter à la force utilisée dans les calculs Hartree-Fock dépendant du temps, pour retrouver les résultats expérimentaux, en particulier une position correcte de la barrière d'interaction.

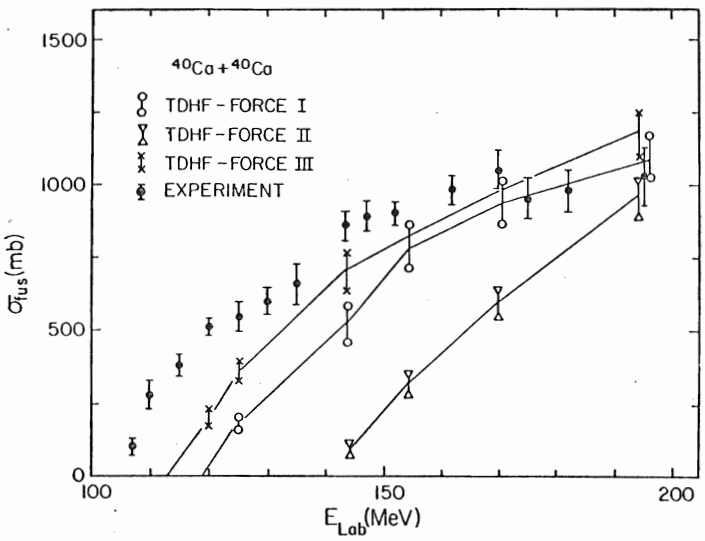

Fig.II.2. Comparaison des résultats expérimentaux sur la fusion $^{40}Ca+^{40}Ca$ aux prédictions théoriques de plusieurs calculs Hartree-Fock dépendants du temps. Cette figure est tirée de la référence [Bo 77].

IV - BILAN DES REACTIONS $^{40}Ca+^{40}Ca$ EN FONCTION DE L'ENERGIE.

La figure II.3, tirée de la référence [Ro78], illustre le bilan des réactions auxquelles donne lieu le système $^{40}Ca+^{40}Ca$, en fonction de l'énergie. Cette figure montre que jusqu'à 75 MeV

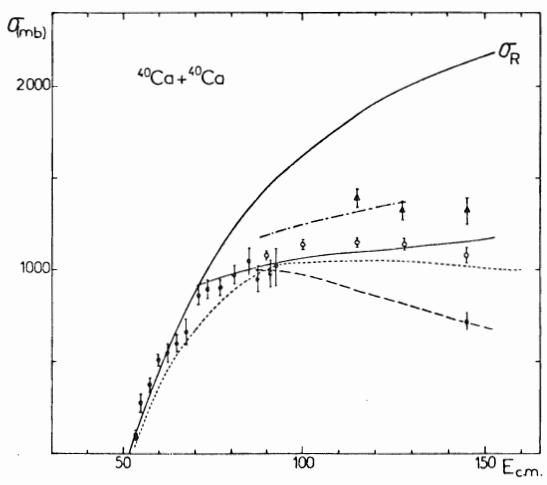

Fig.II.3. Bilan des réactions $^{40}Ca+^{40}Ca$ en fonction de l'énergie incidente. La section efficace totale de réaction apparaît en trait épais, le trait fin continu donne la section efficace de fusion. En tirets longs, la section efficace d'évaporation. En tirets courts, les prédictions de Gross et Kalinowski [Gr 77] pour la section efficace de fusion, et en tirets longs et courts, leur prédiction pour des réactions ayant $Q < -10$ MeV.

(c.m.) la quasi-totalité de la section efficace passe en formation du noyau composé. Au-delà de cette énergie, les processus très inélastiques apparaissent, tandis que la section efficace totale de fusion reste approximativement constante, ne dépassant que lentement la valeur de 1000 mb.

A une énergie donnée, on peut donc lire la part respective des différents processus. Nous faisons les deux remarques suivantes :

- les sections efficaces de formation de noyau composé et de processus très inélastiques que calculent Gross et Kalinowski [Gr 77] sont en bon accord avec nos résultats expérimentaux (de même qu'avec la section efficace totale de réaction que nous avons déduite de nos mesures de diffusion élastique)

- la part des processus quasi-élastiques (obtenue par soustraction) est très loin d'être négligeable (400 mb à 100 MeV, 750 mb à 150 MeV). Ce résultat surprend et est aussi difficile à contrôler expérimentalement. Il devrait être en particulier imputé aux réactions de type inélastique ou transferts de quelques particules, sans trop de dissipation d'énergie. Une telle proposition de processus inélastiques interdit certainement la présence d'une structure dans la voie élastique.

CHAPITRE III

EFFETS D'INTERFERENCE DANS LES FONCTIONS D'EXCITATION ET LES DISTRIBUTIONS ANGULAIRES DE LA DIFFUSION ELASTIQUE

I - INTRODUCTION.

L'absence totale de structure est un résultat tout à fait remarquable de l'étude de la diffusion élastique $^{40}Ca+^{40}Ca$. Avant de tirer des conclusions sur les propriétés des noyaux, l'influence de la masse ou de la charge des ions en présence sur l'allure des fonctions d'excitation peut être mise en cause. En essayant d'introduire quantitativement ces grandeurs dans l'analyse des données expérimentales, on est amené à décomposer l'amplitude de diffusion en composantes variant de façon monotone avec θ et E, auxquelles on peut attribuer une signification physique.

Considérons le développement bien connu de l'amplitude de diffusion élastique en ondes partielles :

$$f(\theta) = \frac{1}{2ik}\sum_{\ell}(2\ell+1)\ (S_\ell - 1)\ P_\ell(\cos\theta) = f_c(\theta) + f_N(\theta) = f_c(\theta) + \frac{1}{2ik}\sum_{\ell}(2\ell+1)\ e^{2i\sigma_\ell}(S_{\ell,N}-1)\ P_\ell(\cos\theta) \tag{1}$$

on peut envisager au moins trois types de décompositions.

a. Une décomposition angulaire : comme il a déjà été dit, cette décomposition apparaît sur la forme asymptotique des polynômes de Legendre :

$$P_\ell(\cos\theta) \simeq \left(\frac{1}{\pi(2\ell+1)\sin\theta}\right)^{1/2}\left\{e^{i[(\ell+\frac{1}{2})\theta - \frac{\pi}{4}]} + e^{-i[(\ell+\frac{1}{2})\theta - \frac{\pi}{4}]}\right\} \tag{2}$$

La nécessité d'une décomposition exacte, lorsque beaucoup d'ondes partielles, y compris des ondes partielles basses, contribuent, conduit Fuller [Fu 75] à écrire :

$$P_\ell(\cos\theta) = \tilde{Q}_\ell^{(+)}(\cos\theta) + \tilde{Q}_\ell^{(-)}(\cos\theta) \tag{3}$$

Fuller donne également la décomposition en ondes circulaires de l'amplitude coulombienne $f_c(\theta)$. On utilisera donc, suivant les cas :

$$f(\theta) = f^{(+)}(\theta) + f^{(-)}(\theta)$$

ou

$$f(\theta) = f_c^{(+)}(\theta) + f_N^{(+)}(\theta) + f_c^{(-)}(\theta) + f_N^{(-)}(\theta) \qquad (4)$$

b. Une décomposition "radiale" : il peut être utile de mettre en évidence le rôle joué par la barrière extérieure (coulombienne + centrifuge), et de l'opposer à celui de la partie la plus interne du potentiel. Ce type de décomposition s'est avéré intéressant dans l'étude semi-classique [Br 76] de l'anomalie de la diffusion élastique α-noyau à grand angle (A.L.A.S.). Dans ce cas, la décomposition porte sur la matrice S_N elle-même, que l'on écrit :

$$S_{N,\ell} = S_{N,\ell}^{(B)} + S_{N,\ell}^{(I)} \qquad (5)$$

ce qui définit les amplitudes "barrière" et interne par :

$$f_N^{B \text{ ou } I}(\theta) = \frac{1}{2ik} \sum_{\ell} (2\ell+1)\, e^{2i\sigma_\ell} \left(S_{N,\ell}^{B \text{ ou } I} - 1 \right) P_\ell(\cos\theta) \qquad (6)$$

On attribue arbitrairement l'amplitude coulombienne à la partie "barrière" de l'amplitude totale.

c. Une décomposition en fonction de la parité : évidemment sans objet dans le cas de particules identiques, elle a été appliquée récemment [Ga 77] au système $^{16}O+^{12}C$. Il est certainement intéressant de dissocier les contributions paire et impaire à l'amplitude de diffusion lorsque le potentiel d'interaction entre deux noyaux susceptibles d'échanger une particule α dépend de la parité du mouvement relatif [Vo 70]. Ceci ne pose aucun problème particulier.

Après quelques rappels, il est montré dans la première partie de ce chapitre comment la section efficace élastique résulte de l'interférence de deux ondes progressives, tournant en sens inverse, et on applique ce résultat à la compréhension des fonctions d'excitation élastiques à 90°. Dans la seconde partie, cette décomposition est poussée un degré plus loin, en séparant les rôles respectifs de la barrière et de la partie interne du potentiel.

Ces questions ont été abordées rapidement dans un article [Do 77d] que nous avons placé en annexe.

II - RAPPELS.

Il n'est peut-être pas inutile de rappeler ici les définitions de quelques termes empruntés à l'optique et fréquemment employés dans l'analyse des réactions par ions lourds. Il règne sur la signification de ces termes une certaine confusion, certainement due à la difficulté de séparer les phénomènes physiques qui leur donnent lieu. Les définitions présentées ici devraient au moins donner une certaine cohérence à ce qui suit.

Qualitativement, on désigne sous le nom de réfraction le changement de direction des trajectoires au cours de l'interaction : il est essentiellement dû au potentiel réel. La diffraction, au contraire, est surtout due à l'absorption plus ou moins rapide de l'onde qui passe à portée de la partie imaginaire du potentiel optique; plus généralement, elle a pour origine la région de l'espace où celui-ci varie rapidement.

La réfraction peut trouver une illustration simple dans la figure III.1 qui donne les trajectoires associées à différents paramètres d'impact. Dans le cas de trajectoires réfractées, il y a une correspondance entre l'angle de déflection et le paramètre d'impact.

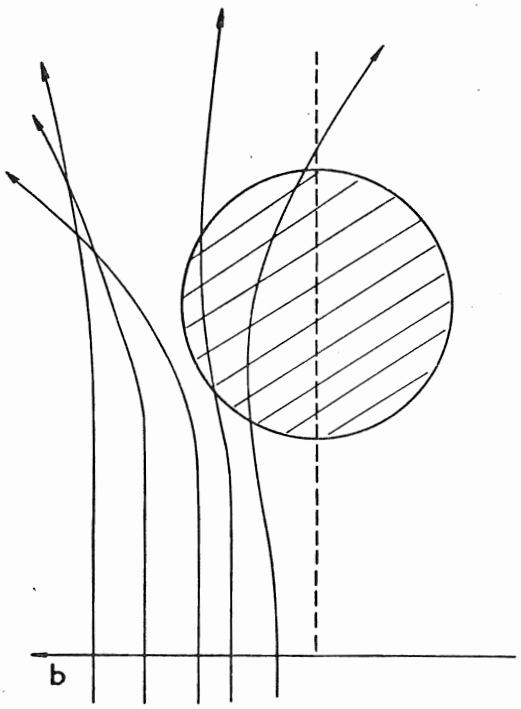

Fig.III.1. Illustration du phénomène de réfraction. Trajectoires dans le champ nucléaire en fonction du paramètre d'impact b.

Pour illustrer le phénomène de diffraction, il est commode d'introduire la décomposition de Poisson [Ro 76]. On sait que toute série peut être écrite [Mo 53] de la façon suivante :

$$f(\theta) = \sum_{\ell=0}^{\infty} f_\ell(\theta) = \sum_{n=-\infty}^{+\infty} f_m(\theta)$$

où la composante de Poisson d'ordre m, s'obtient par :

$$f_m(\theta) = \int_{-1/2}^{\infty} f_\ell(\ell)\ e^{2i\pi m\ell}\ d\ell$$

Cette expression permet la remarque suivante : une approximation semi-classique [Fo 59] souvent utilisée remplace la série d'ondes partielles par une intégrale sur ℓ :

$$f_{s.c} = \frac{1}{2ik} \int_{o}^{\infty} (2\ell+1)(S_\ell - 1)\ P_\ell(\cos\theta)\ d\ell$$

L'argument utilisé est ici le grand nombre d'ondes partielles qui participent à une réaction entre ions lourds ; on voit que cette approximation équivaut à ne garder que le seul terme

$m = 0$ de la série de Poisson. Rowley et Marty [Ro 76] ont montré que cette approximation n'est pas toujours justifiée.

Après la décomposition angulaire mentionnée au paragraphe III.1, on a besoin des composantes tournantes de Poisson :

$$f_m^{(\pm)}(\theta) = \int_{-1/2}^{\infty} f_\ell^{(\pm)} \, e^{2i\pi m\ell} \, d\ell$$

avec évidemment :

$$f^{(\pm)}(\theta) = \sum_{n=-\infty}^{+\infty} f_n^{(\pm)}(\theta)$$

Quand on calcule ces composantes par la méthode de la phase stationnaire, ou mieux par celle du col, on trouve qu'à chaque angle d'observation est associée une infinité de termes de Poisson correspondant à toutes les valeurs de m, positives ou négatives et dont l'angle de déflection vaut $(\pm\theta+2m\pi)$. La figure III.2 donne, pour un tel angle, quelques trajectoires associées ayant $m \geq 0$. On voit immédiatement que ces trajectoires subissent le phénomène de réfraction. Dès que m est plus grand que zéro, l'amplitude des contributions correspondantes va se trouver sévèrement atténuée par l'absorption.

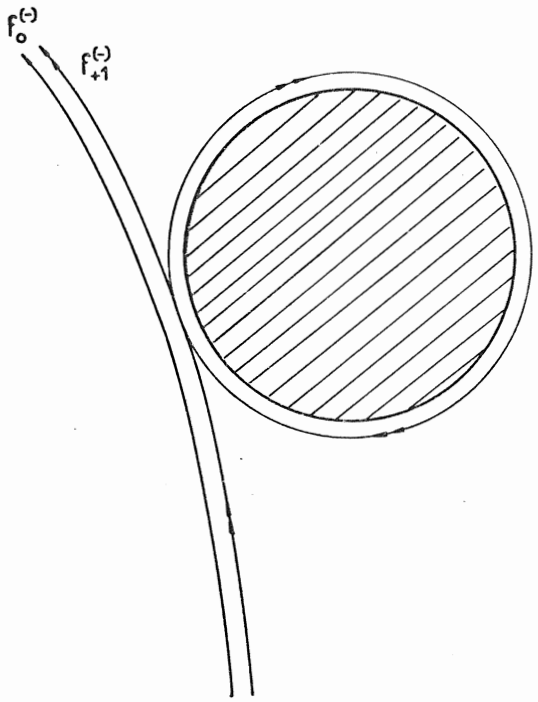

Fig.III.2. Deux composantes de Poisson de l'amplitude $f^{(-)}(\theta)$.

Par contre, on ne peut associer de trajectoires aux termes $m < 0$, qui correspondent à des déflections supérieures à π. Ces contributions sont le résultat des variations brusques des parties réelle et imaginaire du potentiel ; elles sont qualifiées de diffractives.

Pour calculer les différents termes de la décomposition de Poisson, il faut évaluer les intégrales sur l'axe réel:

$$f_m^{(\pm)}(\theta) \propto \frac{1}{(\sin\theta)^{1/2}} \int_o^{\infty} \lambda^{1/2} \, \exp[i\lambda(\pm\theta+2m\pi)] \, S_{\lambda-1/2} \, d\lambda$$

où l'on a posé $\lambda = \ell + 1/2$.

Les intégrales $f_m^{(\pm)}(\theta)$ peuvent souvent être commodément calculées ou estimées par déformation du contour d'intégration dans le plan complexe des moments angulaires. Ceci n'est évidemment possible que connaissant les propriétés analytiques de la matrice S associée à un potentiel complexe, en particulier ses pôles et ses zéros ainsi que son comportement lorsque $|\ell|$, où ℓ est maintenant complexe, tend vers l'infini. Ces propriétés ont été étudiées par Tamura et Wolter [Ta 72], et il est avantageux pour le calcul de $f_o^{(+)}$ et de $f_m^{(\pm)}$

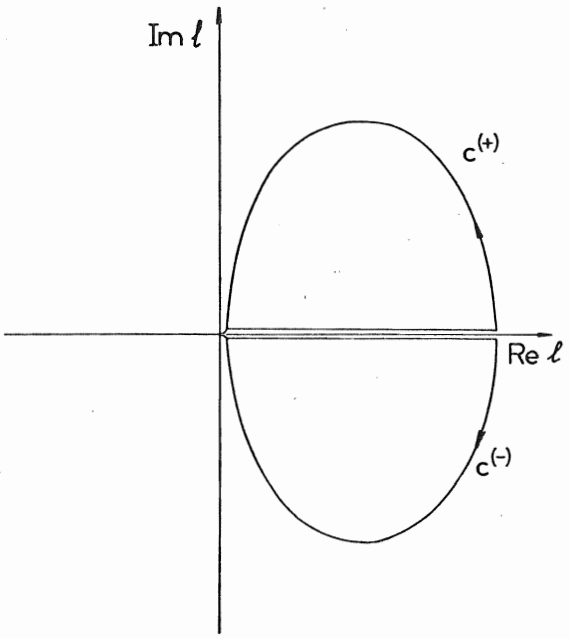

Fig.III.3. Contours d'intégration pour les composantes de Poisson de l'amplitude de diffusion.

lorsque m est positif d'ajouter au demi-axe Re $\ell > 0$, le contour $C^{(+)}$ situé dans le premier quadrant (fig.III.3). Tamura et Wolter ont montré que les pôles de S sont dans le premier quadrant. On trouve alors :

$$\left.\begin{matrix} f_m^{(\pm)} \\ f_o^{(+)} \end{matrix}\right\} = \int_{C^{(+)}} + 2\pi i \sum \text{Résidus}$$

où $\int_{C^{(+)}}$ désigne une intégrale de "background", que l'on ajoute à la contribution des pôles de Regge compris entre $C^{(+)}$ et l'axe réel. Il arrive souvent que la contribution due à l'un (ou quelques uns) de ces pôles soit dominante. Il en résulte alors, comme nous le verrons ci-après, des propriétés remarquables des amplitudes correspondantes. Les composantes $f_m^{(\pm)}(\theta)$, $(m<0)$, et $f_o^{(-)}$ pour lesquelles on utilise le contour $C^{(-)}$ n'ont qu'une contribution de background. Aucun pôle n'intervient dans leur évaluation.

En résumé, les pôles vont contribuer à $f^{(+)}(\theta)$ qui, sauf à l'arrière, est dominée par $f_o^{(+)}$. Le terme $f^{(-)}(\theta)$ peut également être modifié, par ses composantes $f_m^{(-)}$, avec $m > 0$, qui sont présentes aux angles arrière. Dans le cas d'une contribution dominante d'un pôle de Regge unique, la dépendance angulaire sera :

$$f_m^{(\pm)}(\theta) \propto \frac{1}{(\sin\theta)^{1/2}} e^{\pm (\mathrm{Re}\,\Lambda_p + i\,\mathrm{Im}\,\Lambda_p)\theta}$$

$$\propto \frac{1}{(\sin\theta)^{1/2}} e^{\mp(\mathrm{Im}\Lambda_p)\theta} \; e^{\pm i(\mathrm{Re}\Lambda_p)\theta}$$

La présence d'un tel pôle peut alors se reconnaître à une décroissance exponentielle de $\sin\theta\,|f^{(+)}(\theta)|^2$ sur un large domaine angulaire.

De tels pôles sont associés à des ondes de surface : celles-ci ont été introduites en optique [Le 59] sous le nom de trajectoires diffractées, et récemment utilisées par Mc Voy et son groupe [Mc 77] pour analyser les réactions induites par les ions lourds. Dans ce cas, un seul moment angulaire -complexe- est utilisé [Fu 73] : sa partie réelle repère l'onde partielle "active", tandis que sa partie imaginaire donne "l'angle de vie" à l'intérieur duquel l'onde est observable. On a bien, ici encore, un seul moment angulaire, donnant lieu à des trajectoires qui balaient tout un domaine angulaire : c'est le propre d'une composante diffractive.

III - DECOMPOSITION ANGULAIRE DE L'AMPLITUDE DE DIFFUSION.

L'objet de ce chapitre est de montrer que l'interférence entre les deux composantes $f^{(+)}(\theta)$ et $f^{(-)}(\theta)$ est à l'origine des oscillations observées à grand angle (au-delà de $\theta_{1/4}$) et aux énergies des accélérateurs tandem dans les distributions angulaires et les fonctions d'excitation élastiques.

Une méthode approchée due à Frahn [Fr 75,Fr 76] permet de suivre facilement le rôle des différentes quantités physiques. En particulier, on peut en déduire le rôle joué par la charge des noyaux sur la présence d'une structure. La méthode exacte de Fuller [Fu 75] est ensuite appliquée à la compréhension des fonctions d'excitation élastiques.

1. Méthode de Frahn.

Du calcul semi-classique que fait Frahn, il suffit de retenir que les composantes $f^{(+)}(\theta)$ et $f^{(-)}(\theta)$ sont obtenues par la formule :

$$f^{(\pm)}(\theta) = -\frac{i}{k(2\pi\sin\theta)^{1/2}} \int_{-\infty}^{+\infty} d\ell\,(\ell+\tfrac{1}{2})\, S(\ell)\, e^{\pm i[(\ell+\frac{1}{2})\theta - \frac{\pi}{4}]}$$

où $S(\ell)$ est ici la matrice S totale, sans séparation de la partie coulombienne. $S(\ell)$ est paramétrisée, et sa forme est rappelée dans la référence [Do 77b].

On voit rapidement que $f^{(+)}(\theta)$ reçoit sa principale contribution de la région $\ell = L$ où $|S(\ell)|$ varie rapidement dans une situation d'absorption forte, tandis que celle de $f^{(-)}(\theta)$ vient du moment angulaire ℓ_s qui conduit à la déflection θ (seule la composante de Poisson $m = 0$ est considérée, comme on le voit sur la formule ci-dessus). La nature des deux composantes apparaît donc différente : la première tire son origine du phénomène de diffraction, tandis que la seconde a un caractère plus réfractif. Frahn donne des expressions analytiques pour $f^{(\pm)}(\theta)$ qui sont asymptotiques, en ce sens qu'elles sont dérivées à la limite des grands L, ou des grands n.

Nous avons programmé ces expressions, et vérifié que les amplitudes des quantités $f^{(\pm)}(\theta)$ varient doucement avec l'angle et l'énergie. La différence de phase entre les deux composantes est très voisine de $[(2\ell+1)\theta+\pi]$ où L est la valeur de ℓ, autour de laquelle la la matrice S_N varie très rapidement. Cette différence de phase est fonction de l'angle d'observation : ceci est tout à fait cohérent avec l'observation expérimentale reproduite fig.I.1. Nous tirons de la référence [Do 77b] reproduite au chapitre II le tableau III.1 qui compare aux énergies des maximums de la fonction d'excitation, la valeur du moment angulaire rasant donnée par le modèle optique [Go 73] à celle pour laquelle les deux composantes sont en phase dans la théorie de Frahn.

Tableau III.1.

$\theta = 60°$	$E_{c.m.}$(MeV)	22.5		27.	35		43.5
	ℓ_{opt}	16.3		18.8	21.8		24.3
	ℓ_{Fr}	16		19.	22		25.
$\theta = 90°$	$E_{c.m.}$(MeV)	20	24.5	29	33.5	38.5	44.
	ℓ_{opt}	14.7	16.8	19.1	20.8	22.8	24.7
	ℓ_{Fr}	14.5	16.5	18.5	20.5	22.5	24.5

L'accord entre ces valeurs constitue un argument très fort pour l'interprétation de la structure expérimentale en termes d'interférence entre les deux termes $f^{(\pm)}(\theta)$.

2. Rôle de la charge et de la masse sur la présence d'une structure.

Les expressions analytiques que donne Frahn expliquent, sans qu'il soit besoin de faire appel à d'autres propriétés des noyaux, pourquoi il est de plus en plus difficile d'observer une structure dans les fonctions d'excitation lorsque la charge et la masse des ions en présence augmentent. En attribuant la structure à l'interférence des deux amplitudes $f^{(+)}(\theta)$ et $f^{(-)}(\theta)$, le rapport pic-sur-vallée (ou contraste) est donné par :

$$R(\theta) = \left| f^{(+)}(\theta) / f^{(-)}(\theta) \right| \qquad (7)$$

La variation de R(90°) avec l'énergie, lorsqu'on introduit dans le calcul les mêmes valeurs "raisonnables" des paramètres de la matrice S, a été calculée dans trois cas physiquement très intéressants : $^{16}O+^{16}O$, $^{28}Si+^{28}Si$ et $^{40}Ca+^{40}Ca$. Les résultats sont reportés sur la figure III.4, tirée de la référence [Do 77b]. On voit sur cette figure que :

- le rapport R(90°) est une fonction croissante de h
- la masse des noyaux intervient très rapidement pour diminuer R.

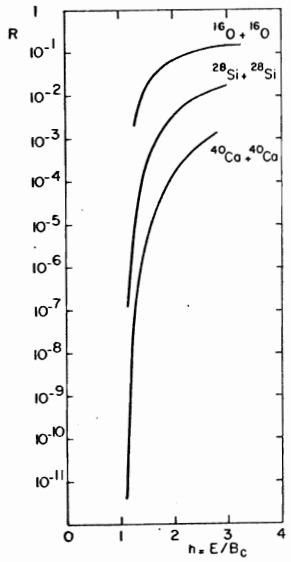

Fig.III.4. Rapport R des deux composantes $f^{(-)}(\theta)$ et $f^{(+)}(\theta)$, pour $\theta = \frac{\pi}{2}$ pour 3 systèmes typiques, en fonction du rapport de l'énergie incidente à la barrière coulombienne.

Les expressions analytiques de Frahn permettent de calculer le rapport R et de comprendre ces résultats. A une approximation d'autant meilleure que le système est lourd, R est donné par l'expression :

$$R = e^{-2\pi\Delta\theta_c} \qquad (8)$$

où θ_c est l'angle associé à la trajectoire de moment angulaire L, et Δ l'étalement de la matrice S_N dans l'espace du moment angulaire. On peut estimer [Do 77b] la quantité Δ pour un système d'ions identiques ayant A = 2Z

$$\Delta = 6.6\ 10^{-2}\ \frac{d(2h-1)}{[r_o(h-1)]^{1/2}}\ A^{4/3} \qquad (9)$$

avec

$$h = E/B_c \qquad (10)$$

La nature spécifique des noyaux considérés apparaît sur le seul paramètre d que Frahn relie à la diffusivité de la partie imaginaire du potentiel optique ; on voit qu'augmenter d contribue à atténuer l'amplitude des oscillations.

En résumé, tous les faits expérimentaux associés à l'observation d'une structure dans les fonctions d'excitation élastiques sont qualitativement reproduits par ce modèle. En particulier, le résultat essentiel, c'est-à-dire le contraste plus faible des oscillations lorsque la charge et la masse des ions en présence augmentent, est obtenu.

Cependant la faiblesse essentielle de la méthode de Frahn tient à l'utilisation d'une matrice S_N paramétrique. On sait que, dans le cas de systèmes comme $^{16}O+^{16}O$ ou $^{12}C+^{12}C$, les petites ondes partielles, par exemple, jouent un rôle essentiel. C'est la nécessité d'inclure ces contributions dans la matrice S_N qui conduit à préférer la méthode de Fuller [Fu 75] : la matrice S_N est beaucoup plus riche en informations (et elle reproduit mieux les résultats expérimentaux !).

3. La méthode de Fuller [Fu 75].

Elle remédie aux insuffisances de celle de Frahn, en permettant l'utilisation de n'importe quelle matrice S, quelle que soit sa complexité, et elle traite correctement toutes les ondes partielles, même les plus basses. Un code a été écrit par E.Plagnol qui permet le calcul des polynômes $\tilde{Q}_\ell^{(\pm)}$ et donne donc les composantes $f^{(\pm)}(\theta)$, par sommation sur les ondes partielles.

Quelques-uns des résultats les plus intéressants de la méthode seront d'abord illustrés par l'analyse d'une distribution angulaire. Celle-ci est obtenue à partir d'un potentiel optique dont les paramètres sont reportés sur le tableau III.2, etproposés par Siemssen [Si 71] pour le cas $^{16}O+^{16}O$ à $E_{c.m.} = 25$ MeV. Ici la symétrisation a été supprimée pour ne pas masquer des effets apparaissant au-delà de 90° (fig.III.5). Cette distribution angulaire peut être

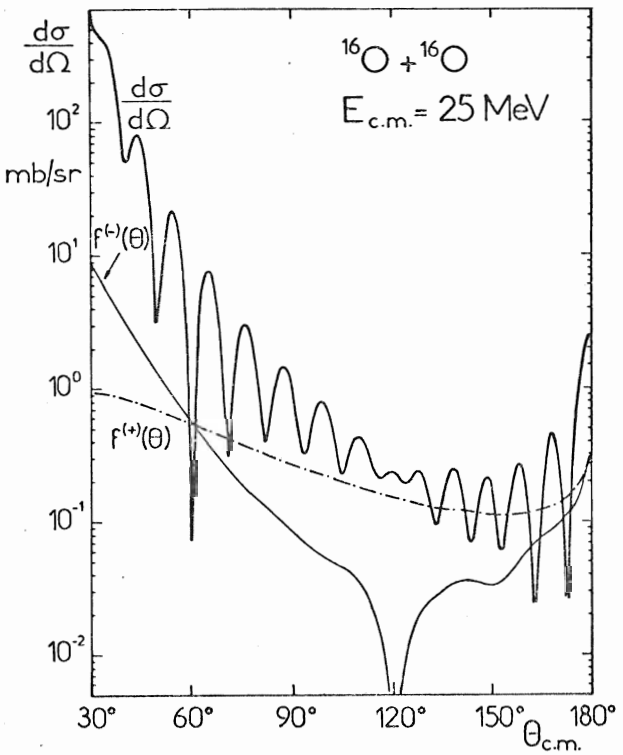

Tableau III.2.

	V(MeV)	r_R(fm)	a_r(fm)	W(MeV)	r_I(fm)	a_I(fm)
Siemssen	18.25	1.35	0.49	0.4+0.1 $E_{c.m.}$	1.35	0.49
Maher	17	"	"	0.4+0.1 $E_{c.m.}$	"	"
Gobbi	17	"	"	0.8+0.2 E	1.27	0.15

Tableau III.2. Potentiels optiques utilisés pour le système $^{16}O+^{16}O$.

Fig.III.5. Décomposition de l'amplitude de diffusion en composantes progressives $f^{(+)}(\theta)$ et $f^{(-)}(\theta)$. Illustration des phénomènes de diffraction de Fraunhofer ($\theta \simeq 60°$) et du phénomène de "glory" ($\theta \simeq 180°$).

décrite de la manière suivante :

- Tout à fait à l'avant, l'amplitude coulombienne l'emporte évidemment, et l'on a:

$$\left| \frac{f_c^{(+)}}{f_c^{(-)}} \right| \underset{\theta \to 0}{\sim} e^{-2\pi\eta}$$

Les deux amplitudes sont d'autant plus éloignées l'une de l'autre que le paramètre de Sommerfeld est grand.

- Le potentiel optique utilisé est un potentiel extrêmement transparent pour les ondes partielles de surface. L'influence du potentiel réel est donc ressentie et a pour résultat un déphasage réel non nul pour ces ondes qui donnent la contribution la plus importante à la section efficace. Ce déphasage réel se lit sur la figure III.5 à la différence très nette de pente observée pour $\theta < 90°$ entre les deux composantes $f^{(+)}(\theta)$ et $f^{(-)}(\theta)$.

- Comme les deux amplitudes se rapprochent, la figure d'interférence devient plus nette et est maximale à 60°. Ensuite $f^{(+)}(\theta)$ l'emporte sur $f^{(-)}(\theta)$ et décroît presque exponentiellement (on peut vérifier que $\log[\sqrt{\sin\theta}\,|f^{(+)}(\theta)|]$ décroît comme une droite). Les oscillations s'atténuent.

- Tout à fait à l'arrière, les deux composantes se rejoignent à nouveau et donnent lieu aux oscillations importantes qu'on appelle phénomène de "glory" ou "auréole" [Fo 59]. Ceci est attendu : on déduit en effet des propriétés analytiques des $\tilde{Q}_\ell^{(\pm)}(\cos\theta)$ que les amplitudes $f_N^{(+)}(\theta)$ et $f_N^{(-)}(\theta)$ sont égales à $\theta = \pi$, comme le sont $f_c^{(+)}(\theta)$ et $f_c^{(-)}(\theta)$.

Il est assez difficile de comprendre cette remontée de $f^{(-)}(\theta)$ à l'arrière. Il faut y voir l'influence prépondérante de la composante de Poisson $f_{+1}^{(-)}(\theta)$ tandis qu'à l'avant, seule $f_o^{(-)}(\theta)$ était importante [Ro 76].

Bien évidemment, une description en termes d'interférence doit étudier la phase de chaque composante. Celle-ci s'obtient aisément. Si l'on écrit [Fu 75] :

$$\tilde{Q}_\ell^{(\pm)}(\cos\theta) = |\tilde{Q}_\ell^{(\pm)}(\cos\theta)|\, e^{\pm i\phi_\ell(\theta)}$$

on a asymptotiquement :

$$\frac{d\phi_\ell}{d\theta} \sim \ell + 1/2$$

On peut, par extension, définir le moment angulaire emmené par chaque composante $f^{(\pm)}(\theta)$ comme étant la dérivée de sa phase par rapport à θ (dérivée obtenue numériquement). Les quantités associées $\ell^{(\pm)}$ sont reportées sur la figure III.6 pour l'exemple précédent. On remarque un comportement très différent des deux composantes et aussi que $f^{(+)}(\theta)$ emporte un moment angulaire pratiquement constant ($\ell = 18$) sur tout le domaine angulaire étudié. La situation considérée ici est un bel exemple où cette composante $f^{(+)}$ est dominée par un seul pôle, et est donc caractéristique d'une onde de surface. Pour $f^{(-)}(\theta)$, la contribution des ondes partielles les plus petites augmente avec l'angle de diffusion, ce qui est bien ce qu'on attend. A 120°, la composante $f_{+1}^{(-)}$ devient égale à $f_o^{(-)}$ et la phase est mal définie, mais $\ell^{(-)}$ remonte ensuite rapidement jusqu'à $\ell \simeq 19$, donc devient égale à $\ell^{(+)}$, ce qu'on attend pour une composante aussi périphérique de $f_{+1}^{(-)}$. C'est cette interprétation que nous avons transposée au cas des fonctions d'excitation.

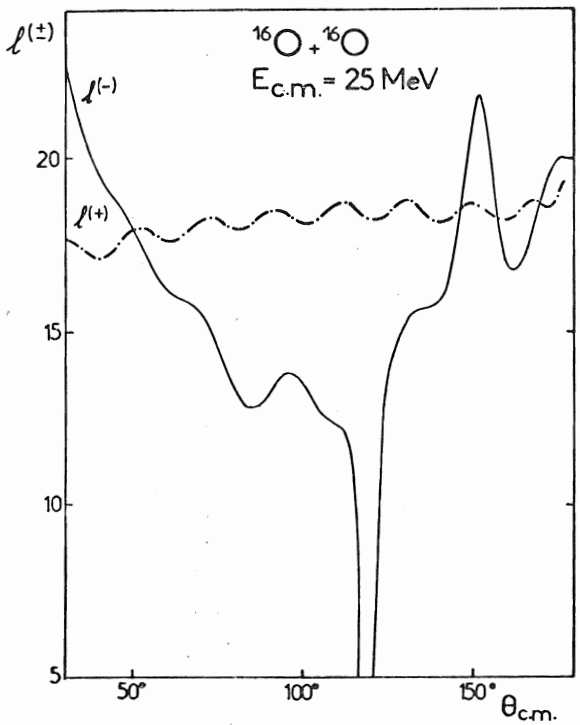

Fig.III.6. Moments angulaires associés aux composantes $f^{(+)}$ et $f^{(-)}$, en fonction de l'angle de diffusion.

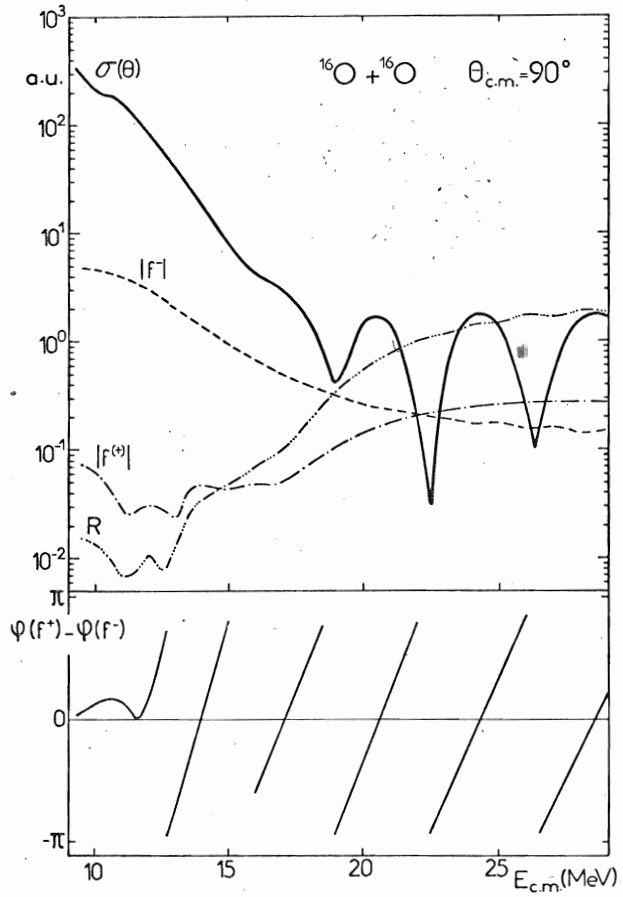

Fig.III.7. Décomposition de l'amplitude de diffusion, et amplitudes des composantes $f^{(\pm)}(\theta)$ en fonction de l'énergie dans le cas du système $^{16}O+^{16}O$, ainsi que leur différence de phase.

Nous présentons sur la figure III.7, sur le cas du système $^{16}O+^{16}O$, toutes les quantités dont nous avons besoin pour une description en termes d'interférence de la fonction d'excitation à 90°. Ces quantités ont été calculées avec le potentiel de Gobbi [Go 73] qui décrit au mieux l'ensemble des données du système $^{16}O+^{16}O$. On observe qu'à 90°, la composante $f^{(-)}$ décroît lentement en fonction de l'énergie. Ceci peut s'expliquer : nous verrons plus loin que $f^{(-)}$ résulte d'une interférence presque totalement destructive entre $f_c^{(-)}$ et $f_N^{(-)}$ car ces deux amplitudes sont toujours de modules presque égaux ; en supposant leur différence de phase constante avec l'énergie, on obtient pour $f^{(-)}(\theta)$ la même décroissance avec l'énergie que $f_c^{(-)}(\theta)$. Il n'en est pas de même pour la composante $f^{(+)}(\theta)$. Celle-ci doit contourner le noyau ; son amplitude croît lentement avec l'énergie car l'absorption est inversement proportionnelle à la vitesse relative des deux ions. Le maximum d'interférence est trouvé pour R = 1, c'est-à-dire à une énergie centre-de-masse $E_{c.m.} = 22.5$ MeV. Enfin, la différence de phase (calculée numériquement) entre $f^{(+)}$ et $f^{(-)}$ confirme entièrement cette description ; les minimums de section efficace étant observés lorsque cette différence de phase vaut π.

Ainsi la structure qui a été observée aux énergies tandem sur les différents systèmes de masse voisine de 16 peut être considérée comme le résultat d'une interférence entre les deux composantes $f^{(+)}$ et $f^{(-)}$. Nous avons montré, par la comparaison des trois systèmes $^{16}O+^{16}O$, $^{18}O+^{18}O$ et $^{40}Ca+^{40}Ca$ que les fonctions d'excitation à 90° (c.m.) par exemple, reproduisent cette interférence : le rapport pic-sur-vallée de la structure dépend des amplitudes respectives des deux composantes, et sa périodicité de leur phase relative. Cette comparaison a fait l'objet d'une lettre [Pl 77] que nous reproduisons ici.

INTERFERENCE EFFECTS IN THE ELASTIC SCATTERING EXCITATION FUNCTIONS OF IDENTICAL HEAVY-IONS

E.PLAGNOL, H.DOUBRE and C.MARTY

Institut de Physique Nucléaire, BP n°1, 91406 Orsay, FRANCE

INTERFERENCE EFFECTS IN THE ELASTIC SCATTERING EXCITATION FUNCTIONS OF IDENTICAL HEAVY-IONS

E. PLAGNOL, H. DOUBRE and C. MARTY
Institut de Physique Nucléaire[1], *91406 Orsay Cedex, France*

Received 24 November 1976
Revised manuscript received 28 February 1977

Gross structures, when present, in excitation functions of identical heavy ion systems are related to interference phenomena. This interpretation is valid in the framework of the optical model.

Recently, a large amount of work has been devoted to get further insight on the mechanisms leading to the observed heavy-ion elastic scattering cross sections. A common feature to these analyses has been to trace the occurrence of oscillations in the angular distribution back to some interference between two components of the scattering amplitude having different physical origin [1–3].

The aim of this paper is to apply such procedures to analyse the variation of the elastic cross section as a function of the energy and to show how a few simple arguments, based on interference effects, can explain the qualitative difference observed in the excitation functions of systems of different masses. As we restrict ourselves to identical heavy-ion systems ($^{16}O + {}^{16}O$, $^{18}O + {}^{18}O$, $^{40}Ca + {}^{40}Ca$), it is natural to look at excitation functions at 90° (center of mass) where symmetrization effects are trivial. In this analysis we use S-matrices obtained from optical model potentials which are considered to give the best fit to the experimental data (table 1). Results with parametric S matrices have already been reported [4–6].

On fig. 1a the excitation functions defined as the ratio of the differential cross section σ to the Rutherford one σ_R are shown for the three different systems as a function of the ratio $h = E/E_B$ of the incident energy E to the Coulomb barrier E_B as given by the optical model (cf. table 1). The behaviour of these excitation functions are different in nature:

(i) $^{16}O + {}^{16}O$ has its Rutherford value until $h \approx 1$. It then decreases relatively slowly until $h \approx 2$ where it displays the well known gross structure.

(ii) For low energy ($h \lesssim 2$) $^{18}O + {}^{18}O$ shows a variation very close to that of the latter system. However, for higher energies σ/σ_R continues to decrease and only for $h = 2.5$ some oscillations appear.

(iii) $^{40}Ca + {}^{40}Ca$ shows a very simple and different aspect. The excitation function diminishes very steeply from $\sigma/\sigma_R = 1$ for $h = 1$ to 10^{-7} for $h = 2$ where some oscillations are apparent. These structures lie in an energy region which, for this angle, has not been investigated experimentally.

[1] Division de Physique Théorique, Laboratoire associé au C.N.R.S.

Table 1
Values of the parameters of the optical-model potentials used for the calculations of all the quantities shown in the figures. Also indicated are the values of the Coulomb barrier (E_B).

	Real potential			Imaginary potential				
	V (MeV)	r_0 (fm)	a (fm)	V (MeV)	r_0 (fm)	a (fm)	E_B (MeV)	Ref.
$^{16}O + {}^{16}O$	17	1.35	0.49	$0.8 + 0.2E_{c.m.}$	1.27	0.15	10.33	[8]
$^{18}O + {}^{18}O$	17	1.35	0.49	$1.4 + 0.35E_{c.m.}$	1.35	0.57	9.97	[9]
$^{40}Ca + {}^{40}Ca$	35	1.35	0.49	12.13	1.35	0.43	52.27	[4]

107

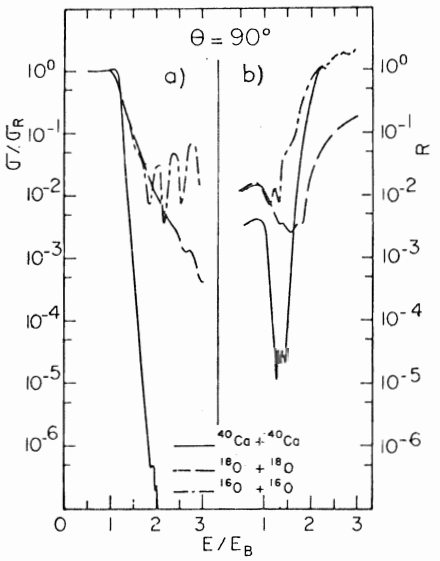

Fig. 1. Optical-model excitation function σ/σ_R and $R = |f^+/f^-|$ for $\theta = 90°$ for $^{16}O + ^{16}O$ (dot-dashed line), $^{18}O + ^{18}O$ (dashed line) and for $^{40}Ca + ^{40}Ca$ (full line) as a function of the ratio of the incident energy (c.m.) to the Coulomb barrier (E_B).

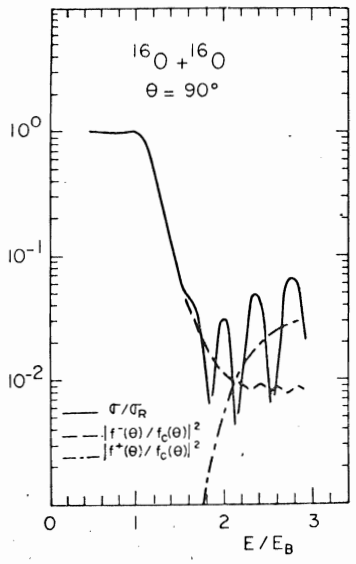

Fig. 2. Optical-model excitation functions σ/σ_R, $|f^+(\theta)/f_c(\theta)|^2$ and $|f^-(\theta)/f_c(\theta)|^2$ ($\theta_{c.m.} = 90°$) for $^{16}O + ^{16}O$ as a function of the ratio of the incident energy (c.m.) to the Coulomb barrier (E_B)

These behaviours have a common origin in the interference effects mentioned above. Following Fuller [1] the elastic amplitude $f(\theta)$ is split into two components:

$$f^{\pm}(\theta) = (2ik)^{-1} \sum_{l=0}^{\infty} (2l+1) S_l \widetilde{Q}_l^{\pm}(\cos\theta) \quad (\theta \neq 0 \text{ and } \pi). \tag{1}$$

Eq. (1), where S_l is the full S-matrix and k the wave number, is very similar to the standard partial-wave expansion of $f(\theta)$ except that the Legendre polynomials are replaced by the $Q_l^{\pm}$ as defined in ref. [1]. For large l values, $\widetilde{Q}_l^{\pm}(\cos\theta)$ behave like $\exp[\pm i(l+1/2)\theta]$ and therefore $f^{\pm}(\theta)$ represent the amplitudes corresponding to travelling waves turning one side or the other of the scattering potential [1–3].

Such an analysis is illustrated in fig. 2 where the excitation has been plotted versus h for $^{16}O + ^{16}O$. Also shown for $\theta = 90°$ are the ratios $|f^-(\theta)/f_c(\theta)|^2$ (dashed curve) and $|f^+(\theta)/f_c(\theta)|^2$ (dot-dashed curve) where $f_c(\theta)$ is the Rutherford amplitude. Several remarks can be made: (i) both components are smoothly varying with the energy, except for very small oscillations in $|f^-/f_c|$ at high energies. These oscillations have too small an amplitude to be the sole origin of the large diffractive pattern of the excitation function. Their origin will be discussed later. (ii) At low energies only f^- contributes significantly. (iii) For higher energies the components become of comparable importance so that the cross section which results from their interference shows strong maxima and minima. An immediate conclusion is that the existence of such gross structures is the signature of the relative importance of f^+ with respect to f^-. An interesting parameter to study is therefore $R = |f^+(90°)/f^-(90°)|$. On fig. 1b are plotted the variations of R as a function of h for the three systems studied. In all cases the qualitative behaviour of the ratio R is very similar. For $h < 1$ it begins to increase slowly until it reaches an energy ($h \approx 0.9$) where it decreases. After having reached a minimum value where some oscillations are present ($1 < h < 1.5$), R increases very strongly at first then seems to tend to some maximum value which depends on the system studied. If this maximum value is close to unity (as in $^{16}O + ^{16}O$) large oscillations in the excitation function are observed.

The simple framework adopted so far is not sufficient to explain the behaviour of R around its minimum value. It is then convenient to analyse each $f^{\pm}$ amplitude in terms of Poisson contributions defined

108

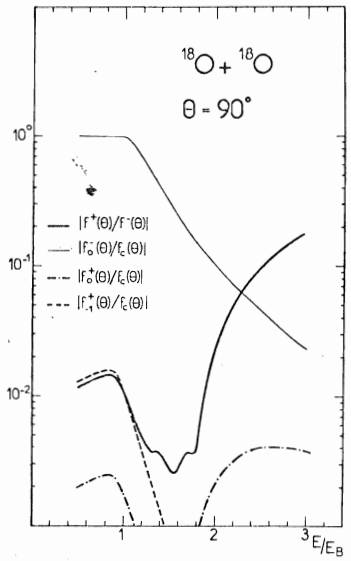

Fig. 3. Optical-model excitation functions ($\theta_{c.m.} = 90°$) of the different Poisson terms (for definition see text) which contribute to the cross section of $^{18}O + ^{18}O$, as a function of the ratio of the incident energy (c.m.) to the Coulomb barrier (E_B).

by [3] $f^{\pm}(\theta) = \Sigma_{m=-\infty}^{+\infty} f_m^{\pm}(\theta)$ where

$$f_m^{\pm}(\theta) = (2ik)^{-1} \int_{-1/2}^{\infty} (2l+1) S_l \widetilde{Q}_l^{\pm}(\cos\theta)\, e^{2i\pi m l}\, dl \qquad (2)$$

($\theta \neq 0$ and π).

Note that in eq. (2) S_l and $\widetilde{Q}_l^{\pm}$ have to be defined for non-integer l values. This is trivial for $\widetilde{Q}_l^{\pm}$. For S_l one can either use an interpolation method or solve the Schrödinger equation for the corresponding l value, using Wolter's code [7] for instance. For $^{16}O + ^{16}O$ at 25 MeV (c.m.) it has been checked that both methods give similar results, so the former one has been used throughout this letter.

Fig. 3 shows how the moduli of the leading Poisson terms, relative to f_c, vary as a function of h for the $^{18}O + ^{18}O$ system. All the $f_m^{\pm}/f_c$ not reported in this figure were found to be of negligible importance. At low energies f_0^- reproduces very closely the full scattering amplitude. The only contribution to f^+ comes from f_{-1}^+, as expected [11]. Just below the barrier ($h \approx 0.9$) f_{-1}^+ begins to decrease (and consequently R) due to the onset of nuclear scattering. As nuclear attraction sets in, the deflection to small negative angles increases giving therefore an important contribution to f_0^+. Although f_0^- decreases (due to the absorption or/and the attractive nature of nuclear interaction), it retains its smooth behaviour. When f_0^+ reaches values comparable to f_{-1}^+, oscillations are observed in R. For still higher energies f_0^+ becomes the leading term in f^+ and R increases. Apart from details due to the potentials involved, this description of the variation of R is valid for the three systems studied. It has also been checked for $^{16}O + ^{16}O$ that the small f^- oscillations of fig. 2 are not due to interferenee between Poisson terms, but are genuine oscillations of f_0^- due to interference between low partial waves.

In view of these results one can analyse and compare the excitation functions (fig. 1a) of the three systems. A comparison between $^{16}O + ^{16}O$ and $^{18}O + ^{18}O$ shows that in both cases the f_0^- are very nearly identical whereas the f_0^+ differ, over most of the energy range, by an order of magnitude. This difference is related, in terms of the optical model, to the variation of the imaginary component of the potential (cf. table 1) and is responsible for the difference observed in the excitations functions. Due to the important absorption in $^{18}O + ^{18}O$, the flux in the elastic channel is lowered as the angle of deflection increases, thus reducing the importance of f_0^+. Inversely, for $^{16}O + ^{16}O$, a more transparent imaginary potential produces a greater sensitivity to the nuclear attraction. The comparison between $^{16}O + ^{16}O$ and $^{40}Ca + ^{40}Ca$ offers a different view of the scattering mechanism. Indeed for the two systems R reaches a value close to unity for $h \approx 2$. However, for the latter system the cross-section has diminished by seven orders of magnitude between $h = 1$ and 2. This strong decrease of f_0^- and f_0^+ is a very general feature of heavy ion scattering and is contained even in the simplest models as the sharp cut-off one (see for instance [10]).

In conclusion the aim of this letter is to exhibit the interference effects on the excitation functions of heavy ions. These interferences are due to two smoothly varying amplitudes $f^+(\approx f_0^+)$ and $f^-(\approx f_0^-)$. This is particularly sensitive for the $^{16}O + ^{16}O$ case where the two components are of comparable importance for high energies giving rise to the observed gross structure.

We thank Drs. N. Rowley and J.C. Roynette for many interesting and helpful suggestions. We are espe-

cially indebted to Dr. H. Wolter who kindly provided us with values of the S matrix for non integer l.

References

[1] R.C. Fuller, Phys. Rev. C12 (1975) 1561.
[2] W.E. Frahn, in: Heavy-ion, high-spin states and nuclear structure (IAEA, Vienna, 1975) p. 157.
[3] N. Rowley and C. Marty, Nucl. Phys. A266 (1976) 494.
[4] H. Doubre et al., submitted to Phys. Rev. C.
[5] H. Doubre et al., Europ. Conf. on Nuclear physics with heavy-ions, Caen, 6–10 September 1976, p. 16.
[6] W.E. Frahn, Lett. Nuovo Cim. 1 (1971) 561; W.E. Frahn and K.E. Rehm, Europ. Conf. on Nuclear physics with heavy-ions, Caen, 6–10 September 1976, p. 8.
[7] T. Tamura and H.H. Wolter, Phys. Rev. C6 (1972) 1976.
[8] A. Gobbi et al., Phys. Rev. C7 (1973) 30.
[9] R.W. Shaw, Jr., R. Vandenbosch and M.K. Mehta, Phys. Rev. Lett. 25 (1970) 457.
[10] J.R. Birkelund et al., Phys. Rev. C13 (1976) 133.
[11] N. Rowley, private communication.

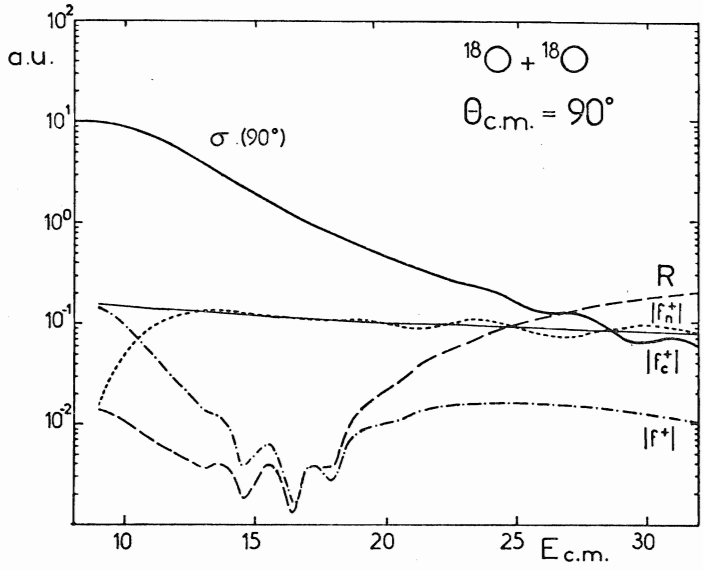

Fig.III.8. Décomposition de l'amplitude de diffusion, en fonction de l'énergie incidente, pour le système $^{18}O+^{18}O$. Le potentiel utilisé est celui de la référence [Va 71].

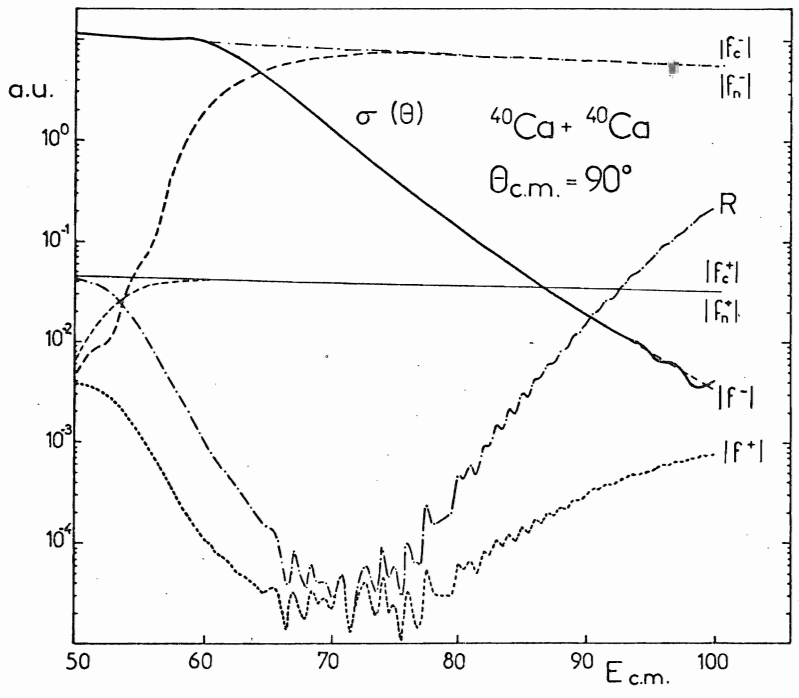

Fig.III.9. Même chose que la figure III.8, pour le système $^{40}Ca+^{40}Ca$, avec le potentiel de la référence [Do 77b].

On peut détailler ces résultats en montrant, sur les figures III.8 et III.9, le comportement en fonction de l'énergie de toutes les quantités qui entrent dans cette description pour les systèmes $^{18}O+^{18}O$ et $^{40}Ca+^{40}Ca$. La similarité des comportements est frappante. Lorsque l'énergie dépasse assez largement celle de la barrière coulombienne, on constate qu'à grand angle les termes $f^{(+)}(\theta)$ et $f^{(-)}(\theta)$ sont l'un et l'autre le résultat d'une interférence presque totalement destructive entre leurs propres composantes coulombiennes et nucléaires. Mais surtout on remarque que l'influence de l'absorption se lit sur la composante $f^{(+)}$. Si le système n'est pas trop absorbant, cette composante croît avec l'énergie. Dans le cas de $^{18}O+^{18}O$, cette remontée n'est observée que sur quelques MeV, puis $f^{(+)}$ atteint un maximum et décroît de nouveau.

Il apparaît maintenant clairement que le phénomène de structure sur les fonctions d'excitation élastiques, aux énergies étudiées, relève uniquement de l'interférence entre les deux composantes $f^{(+)}(\theta)$ et $f^{(-)}(\theta)$. Les différences qui sont trouvées expérimentalement entre les systèmes résultent donc des conditions particulières dans lesquelles cette interférence se produit. L'interprétation proposée traduit mathématiquement le terme de "diffraction", souvent employé, et permet de préciser le rôle attribué à la nature des noyaux qui participent à la collision.

IV - DIFFRACTION DE FRAUNHOFER, DE FRESNEL, BATTEMENTS... ET DIFFUSION ELASTIQUE.

Trois types d'interférence peuvent se rencontrer en diffusion élastique, qui sont schématisés sur la figure III.10 (tirée de [Do 77d]).

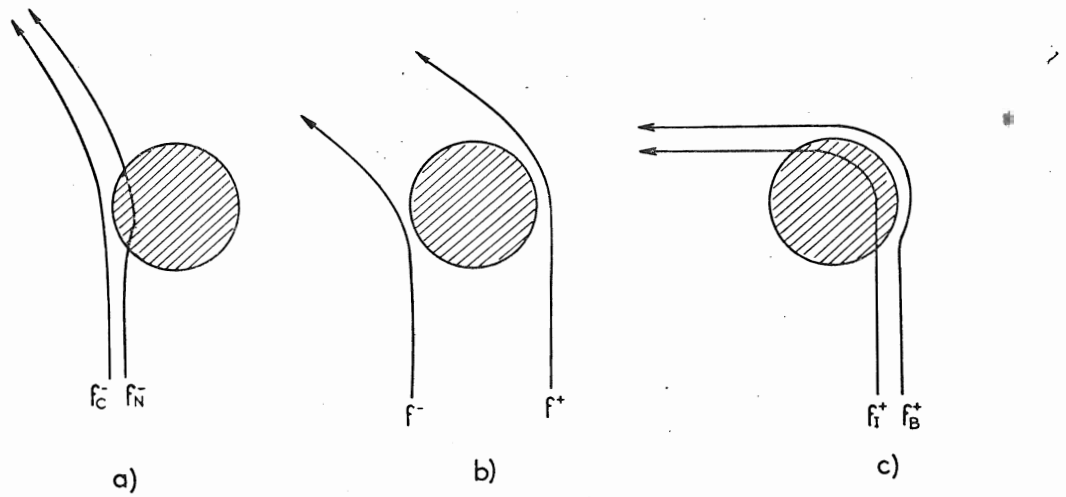

Fig.III.10. Trois décompositions de l'amplitude de diffusion élastique. Cette figure est tirée de la référence [Do 77d].

1. Diffraction de Fraunhofer.

Nous venons de voir que l'interférence entre les deux composantes $f^{(+)}(\theta)$ et $f^{(-)}(\theta)$ est responsable de la structure observée à grand angle, dans les fonctions d'excitation élastiques. Elle correspond au schéma b). On a gardé le nom de diffraction de Fraunhofer pour cette interférence, par analogie au phénomène optique de diffraction à l'infini dû à une sphère opaque. On rappelle que dans ce cas [Br 72], la période des oscillations d'une distribution angulaire est voisin de :

$$\Delta\theta = \pi/L_c$$

où L_c est le moment angulaire rasant.

2. Diffraction de Fresnel.

On a gardé aussi pour la situation a) le nom de diffraction de Fresnel. Elle est évidemment observée dans le cône $\theta < \theta_{1/4}$. On peut montrer [Fu 77] qu'elle résulte de l'interférence :

$$f(\theta) = f_c(\theta) + f_N(\theta)$$

où $f_c(\theta)$ est l'amplitude de Coulomb et où l'amplitude nucléaire (obtenue par différence) est bien décrite par un polynôme de Legendre de degré complexe $P_\alpha(\cos\theta)$ comme on l'observe sur la figure III.11. La partie réelle de α est proche du moment angulaire rasant. Comme on le voit sur la figure III.11, ces deux composantes sont, à l'angle $\theta_{1/4}$, en opposition de phase :

$$f_c = -2f_N$$

et elles le demeurent à plus grand angle. Aux angles plus petits que $\theta_{1/4}$, cette différence de phase varie comme

$$(\ell_N - \ell_c)\theta = (\alpha_r - n \cot g\frac{\theta}{2})\theta$$

où ℓ_N et ℓ_c sont les moments angulaires des composantes f_N et f_c. D'où la périodicité des oscillations observées sur σ/σ_{Ruth}

$$\Delta\theta = 2\pi/\mathrm{Re}(\alpha)$$

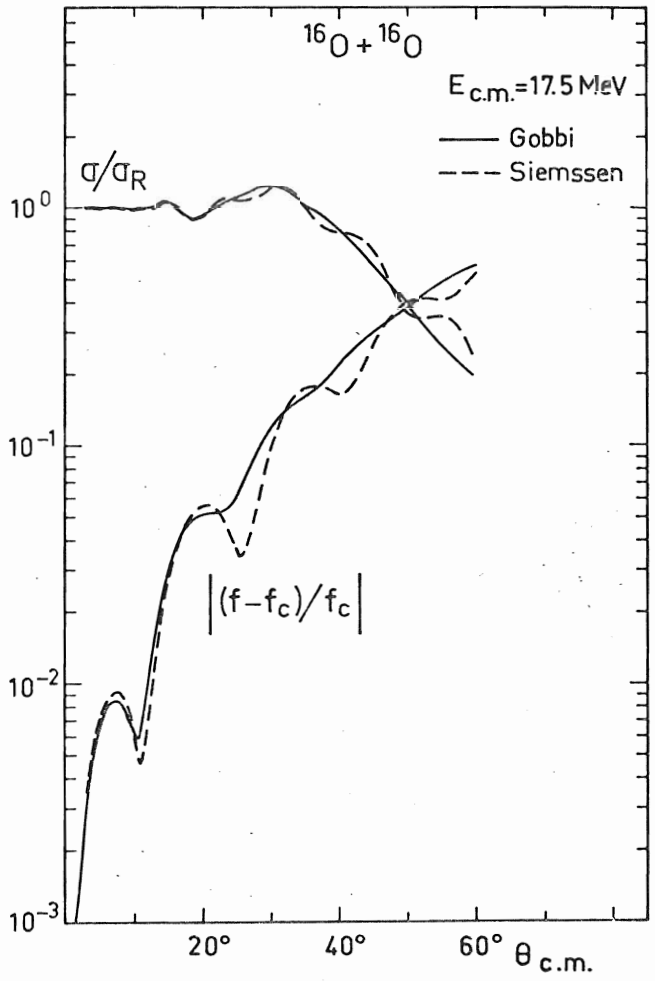

Fig.III.11. Décomposition de l'amplitude de diffusion à l'avant. Mise en évidence d'une composante "nucléaire".

3. Battements à grand angle.

Ces battements correspondent au cas c) de la figure III.10. Dans ce cas, les deux composantes considérées contournent toutes deux le noyau. Les composantes correspondantes de $f^{(-)}(\theta)$ ont alors une amplitude beaucoup trop faible pour apparaître dans l'amplitude de diffusion : un tel phénomène n'aura donc lieu qu'aux angles bien supérieurs à l'angle d'absorption forte, c'est-à-dire dans une région classiquement interdite. A de tels angles, nous montrons plus bas que la contribution des petites ondes partielles est loin d'être négligeable, et peut considérablement distordre une distribution angulaire.

C'est cette situation que nous étudions maintenant.

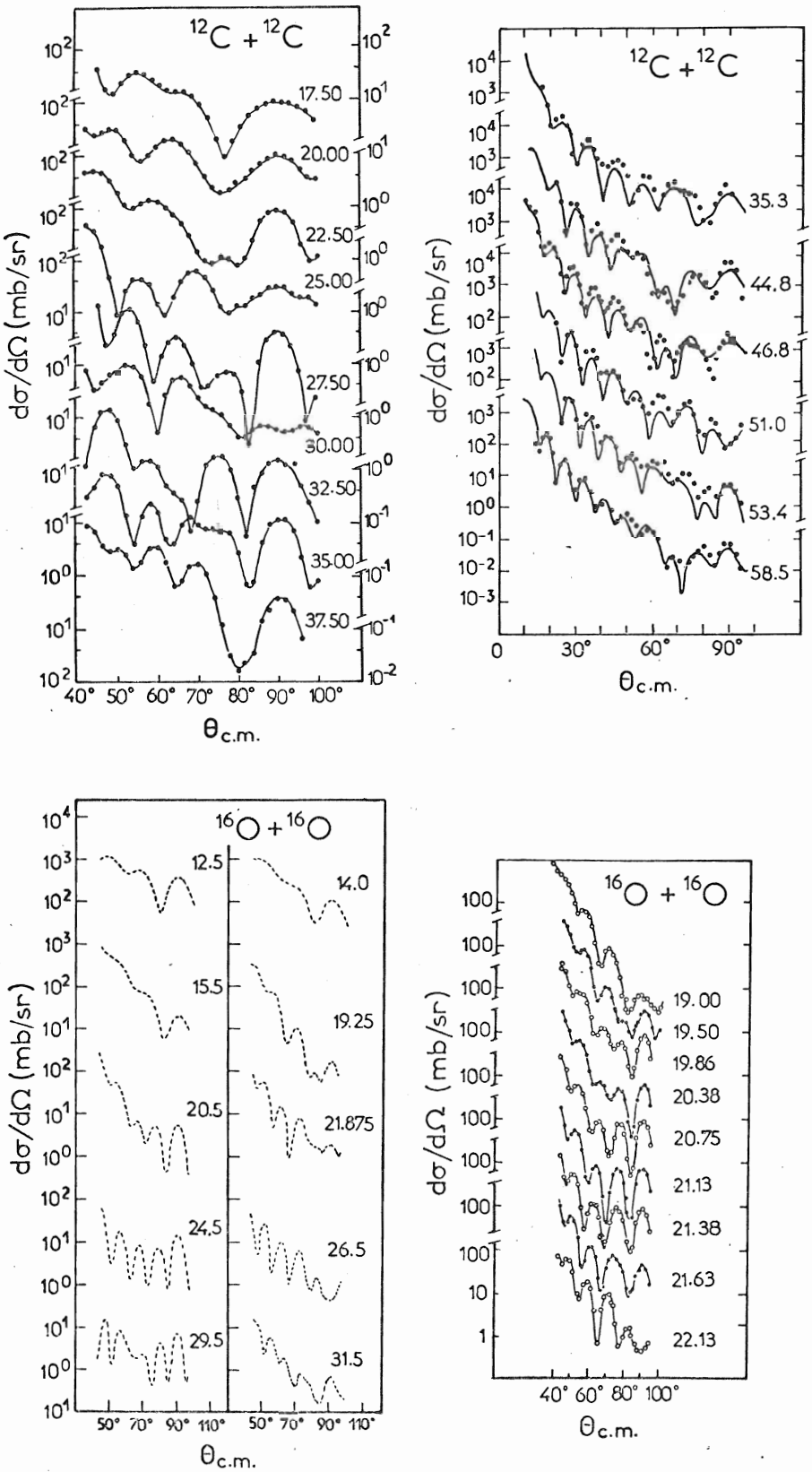

Fig.III.12. Distributions angulaires des systèmes $^{12}C+^{12}C$ et $^{16}O+^{16}O$, montrant que l'existence d'un minimum à 90° est un fait expérimental relativement peu fréquent. Les données sont tirées des références [Ma 69],[Re 73] et [Wi 76].

V - ALLURE DES DISTRIBUTIONS ANGULAIRES AU VOISINAGE DE 90° DANS LE CAS DE BOSONS IDENTIQUES.

1. Présentation du problème.

Cette étude de l'influence de la symétrie de la voie d'entrée sur les distributions angulaires part de la constatation suivante : de toutes celles publiées par Maher et al. [Ma 69], seules deux distributions angulaires, à 22.5 MeV et 26.5 MeV c.m., présentent un minimum à 90° dans le cas du système $^{16}O+^{16}O$. Dans le cas du système $^{12}C+^{12}C$ [Re 73], une distribution angulaire, à 30 MeV c.m., présente un minimum très aplati à 90° ; à $E_{c.m.} = 52$ MeV, Wieland et al. [Wi 76] ont trouvé un minimum très prononcé. La situation expérimentale est résumée sur la figure III.12.

Non seulement, en diffusion élastique d'ions lourds, ce phénomène s'observe uniquement à quelques énergies bien définies, mais encore il est très difficile de le reproduire lorsqu'on utilise des potentiels optiques "classiques" de type Saxon-Woods. Ainsi le potentiel de Yale [Re 73a] ne reproduit pas le minimum à 30 MeV du système $^{12}C+^{12}C$. Pour obtenir le minimum trouvé expérimentalement à $E_{c.m.} = 52$ MeV, Wieland et al.[Wi 76] ont dû donner au potentiel optique une partie réelle de profondeur voisine de 500 MeV. Dans le cas $^{16}O+^{16}O$, le potentiel de Gobbi [Go 73], pourtant reconnu excellent sur un large domaine d'énergies, prédit le minimum à 22.25 MeV, mais pas le suivant à 26.5 MeV. La figure III.13 donne les sections efficaces non symétrisées et symétrisées que prévoit le potentiel de Gobbi au voisinage de ces deux énergies. Cette figure montre que les situations physiques diffèrent dans les deux domaines d'énergie. Ceci se vérifie également sur la figure III.14 où la fonction

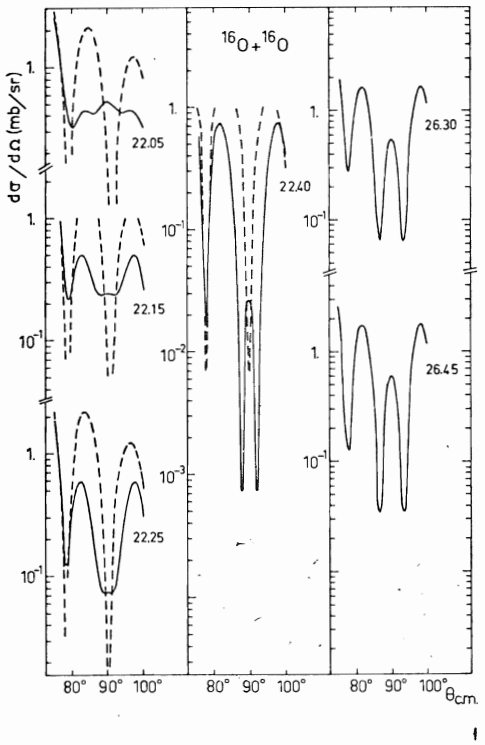

Fig.III.13. Prédictions du potentiel de Gobbi pour le système $^{16}O+^{16}O$: distributions angulaires symétrisées et non symétrisées au voisinage de 90°.

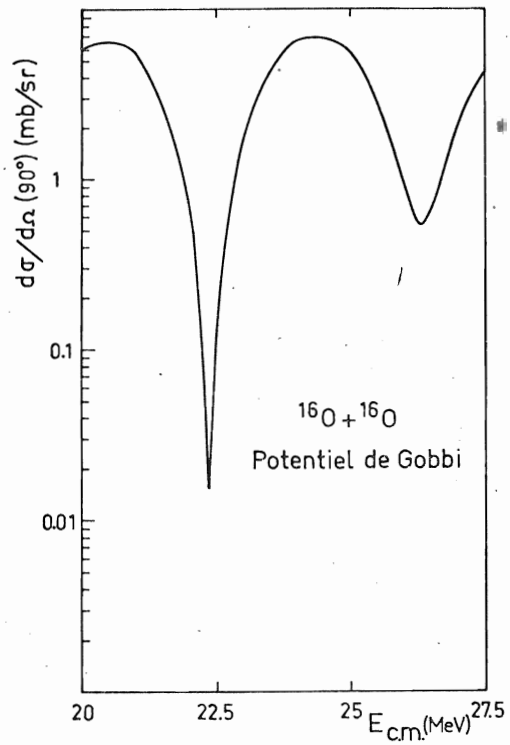

Fig.III.14. Prédictions du potentiel de Gobbi pour la fonction d'excitation à 90° du système $^{16}O+^{16}C$

d'excitation à 90° c.m. calculée tous les 50 keV dans le c.m., montre nettement quel pas en énergie est compatible avec l'étude de la diffraction.

Le problème posé par le système $^{12}C+^{12}C$ à $E_{c.m.} = 51.05$ MeV a d'abord été étudié, car un potentiel optique est connu, qui reproduit les résultats expérimentaux. Cette étude a fait l'objet d'une lettre [Ro 77a] insérée ci-dessous.

2. Le cas $^{12}C+^{12}C$ à $E_{c.m.} = 51$ MeV.

LOW PARTIAL WAVES IN $^{12}C+^{12}C$ ELASTIC SCATTERING

N.ROWLEY

Department of Applied Mathematics and Theoretical Physics,
University of Liverpool, P.O.Box 147, Liverpool L69 3BX, UK.

and

H.DOUBRE and C.MARTY

Institut de Physique Nucléaire, BP n°1, 91406 Orsay, FRANCE

LOW PARTIAL WAVES IN $^{12}C + ^{12}C$ ELASTIC SCATTERING

N. ROWLEY
Department of Applied Mathematics and Theoretical Physics, University of Liverpool, P.O. Box 147, Liverpool L69 3BX, UK

and

H. DOUBRE and C. MARTY[1]
Institut de Physique Nucléaire, 91406 Orsay Cedex, France

Received 1 April 1977

A correlation between minima at 90° in the angular distributions and deep minima in the 90° excitation functions for the elastic scattering of identical light ions is noted. In the case of $^{12}C + ^{12}C$ at $E_{c.m.} = 51$ MeV, it is shown that the low partial waves are essential to reproduce this effect.

The particular interest of the elastic scattering of identical particles is that information on the phase of the amplitude is available from the interference of $f(\theta)$ with $f(\pi - \theta)$. This information may be useful in removing the usual optical-model ambiguities. In the case of spin-0 bosons the above amplitudes always interfere constructively at 90°. The cross section at this angle will therefore possess an extremum which might be expected to be a maximum, unless the non-symmetrised amplitude itself possesses a minimum at 90°. If we write the unsymmetrised amplitude as $|f(\theta)| \exp i\phi(\theta)$, the symmetrised cross section $\sigma(\theta)$ near 90° reads

$$\frac{\sigma(\pi/2) \pm \epsilon))}{\sigma(\pi/2)} = 1 + \epsilon^2 \left[\frac{|f|''}{|f|} - \phi'^2\right]_{\theta=\pi/2},$$

where the primes denote differentiation with respect to θ. We see, therefore, that the bigger ϕ'^2 is, the less likely we are able to observe a minimum. In heavy ion reactions, the phase will indeed vary rapidly, ϕ' being of the order, for example, of the grazing angular momentum l_g [1, 2]. In this case, it will only be possible to find a minimum in $\sigma(\theta)$ at 90° if $|f|$ itself is very small, i.e. if the non-symmetrised amplitude possesses a deep interference minimum and the cross section is very small. We are therefore more likely to find such minima at energies where the 90° excitation function possesses a pronounced minimum.

A study of $^{12}C + ^{12}C$ [3, 4] and $^{16}O + ^{16}O$ [5, 6] elastic scattering over a large range of energies produces a total of only 4 examples of minima in $\sigma(\theta)$ at 90° and each case does correspond to a very deep minimum in the excitation function: $E_{c.m.} = 30$ and 51 MeV for ^{12}C and $E_{c.m.} = 22.1$ and 26.5 MeV for ^{16}O. In the case of α--α scattering [7], minima in $\sigma(\theta)$ at 90° are more frequent since ϕ'^2 is much smaller (smaller l_g) than for $^{12}C + ^{12}C$ or $^{16}O + ^{16}O$.

Wieland et al. [4] have obtained reasonable fits to the cross section for $^{12}C + ^{12}C$ elastic scattering over a large energy range, including the 51 MeV case mentioned above. This latter energy is about 7 times the barrier height and corresponds to a Sommerfeld parameter of 1.95. The above authors claim that their fit requires a deep real potential (about 500 MeV at the origin) which was obtained by a folding procedure due to Satchler and Love [8]. Their attempts to use a conventional Saxon-Woods potential were successful up to about 60° but between 60° and 90° the oscillatory structures were not reproduced. It is clear then that this folded potential gives a contribution to the scattering amplitude which is not present in a conventional analysis.

Reading the real potential from ref. [4], welhave calculated the elastic S-matrix $S_l = \eta_l \exp(2i\delta_l)$ at 51 MeV and observed that the above contribution is due to the non-negligible presence of low partial

[1] Division de Physique Théorique, Laboratoire associé au C.N.R.S.

119

waves. This incomplete absorption arises because the deep real potential gives a large relative velocity in the nuclear interior. The effect of these partial waves was confirmed by a calculation in which they were suppressed by strongly increasing the imaginary potential in the nuclear interior while leaving it unchanged near and outside the barrier. So long as the imaginary potential is sufficiently strong inside, such a procedure gives an S-matrix S_B which is *independent* of the potential in the nuclear interior and can therefore be solely attributed to reflection at the external potential barrier. The part S_I of the S-matrix which is suppressed by this procedure can be attributed to the flux which enters the nuclear interior and leaves again after a single or multiple reflections [9]. In fig. 1, we show for these two parts of the S-matrix the reflection coefficients η_l and the deflection function

$$\Theta_{l+1/2} = 2(\delta_{l+1} - \delta_l) + \Theta^c_{l+1/2},$$

where $\Theta^c_{l+1/2}$ is the Coulomb deflection function [10] defined similarly. The barrier contribution is seen to be a typical strong-absorption S-matrix [2, 11]. It is totally insensitive to the nuclear interior and the potentials which give this S-matrix are subject to the usual continuous ambiguities. It is also responsible for the typical Fraunhofer diffraction oscillations observed at forward angles. As noted in ref. [4], the conventional Saxon-Woods potential also fits the cross sections up to about 60° and this is because it gives the barrier part of the above S-matrix. The folded potential, however, also gives the internal contribution which is responsible for the oscillations at large angles. Note that η_l is actually rather small for S_I, and that since we will be discussing the non-symmetrised scattering amplitude, we have shown both even and odd partial waves.

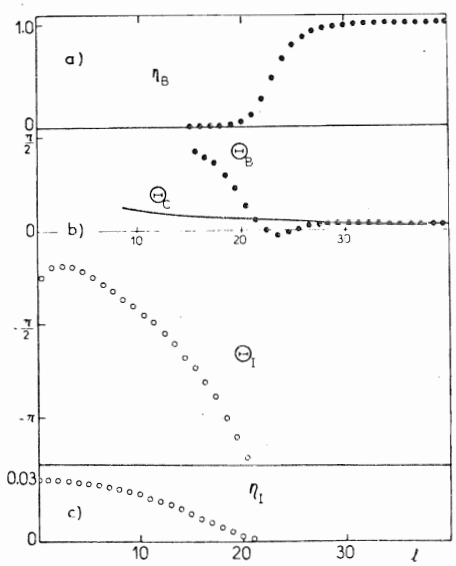

Fig. 1. Decomposition of the S-matrix into barrier and internal contributions: (a) and (c) show the respective reflection coefficients (note the exaggerated scale of η_I) and (b) shows the corresponding deflection functions (as defined in the text) along with that for pure Coulomb scattering.

The appealing feature of the above decomposition is that each of the contributions to the S-matrix is smooth and well-behaved. This is not necessarily true of the sum, in the region of their overlap ($l \approx 20$), due to the rapid variation of their relative phase. We might therefore expect each part of the S-matrix to give a smoothly varying contribution to the scattering amplitude which will make the origin of the interference structure in the cross section more evident.

Although the folded potential is very successful in fitting the data, it is not expected to be good in regions of large overlap and we physically do not expect so deep an internal potential. We can ask then if it is possible to change this part of the potential and still obtain the same internal contribution (low partial waves) to the scattering amplitude.

Intuitively the absorption $A(r)$ at the point r is proportional to the absorptive potential and inversely proportional to the instantaneous relative velocity

$$A(r) \propto \frac{W(r)}{\sqrt{2m(E_{\mathrm{c.m.}} + |U(r)| - V_c - V_l)}},$$

where $V(r) = U(r) + iW(r)$ is the nuclear potential, V_c and V_l are the Coulomb and centrifugal potentials and m is the reduced mass. Since the real potential we are considering is so deep in the interior, we can neglect the centrifugal and Coulomb terms and the incident energy to obtain $W^2/U \approx$ constant as an approximate condition for constant absorption. We modified the interior with the form factors g_U and g_W giving

$$\tilde{U}(r) = U(r)\,g_U(r) = U(r)\left(\frac{1 + \beta_U\, e^{-(r-R)/a}}{1 + e^{-(r-R)/a}}\right)^2$$

$$\widetilde{W}(r) = W(r)\, g_{W'}(r) = W(r)\, \frac{1 + \beta_W e^{-(r-R)/a}}{1 + e^{-(r-R)/a}} .$$

(These form factors tend to 1 for large r and to β_U^2 and $\beta_{W'}$ for small r.) We have used $R = 2 \times 0.8 \times (12)^{1/3}$ fm and $a = 0.3$ fm: these values are such that we do not touch the potential in the region of the barrier. If the above condition for constant absorption holds then $\beta_U = \beta_{W'}$. We took $\beta_{W'} = 0.9$ and actually found it necessary to use $\beta_U = 0.87$ to obtain the same internal reflection coefficients η_I. The integral deflection function Θ_I is given by the relative phases of the low partial waves so if it changes we do not expect the same internal scattering amplitude even if η_I is unchanged. Surprisingly, however, the above modification results in almost exactly the same deflection function as before. This can be understood qualitatively from the W.K.B. formula for the phase

$$\delta_l \sim \frac{1}{\hbar}\int \sqrt{2m[E_{\text{c.m.}} - V(r) - V_c - V_l]}\, dr .$$

Since the potential is very deep, then apart from a small region close to the origin, $V_l = (l+\frac{1}{2})^2/2mr^2$ is negligible over the entire region in which we have changed the potential. Consequently the phase change we have introduced is roughly l-independent and Θ_I is essentially unchanged. This means that the entire amplitude $f_I(\theta)$ coming from S_I has only been modified by an overall phase, i.e. it becomes $f_I(\theta)\exp(i\alpha)$. This additional phase α will clearly shift the interference between f_I and the barrier amplitude f_B and we will only reobtain the original cross section if α is a multiple of 2π. We have varied the parameters β_U and β_W in such a way as to obtain $\alpha = 2\pi$ with $\beta_U = 0.69$, $\beta_{W'} = 0.75$. The positions of the interference minima are actually very sensitive to α and thus β_U and β_W can only take well-defined values for any given form factors g_U and $g_{W'}$, thus giving rise to *discrete* potential ambiguities. Clearly it may also be possible to find other modifications to the potential which give the same S_I. The above value of β_U reduces the real potential in the nuclear interior to about 48% ($\approx$ 250 MeV) of its original value.

To understand the sensitivity of the interference pattern to the value of α, and hence why it is difficult to obtain an optical-model fit to the data, we shall now decompose the contributions f_I and f_B of the total unsymmetrised amplitude into travelling waves. This is usually done by replacing the $P_l(\cos\theta)$ by their asymptotic forms which contain $\exp(\pm il\theta)$. However, since the internal S-matrix explicitly contains low partial waves, we shall not take these expressions but shall use the $\widetilde{Q}_l^{\pm}$ of Fuller [1], to define

$$f_{I,B}^{\pm} = \sum_l (2l+1)\, \widetilde{Q}_l^{\pm}\, e^{2i\sigma_l} S_{l;I,B} ,$$

where $f(\theta)$ is exactly the sum of these four terms and σ_l are the Coulomb phases. The moduli of $f_{I,B}^{+}$ and $f^{-} = f_I^{-} + f_B^{-}$ are shown in fig. 2 as a function of θ. At forward angles f^{-} is almost entirely due to f_B and the oscillations obtained up to about 60° in $\sigma(\theta)$ are the result of the usual Fraunhofer diffraction (interference of f_B^{-} with f_B^{+}). The minimum at 90° and other structure in this region is a result, however, of interference of f_I^{+} and f_B^{+} which have about the same order of magnitude in this region. Thus, as previously noted, the low partial waves are absolutely essential to produce a minimum at 90° which is sufficiently deep to persist in the *symmetrised* cross section. Note that the Fraunhofer diffraction is interference between two waves turning in opposite directions, and thus gives a small angular period $\Delta\theta = \pi/l_g \approx 8°$ where l_g is the grazing angular momentum ($\approx$ 23). On the other hand, f_B^{+} and f_I^{+} represent waves turning in the *same* direction and thus their interference (see f^{+}) is sensitive to

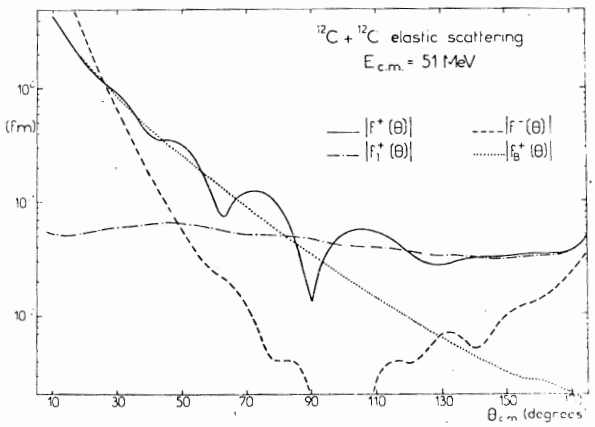

Fig. 2. The non-symmetrised amplitude is split into f^{-} and $f_{I,B}^{+}$. Note the beat structure of f^{+} (see text). The relative flatness of f_I^{+} comes from the fairly even distribution of S_I over all deflections $-\pi \lesssim \Theta_I \lesssim 0$ (see fig. 1) [2].

α and gives beats with a large period $\Delta\theta'$. This period depends on θ, i.e. $\Delta\theta'(\theta) = 2\pi/(l_g - l_I(\theta))$, where $l_I(\theta)$ is the l-region contributing to $f_I^+(\theta)$. Averaging over the two oscillations near 90° we find $\Delta\theta'(\frac{1}{2}\pi) \approx 32°$, giving $l_I(\frac{1}{2}\pi) \approx 12$. This is just the region where $\Theta_I \approx -\frac{1}{2}\pi$ as we would expect from a stationary-phase argument. In the physical (symmetrised) cross section we do not see these beats very clearly because of the additional interference with $f(\pi - \theta)$. In a non-symmetric system, if the low partial waves were important, these beats would give a marked change in the structure of the cross section.

We have shown by studying the $^{12}C + ^{12}C$ data that low partial waves are essential to reproduce the structure at 90° in $\sigma(\theta)$. By the same argument, the low partial waves are essential to reproduce deep minima in the 90° excitation function at energies high above the Coulomb barrier where the diffraction pattern arising from f_B has completely disappeared. This may also be the case for some of the minima seen at high energies in the excitation function for $^{16}O + ^{16}O$ [6].

It remains an open question as to whether the presence of low partial waves is really an effect of direct elastic scattering or, more probably, an effect of coupling to inelastic channels.

One of the authors (NR) is grateful to the IN2P3 for financial support during a visit to the Division de Physique Théorique, Orsay, where most of this work was performed. He would also like to acknowledge a Science Research Council Fellowship.

References

[1] C. Fuller, Phys. Rev. C12 (1975) 1561.
[2] N. Rowley and C. Marty, Nucl. Phys. A266 (1976) 494.
[3] W. Reilly et al., Nuovo Cim. 13A (1973) 913.
[4] R.M. Wieland, R.G. Stokstad, G.R. Satchler and L.D. Rickertsen, Phys. Rev. Lett. 37 (1976) 1458.
[5] J.V. Maher et al., Phys. Rev. 188 (1969) 1665.
[6] M.L. Halbert et al., Phys. Lett. 51B (1974) 341.
[7] J.L. Russell Jr., G.C. PHilips and C.W. Reich, Phys. Rev. 104 (1956) 135.
[8] G.R. Satchler and W.G. Love, Phys. Lett. 65B (1976) 415.
[9] D.M. Brink and N. Takigawa, Nucl. Phys. A, in press.
[10] N. Rowley and E. Plagnol, Phys. Lett. 56B (1975) 221.
[11] W.E. Frahn, Ann. Phys. (N.Y.) 24 (1963) 243.

Une décomposition de l'amplitude de diffusion, correspondant au cas c) de la figure III.10, vient donc d'être obtenue en divisant la matrice S en une partie interne et une partie "barrière". Evidemment cette décomposition est plus difficile que dans le cas de la diffraction de Fresnel, où l'amplitude de Coulomb se propose immédiatement comme l'une des deux composantes.

Cette méthode est proche de celle obtenue, à l'approximation semi-classique, par Brink et Takigawa [Br 76], mais plus empirique et plus générale. La méthode de Brink et Takigawa ne pouvait être appliquée, en outre, car elle a besoin de facteurs de forme analytiquement connus.

3. Les fonctions d'excitation de $^{16}O+^{16}O$ et de $^{12}C+^{12}C$ à haute énergie.

Les résultats qui précèdent amènent à la conclusion suivante : la structure observée [Ra 74] dans la fonction d'excitation à 90° du système $^{12}C+^{12}C$ (fig.III.15) est d'origine différente suivant l'énergie : à basse énergie ($E_{c.m.} \lesssim 35$ MeV), cette structure résulte de l'interférence $f^{(+)}(\theta)$, $f^{(-)}(\theta)$; à haute énergie, la composante $f^{(-)}$ est devenue négligeable à 90°, et $f^{(+)}(\theta)$ n'a plus un comportement monotone avec l'angle et l'énergie. La structure de la fonction d'excitation est donc toujours d'origine "diffractionnelle", mais maintenant due à l'interférence des ondes partielles les plus basses avec celles de surface. Cette interférence est observable grâce à la grande énergie incidente et la faible répulsion coulombienne entre les ^{12}C.

Un problème posé ici est celui de l'existence d'un potentiel unique, ou variant lentement avec l'énergie, car le potentiel de Yale est très peu profond ($V = 17$ MeV à $r = 0$), contrairement à celui proposé par Satchler et Love [Wi 76]. Il est remarquable (cf la lettre reproduite au paragraphe V.2) que le potentiel optique n'a plus que des ambigüités discrètes, que l'on sait trouver et grâce auxquelles on peut espérer diminuer la profondeur du potentiel réel. On peut espérer ainsi arriver à proposer un potentiel satisfaisant dans les deux régions d'énergie.

Les résultats de cette étude peuvent ainsi aider à la compréhension de la fonction d'excitation du système $^{16}O+^{16}O$, étendue jusqu'à 100 MeV (c.m.) par Halbert et al.[Ha 74]. Ces auteurs observent ici aussi un changement de comportement au-delà de $E_{c.m.} = 40$ MeV et trouvent qu'il n'est possible de reproduire les données expérimentales ni avec le potentiel de Gobbi, excellent à plus basse énergie, ni avec celui de Maher [Ma 69]. A haute énergie, à cause de sa transparence, le potentiel de Maher donne à $f^{(+)}(\theta)$ un rôle prépondérant (fig.III.16), mais les ondes partielles basses n'ont ici aucun rôle : la dépendance angulaire de $f^{(+)}(\theta)$ indique purement le comportement d'une onde de surface. Ce potentiel ne prédit donc pas assez de structure. Le potentiel de Gobbi, au contraire, en prédit une de trop grande amplitude, car l'interférence $f^{(+)}(\theta)$, $f^{(-)}(\theta)$ est présente ici sur tout le domaine angulaire (fig.III.17). Il est d'ailleurs difficile d'expliquer un tel comportement sans faire appel aux ondes partielles basses comme dans le cas $^{12}C+^{12}C$. Dans ce dernier, les ondes partielles basses modifient principalement $f^{(+)}(\theta)$, car elles peuvent traverser le puits de potentiel réel, à cause de sa grande profondeur : on a vu que la partie interne du coefficient de réflexion $\eta_I(\ell)$ a plutôt la forme d'un coefficient de transmission. Au contraire, avec le système $^{16}O+^{16}O$, tel qu'il est décrit par le potentiel de Gobbi, les mêmes ondes ne peuvent traverser le puits à cause de leur faible vitesse ; quand l'angle d'observation augmente, la composante $f^{(-)}$ contient de plus en plus d'ondes partielles basses apportées par la réflexion sur la discontinuité du potentiel imaginaire, pratiquement carré. On vérifiera cette hypothèse en comparant les moments angulaires $\ell^{(\pm)}$ transportés par les deux composantes obtenues avec le potentiel transparent de Siemssen (fig.III.6), à ceux que donne le potentiel de Gobbi (fig.III.18). On remarquera, sur cette dernière figure, à quel point $f^{(+)}(\theta)$ est dominée par un pôle unique.

En résumé, on voit qu'on a maintenant les techniques nécessaires à l'analyse des données expérimentales, et qu'il serait très intéressant d'analyser en parallèle les résultats obtenus à haute énergie sur ces deux systèmes. Des mesures ont déjà été entreprises dans ce sens au laboratoire.

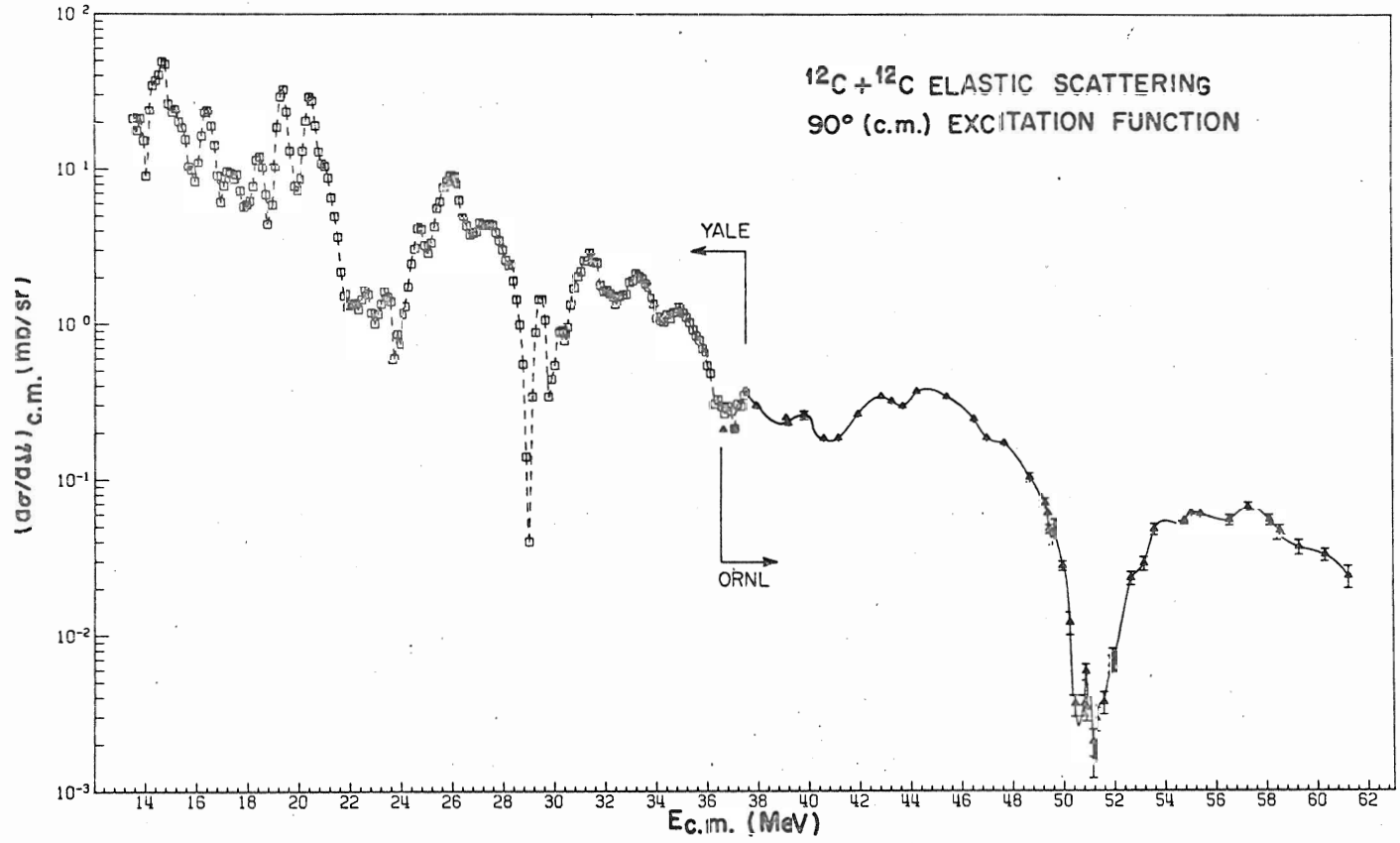

Fig.III.15. Fonction d'excitation à 90° du système $^{12}C+^{12}C$, tirée de la référence [St 77].

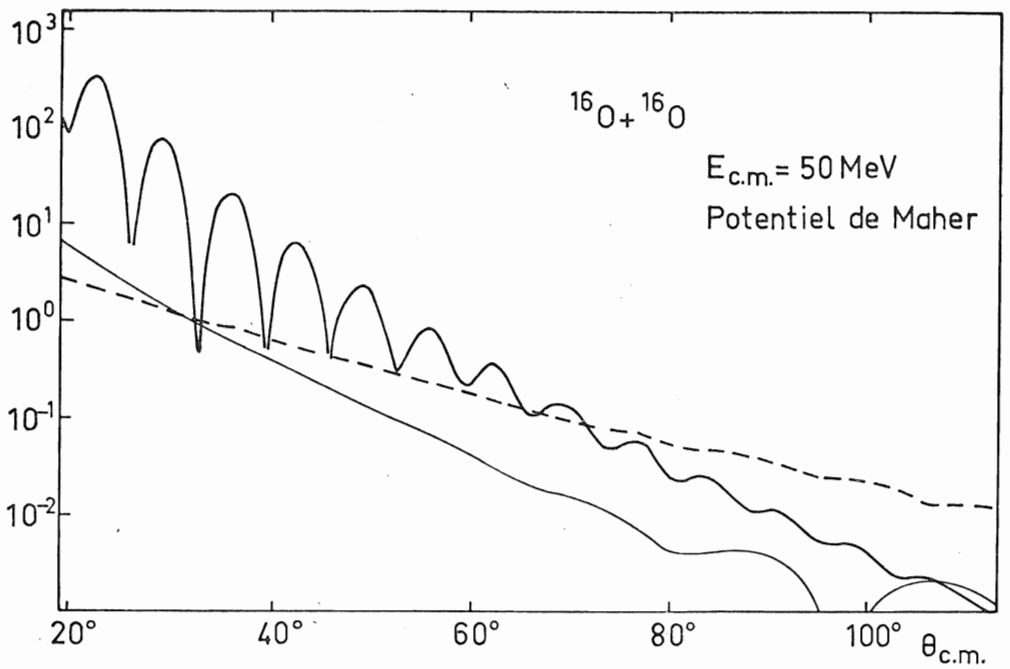

Fig.III.16. Prédictions du potentiel de Maher [Ma 69] pour la diffusion élastique de ^{16}O sur ^{16}O à $E_{c.m.}$ = 50 MeV.

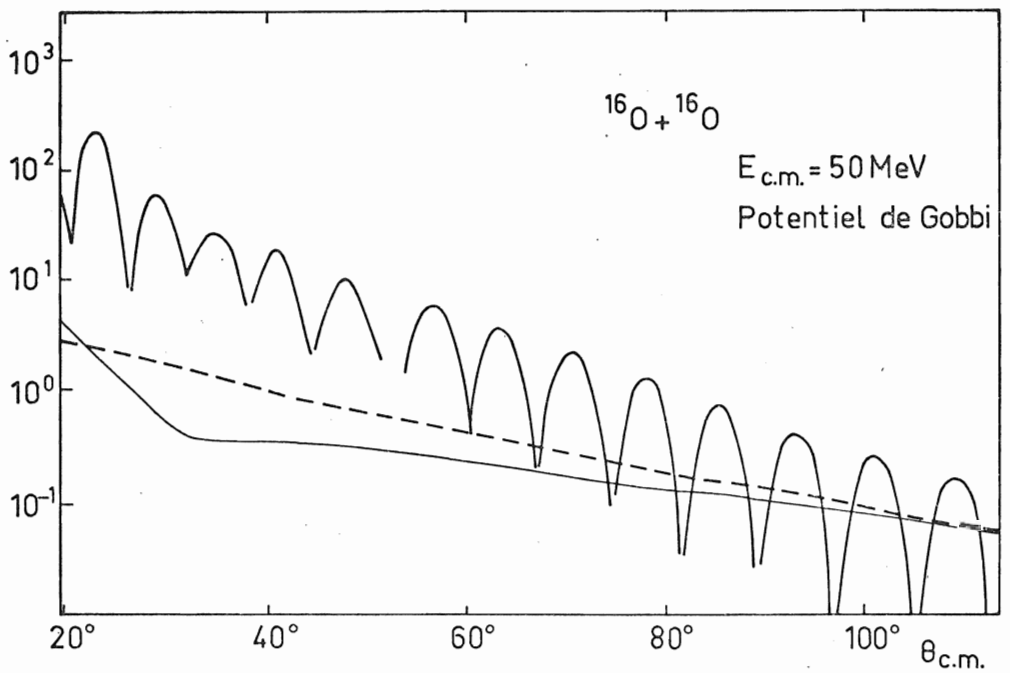

Fig.III.17. Prédictions du potentiel de Gobbi [Go 73] pour la diffusion élastique de ^{16}O sur ^{16}O à $E_{c.m.}$ = 50 MeV.

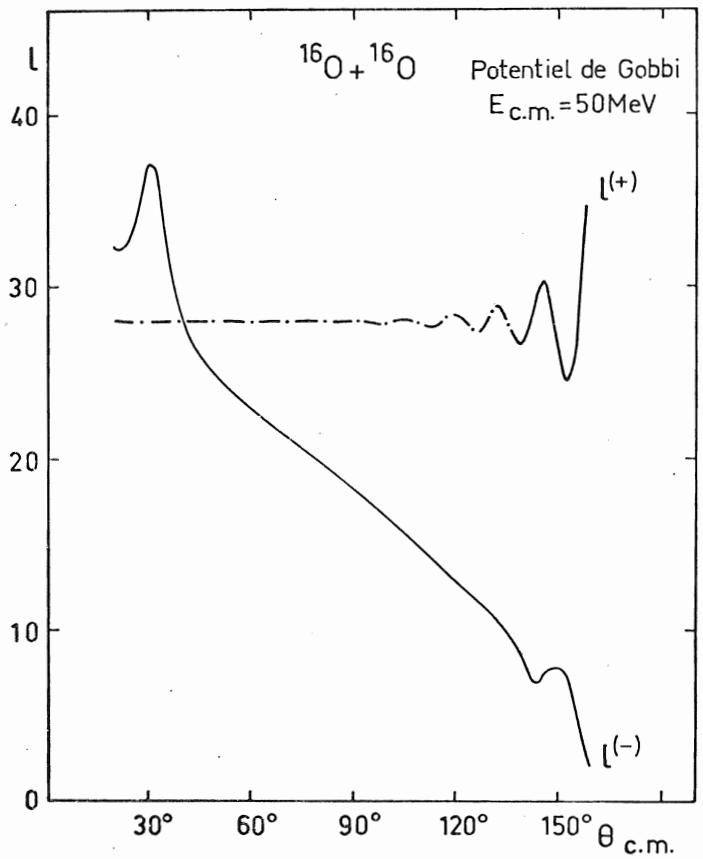

Fig.III.18. Moments angulaires associés aux composantes $f^{(+)}$ et $f^{(-)}$, en fonction de l'angle de diffusion, pour la diffusion élastique $^{16}O+^{16}O$ à 100 MeV.

V - CONCLUSION.

Nous avons présenté une méthode d'analyse de la diffusion élastique entre ions lourds, qui permet d'apporter des conclusions quantitatives sur les rôles respectifs de l'absorption entre ces ions, de leur masse et charge, de la réflexion sur une barrière de potentiel... La décomposition de l'amplitude de diffusion élastique et ses deux composantes progressives $f^{(+)}$ et $f^{(-)}$ introduit une simplification immédiate pour l'analyse du phénomène. Les ambiguïtés discrètes,qui ont été observées il y a longtemps déjà [Dr 63], ne sont par exemple que la succession de situations où le déphasage relatif entre les deux composantes a varié de 2π. Cette méthode constitue aussi un guide pour la recherche du potentiel optique, que nous avons utilisé à la référence [Do 77a] : on y voit comment les variations avec l'angle des modules $|f^{(+)}(\theta)|$ et $|f^{(-)}(\theta)|$,pour le système $^{12}C+^{20}Ne$,peuvent être prévues et comparées à celles du système $^{16}O+^{16}O$.

Enfin, cette méthode peut fournir une indication précieuse sur la situation physique que reproduit la distribution angulaire. Par exemple Fuller a montré [Fu 73] que si la quantité $\sin\theta|f^{(+)}(\theta)|^2$ décroît exponentiellement lorsque θ augmente, c'est une bonne indication pour décrire $f^{(+)}(\theta)$ comme la seule contribution d'un pôle de Regge, ce pôle décrivant l'effet cohérent d'un ensemble d'états excités dans le continu par le processus. Les résonances qui ont lieu dans de telles réactions sont plutôt le résultat de la coïncidence, à certaines énergies, de la partie réelle α_r du pôle de Regge avec une valeur entière du moment angulaire. On peut aussi montrer [Al 65] que la partie imaginaire α_i du pôle de Regge mesure

le rapport de la largeur de ces états excités à leur espacement. A titre d'exemple, nous avons comparé la situation dans les systèmes $^{16}O+^{16}O$ et $^{18}O+^{18}O$ sur la figure III.19.

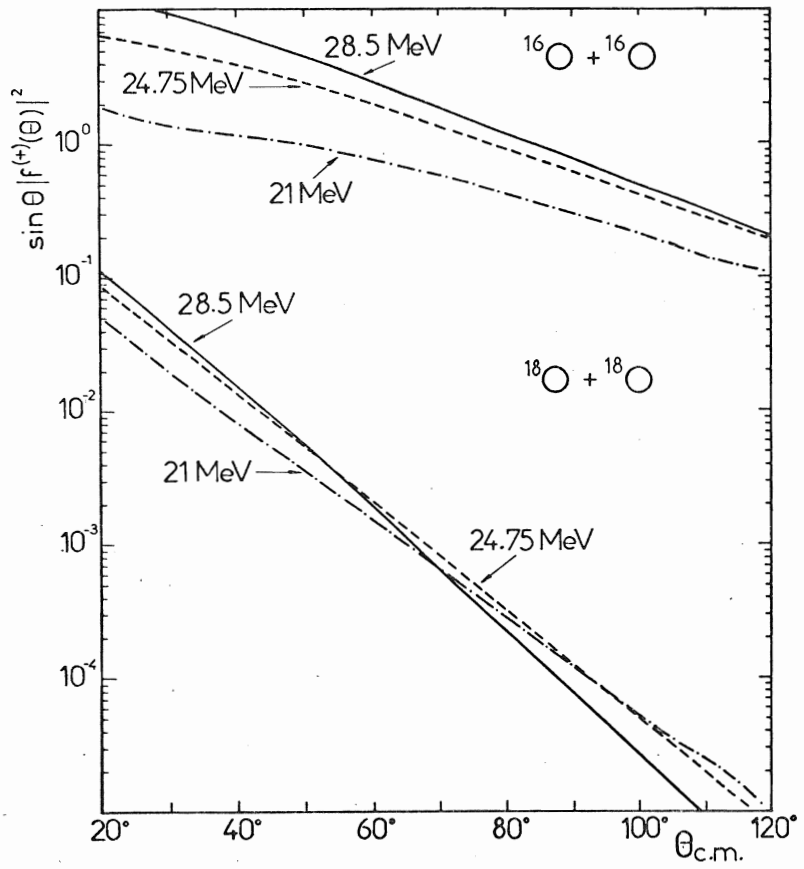

Fig.III.19. Distributions angulaires pour la seule composante $f^{(+)}(\theta)$.

On trouve, aux énergies considérées, les valeurs de α_r et α_i suivantes : (tableau III.3).

$^{16}O+^{16}O$	$E_{c.m.}$ =	21	24.75	28.5
	α =	16.2+0.974 i	18.3+1.118 i	20.12+1.26 i
$^{18}O+^{18}O$	$E_{c.m.}$ =	21	24.75	28.5
	α =	18.66+2.81 i	21.03+2.69 i	23.23+3.03 i

Fig.III.19. Distributions angulaires pour la seule composante $f^{(+)}(\theta)$.

On remarque que α_r est proche du moment angulaire rasant [Fr 77], que la dépendance de α_i avec l'énergie est faible, mais la différence entre les deux systèmes sur la valeur de α_i est frappante. Cette spectroscopie d'états du continu, états se recouvrant et excités de façon cohérente en diffusion élastique, mérite certainement d'être approfondie à l'avenir.

CONCLUSION

Un des buts de ce travail a été d'élucider le mécanisme qui gouverne la diffusion élastique entre ions lourds.

Dans une première partie, nous avons montré que la forme des distributions angulaires, et surtout des fonctions d'excitation, est caractéristique de l'absorption qui agit dans la voie élastique. Cette absorption a pour origine les voies directes immédiatement couplées à la voie d'entrée, comme notre étude du système $^{12}C+^{20}Ne$ et sa comparaison à $^{16}O+^{16}O$ l'ont fait apparaître d'une manière quantitative. Toutefois, les données expérimentales présentées pour le système $^{20}Ne+^{20}Ne$ conduisent à envisager une hiérarchie parmi ces voies : celles-ci interviennent sans doute avec un poids différent dans l'absorption, selon qu'elles résultent d'un transfert (d'un nucléon, d'un alpha...) ou d'une diffusion élastique. Ce résultat est important car il atténue l'opposition faite entre systèmes transparents et systèmes absorbants, et pour la première fois il est montré que, non seulement les excitations de basse énergie, mais aussi d'autres propriétés intrinsèques des noyaux (diffusivité de la surface, configurations disponibles au cours de la collision) peuvent influer grandement sur la distribution du flux incident entre les différentes voies.

En s'intéressant, dans la seconde partie, à un système beaucoup plus lourd ($^{40}Ca+^{40}Ca$), et en y recherchant de semblables manifestations d'une plus ou moins grande absorption, notre étude prolonge celles consacrées aux systèmes plus légers. L'analyse que nous avons effectuée de l'absence de structure dans les données expérimentales a révélé que les effets coulombiens peuvent masquer totalement ceux dus à la structure des noyaux. Dans le cas du système $^{40}Ca+^{40}Ca$, ces effets nucléaires ne peuvent apparaître qu'à une énergie où les sections efficaces élastiques deviennent extrêmement petites, et les incertitudes expérimentales prohibitives. On conclut que,dans le cas d'un système aussi lourd, il n'est pas possible d'obtenir des informations fiables et caractéristiques sur les détails de la matrice S : seules sont déterminées les valeurs du rayon d'absorption forte, et des potentiels réel et imaginaire pour cette distance de séparation. Par ailleurs, la fonction d'excitation de la fusion pour le système $^{40}Ca+^{40}Ca$ indique,qu'au moins pour les collisions donnant lieu à la formation d'un noyau composé, les noyaux sont déjà considérablement excités (c'est-à-dire que leur structure initiale a disparu) lorsque la distance critique est atteinte. Ainsi, pour ce système, il est extrêmement difficile de retrouver la trace des propriétés statiques des noyaux isolés dans les résultats de leur collision.

Une description cohérente de la diffusion élastique, -que les noyaux soient légers ou lourds, que les systèmes soient absorbants ou non-, a été présentée, fondée sur la recherche d'une décomposition de l'amplitude de diffusion en composantes variant doucement avec l'angle et l'énergie. Cette méthode offre un grand nombre d'avantages : elle explicite le rôle joué par la charge des noyaux, par l'absorption qui agit entre eux, elle permet une évaluation quantitative des effets dus aux détails de la matrice S. Surtout, elle met en évidence les processus physiques simples (réfraction, réflection, diffraction,...) que les

méthodes semi-classiques ont illustrés, et elle propose ainsi une interprétation claire de la forme d'une distribution angulaire, ou d'une fonction d'excitation, en faisant appel aux phénomènes bien connus d'interférences. Elle a aussi le mérite de guider la recherche des potentiels optiques car elle rend plus évident le rôle de tel ou tel paramètre. Enfin, elle peut être généralisée aux transferts et à la diffusion inélastique.

Un résultat extrêmement important de l'application d'une telle méthode à l'étude de la diffusion élastique d'ions relativement légers a été la part capitale que les ondes partielles les plus basses prennent dans le phénomène, contrairement à ce qui a été souvent répété. On peut penser que leur réflection à la surface nucléaire, ou encore leur relative "pénétration" du noyau offrent la possibilité d'étudier avec précision des mécanismes où la nature de l'ion demeure une donnée essentielle.

Ainsi, il ne fait pas de doute que l'extension vers des énergies plus élevées d'études similaires doit apporter des informations considérables sur la configuration des ions à leur distance minimale d'approche. D'ores et déjà, deux directions sont ouvertes ; d'une part, on compte sur l'investigation de quelques situations compliquées, mais ponctuelles, comme celles où un minimum est observé à 90° dans la distribution angulaire de particules identiques, pour réduire les ambiguïtés du potention ion lourd-ion lourd et fournir des renseignements sur le mécanisme de la diffusion à haute énergie ; d'autre part, une étude systématique de la diffusion entre noyaux de la couche 2s-1d, permettant de suivre les caractéristiques de l'absorption entre noyaux légers dans une région encore peu explorée, où voisinent des noyaux déformés mais rigides, et d'autres aisément déformables, nous paraît prometteuse. Ces études ont été entreprises au laboratoire ainsi que l'analyse des données de diffusion élastique et inélastique à des énergies allant jusqu'à dix fois celle de la barrière.

Parallèlement, sur le plan théorique, il serait important d'examiner, de façon détaillée, l'origine de l'absorption puisque c'est cette dernière qui donne aux divers systèmes leur caractère propre. L'étude des configurations adiabatiques, par exemple, fournit une base d'états accessibles aux nucléons au cours de la collision. Peut-être peut-on relier ces orbitables au phénomène d'absorption, c'est-à-dire de décrire de façon microscopique le stade de transition où un système commence à sortir de la voie élastique. Les techniques mises au point ces dernières années devraient permettre d'envisager un tel programme.

RÉFÉRENCES

[Al 60] : E.ALMQVIST, D.A.BROMLEY and J.A.KUEHNER, Phys. Rev. Lett. 4 (1960) 515.

[Al 65] : V. de ALFARO and T.REGGE,Potential scattering, North Holland ed. (1965).

[Ba 63] : J.B.BALL, ORNL 3311 - UC 34 - TID 4500 (1963), non publié.

[Bo 77] : P.BONCHE et al., preprint Saclay (1977).

[Br 76] : D.M.BRINK and N.TAKIGAWA, Nucl. Phys. A279 (1976) 159.

[Br 72] : D.M.BRINK, Lectures Notes, Orsay (1972).

[Br 77] : D.A.BROMLEY, in Proceedings of the International Conference on Resonances in Heavy Ion Reactions, HVAR (1977).

[Ch 70] : R.A.CHATWIN et al., Phys. Rev. C1 (1970) 795.

[Co 74] : P.COLOMBANI et al., Phys. Lett. 55B (1975) 45.

[Do 75a] : H.DOUBRE et al., J. Physique Lett. 36 (1975) L113.

[Do 75b] : H.DOUBRE et al., Phys. Rev. Lett. 35 (1978) 508.

[Do 77a] : H.DOUBRE et al., IPNO-PhN-77-16, à paraître dans Phys. Rev. C.

[Do 77b] : H.DOUBRE et al., Phys. Rev. C15 (1977) 693.

[Do 77c] : H.DOUBRE et al., IPNO-PhN-77-26 (1977), à paraître dans Phys. Lett. B.

[Do 77d] : H.DOUBRE and C.MARTY, in Proceedings of the International Conference on Resonances in Heavy Ion Reactions, HVAR (1977).

[Dr 63] : R.DRISKO et al., Phys. Lett. 5 (1963) 347.

[Du 75] : M.DUMAIL and J.P.MOUFFRON, Nucl. Inst. Meth. 127 (1975) 305.

[Fe 76] : H.FESHBACH, J. Physique C5, 11 (1976) 177.

[Fo 59] : K.W.FORD and J.A.WHEELER, Ann. Phys. (N.Y.) 7 (1959) 259.

[Fr 75] : W.E.FRAHN, in High Spin States and Nuclear Structure, Vol.I, (IAEA, Vienne 1975) 157.

[Fr 76] : W.E.FRAHN and D.H.E.GROSS, Ann. Phys. (N.Y.) 101 (1976) 520.

[Fr 77a] : W.E.FRAHN, preprint (1977).

[Fr 77b] : W.A.FRIEDMAN and C.J.GOEBEL, Ann. Phys. (N.Y.) 104 (1977) 145.

[Fu 73] : R.C.FULLER, Nucl. Phys. A216 (1973) 199.

[Fu 75] : R.C.FULLER, Phys. Rev. C12 (1975) 1561.

[Fu 77] : R.C.FULLER and P.J.MOFFA, Phys. Rev. C15 (1977) 266.

[Ga 77] : J.GASTEBOIS, in Proceedings of Tokyo Conference (1977).

[Go 73] : A.GOBBI, Phys. Rev. C7 (1973) 30.

[Gr 77] : D.H.E.GROSS and H.KALINOWSKI, Communication privée (1977).

[Ha 74] : M.L.HALBERT et al., Phys. Lett. 51B (1974) 341.

[Hu 76] : J.R.HUIZENGA, J.R.BIRKELUND and W.JOHNSON, in Proceedings of the Symposium on Macroscopic features of heavy-ion collisions, ANL/PHY-76-2 (1976),(unpublished).

[Le 59] : R.LEVY and J.B.KELLER, Comm. Pure Appl. Math. 12 (1959) 159.

[Ma 69] : J.V.MAHER et al., Phys. Rev. 188 (1969) 1665.

[Mc 77] : K.McVOY, Lectures notes, Mexico (1977).

[Mo 76] : L.G.MORETTO and R.SCHMITT, J. Physique C5, 11 (1976) 109.

[Mo 53] : P.M.MORSE and H.FESHBACH, Methods of Theoretical Physics, Mc Graw and Hill ed. (1953).

[Pl 77] : E.PLAGNOL, H.DOUBRE et C.MARTY, Phys. Letters 67B (1977) 377.

[Ra 74] : S.RAMAN et al., in Proceedings of the International Conference on Reactions between complex nuclei, Nashville (1974), Vol.I, p.2.

[Re 73] : W.REILLY et al., Nuovo Cim. 13A (1973) 913.

[Ro 76] : N.ROWLEY and C.MARTY, Nucl. Phys. A266 (1976) 494.

[Ro 77a] : N.ROWLEY, H.DOUBRE et C.MARTY, Phys. Lett. B 69B (1977) 147.

[Ro 77b] : J.C.ROYNETTE et al., Phys. Lett. 67B (1977) 395.

[Ro 78] : J.C.ROYNETTE et al., à paraître.

[Sh 67] : R.W.SHAW et al., Phys. Lett. 184 (1967) 1040.

[Sh 70] : R.W.SHAW et al., Phys. Rev. Lett. 25 (1970) 457.

[Si 67] : R.H.SIEMSSEN et al., Phys. Rev. Lett. 19 (1967) 369.

[Si 71] : R.H.SIEMSSEN, in Proceedings of the Symposium of Heavy Ion Scattering, Argonne (1971) ANL 7837, p.145 (unpublished).

[St 77] : R.G.STOKSTAD et al., ORNL/TM 5935 (1977).

[Ta 72] : T.TAMURA and H.H.WOLTER, Phys. Rev. C6 (1972) 1976.

[Va 71] : R.VANDENBOSCH, in Proceedings of the Symposium of Heavy Ion Scattering, Argonne (1971) ANL 7837, p.103 (unpublished).

[Va 74] : R.VANDENBOSCH, M.WEBB and M.S.ZISMAN, Phys. Rev. Lett. 33 (1974) 842.

[Vo 70] : W.VON OERTZEN, Nucl. Phys. A148 (1970) 529.

[Wi 76] : R.M.WIELAND et al., Phys. Rev. Lett. 37 (1976) 1458.

ANNEXE

INTERFERENCE EFFECTS IN HEAVY-ION ELASTIC SCATTERING

H.DOUBRE and C.MARTY

Institut de Physique Nucléaire, BP n°1, 91406 Orsay, FRANCE

INTERFERENCE EFFECTS IN HEAVY-ION ELASTIC SCATTERING

H. DOUBRE and C. MARTY*
Institut de Physique Nucléaire - 91406 ORSAY Cedex - France

(Invited talk at the International Conference on Resonances in Heavy Ion Reactions, Hvar, (Croatia, Yugoslavia), May 30-June 3,1977)

IPNO/TH 77-28 May 1977

---

* Division de Physique Théorique, Laboratoire associé au C.N.R.S.

Abstract :

At energies well above the Coulomb barrier, interference effets offer an attractive explanation of the oscillations observed in excitation functions and/or angular distributions of light heavy ions systems. The elastic amplitude as given by an optical-model potential can be split up, in several ways, the modulus of each component of the amplitude varying smoothly with energy and angle. The interference between these sub-amplitudes can give rise to the well-known Fraunhofer diffraction, but also to other phenomena which are analyzed here.

A first decomposition is the splitting of the elastic amplitude into negative and positive deflection angle components. This method can explain the presence or absence of oscillations in the excitation functions of $^{16}O + ^{16}O$, $^{18}O + ^{18}O$ and $^{40}Ca + ^{40}Ca$. A second possibility is to consider the S matrix itself as the sum of an internal part containing partial waves of low order and a barrier part. Combining these two decompositions one is able to understand rather rare effects as the presence of a minimum at 90° in the angular distribution of $^{12}C + ^{12}C$ at some energies. Implications on the ambiguities of the potential are also discussed. Finally potential resonances in a complex potential are studied in the semi-classical approximation as a function of the absorption. Regge poles, if present, manifest themselves in the internal part of the S matrix whereas Regge zeroes arise from interference between barrier and internal parts of the scattering matrix. Applications are made to $^{16}O + ^{16}O$ scattering and anomalous large angle scattering of α particles.

The origin of the interference patterns analysed here can be traced back to the complex potentials used. In that sense there is no contradiction between the present interpretation of oscillations and the standard ones based on intermediate structure. The complex potential is nothing but a mean field due to energy averaging, so basically the dynamics of the systems is responsible for both intermediate structure and interference phenomena.

I. Introduction

Since it was recently suggested [1] that the intermediate (≈ 300 keV wide) structure studied at this meeting could provide examples of isolated doorway states excited within energy windows defined by shape resonances in the elastic channel, perhaps it is the proper time to discuss the gross structure observed in heavy-ion elastic scattering. Especially, one would like to disentangle the intrinsic effects from more trivial ones which result from interferences between smooth, well-behaved components of the elastic scattering amplitude.

The origin of the results reported here can be traced back to the following remark : the large oscillations observed [2] at large scattering angles in $^{16}O + ^{16}O$ and energies well above the Coulomb barrier provide evidence for a surface-transparent potential. This transparency is due to the small number of angular momentum-allowed channels for this system [3]. A similar situation exists for the $^{40}Ca + ^{40}Ca$ system. However, the experimental result [4] is negative : no oscillations are observed at 60°, 70° and 90° at energies between one and two times the Coulomb barrier.

The present situation can be summarized in table I and Fig.1. Close to the Coulomb barrier intrinsic effects which can be looked at as the signature of doorway states [5] are present. With increasing incident energy these narrow resonances merge into gross structure, the origin of which has been discussed in many places [6] and especially at this Conference.

An alternative interpretation is possible: if the scattering amplitude $f(\theta,E)$ at an observation angle θ and energy E

found (table 2) to fit angular distributions as well as excitation functions. On fig.3.a) the predictions for the excitation function σ/σ_R where σ is the 90° differential cross section and σ_R the Coulomb cross section are shown. The abscissa is the ratio h of the c.m. energy to the Coulomb barrier. The figure exhibits how the behaviour differs from system to system :

i) the $^{16}O + ^{16}O$ cross-section falls down relatively slowly from its Coulombvalue (at $h \approx 1$) up to $h \approx 2$ where it displays the well-known gross structure.

ii) For low energy ($h < 2$) the $^{18}O + ^{18}O$ variation compares with that of the latter system. However, for higher energies, σ/σ_R continues to decrease and some slight oscillations begin to occur at only h = 2.5.

iii) The $^{40}Ca + ^{40}Ca$ system shows a different and very simple aspect. The excitation function falls very steeply from $\sigma/\sigma_R = 1$ at h = 1 to about 10^{-7} at h = 2 where some oscillations can be found. However, these oscillations lie in an energy region which, for this angle, was not investigated experimentally.

The decrease in σ/σ_R is known to be essentially governed by the Sommerfeld parameter n and is already described by the simplest models such the sharp cut-off one [11] : the larger n is, the more steeply the excitation function decreases with h.

At higher energy, the behaviour of σ/σ_R is understood by splitting the elastic scattering amplitude according to Eq.(3). One notices that at 90° symmetrisation effects are trivial and actually it is only necessary to consider unsymmetrised amplitudes. The results are illustrated in Fig.4. Together with the 90° excitation function plotted as a function of h for $^{16}O + ^{16}O$

are also shown the ratios $|f^-/f_R|^2$ and $|f^+/f_R|^2$ where f_R is the Rutherford amplitude. Several remarks can be made : i) both components are smoothly varying with energy, except for the very small oscillations found in $|f^-/f_R|^2$ at high energy. (Actually, these oscillations have too small an amplitude to be the sole origin of the large diffractive pattern in the excitation function).

ii) As expected, at low energy, only f^- contributes significantly.

iii) With increasing energy the two components become of comparable magnitude so that the cross section which results from their interference shows strong maxima and minima. An immediate conclusion is that the existence of such large-amplitude oscillations could be the signature of the relative importance of f^+ with respect to f^-. The relevant parameter is therefore the quantity :

$$R = |f^+(90°)/f^-(90°)|$$

Fig. 3.b) shows the variation of R as a function of h for the three systems considered. It is striking to observe that in all cases the qualitative behaviour of the ratio R is very similar. Below the Coulomb barrier, R slowly increases until it reaches a maximum at h ≈ 0.9. Decreasing then to a minimum value around which some fluctuations are present ($1 < h < 1.5$), R reproduces the relative importance of f^- already mentioned. After the minimum R at first increases very strongly, then seems to approach some maximum value which depends on the nature of the system studied. It is over this energy range that interference between f^+ and f^- occurs. A sharp interference pattern is observed in the $^{16}O + ^{16}O$ case where the excitation function has not fallen too much. Although the same can be expected in principle for the $^{40}Ca + ^{40}Ca$

can be divided into several contributions $f_1(\theta,E)$, $f_2(\theta,E)\ldots$, each of them being a smooth function of θ and E, oscillations can appear in the cross section $\sigma(\theta,E) = |f(\theta,E)|^2$. Are these oscillations an evidence for a genuine resonance behaviour, which would be present in one or maybe several components, or do they result from the interference between various contributions to $f(\theta,E)$? It is our aim here to show that the second point of view has to be taken seriously.

As early as 1963, Frahn pointed out [7] that the elastic amplitude could conveniently be split up in interfering components. One has :

$$f(\theta,E) \propto \frac{1}{\sqrt{E}} \sum_{\ell=0}^{\infty} (2\ell+1) S_\ell(E) P_\ell(\cos\theta) \qquad (\theta \neq 0) \qquad (1)$$

As in heavy-ion physics one is dealing with large angular momenta, the following asymptotic expression for the Legendre polynomial

$$P_\ell(\cos\theta) \simeq \frac{1}{\sqrt{(\ell+\frac{1}{2})\frac{\pi}{2}\sin\theta}} \cos\left[(\ell+\tfrac{1}{2})\theta - \tfrac{\pi}{4}\right] \qquad (2)$$

can be used. It is a superposition of turning angular waves $\exp(i\ell\theta)$ and $\exp(-i\ell\theta)$. This leads to the decomposition in two terms :

$$f(\theta,E) = f^+(\theta,E) + f^-(\theta,E) \qquad (3)$$

where $f^\pm(\theta,E)$ can be seen as travelling waves corresponding to positive- and negative-deflection angles (Fig.2). Using a parametric S-matrix [8], Frahn computed easily the term $f^+(\theta,E)$, and approximately the term $f^-(\theta,E)$. Actually Fuller has shown [9] that the decomposition (3) is an exact one which can be obtained without using the asymptotic expression (2). S-matrices used here result from optical-model analysis of the data.

An a-posteriori description of the physical process is then obtained : first, the experimental situation is reproduced through an S-matrix and secondly, the resulting behaviour of both components $f^+(\theta,E)$ and $f^-(\theta,E)$ is analyzed.

The decomposition (3) is by no means unique. It is only a natural way to get some insight into the angular dependence of the interference phenomena. But the scattering matrix can itself be decomposed in several pieces. For instance, the JWKB approximation gives for the scattering from complex potentials [10] :

$$S(\ell,E) = S_B(\ell,E) + S_I(\ell,E) \qquad (4)$$

where S_B is referred to as the "barrier" S-matrix, and S_I is the "internal" one. Then with obvious notations :

$$f(\theta,E) = f_B(\theta,E) + f_I(\theta,E) \qquad (5)$$

The inner and barrier contributions to the scattering amplitude can also be submitted to the angular decomposition (3) to study the interference between the negative- and positive-deflection angle barrier (or internal) amplitudes. The usefulness of such decompositions will be shown in some examples.

II. Excitation functions at 90° of identical ions : angular decomposition of the scattering amplitude

For the three systems $^{16}O + ^{16}O$, $^{18}O + ^{18}O$ and $^{40}Ca + ^{40}Ca$, acceptable optical-model potentials have been

$$\frac{\sigma^S(\frac{\pi}{2}\pm\varepsilon)}{\sigma^S(\frac{\pi}{2})} = 1 + \varepsilon^2\left[\frac{|f|''}{|f|} - \phi'^2\right]_{\theta=\frac{\pi}{2}}$$

where the primes denote differentiation with respect to θ . We see, therefore, that the bigger ϕ'^2 is, the less likely we are to be able to observe a minimum. In heavy-ion reactions, the phase will indeed vary rapidly, ϕ' being of the order of the grazing angular momentum ℓ_g [9,18] . In this case, it will only be possible to find a minimum in $\sigma^S(\theta)$ at 90° if $|f|$ itself is very small, i.e. if the non-symmetrised amplitude possesses a deep minimum and the cross section is very small. We are therefore more likely to find such minima in the angular distributions at energies where the 90° excitation function possesses a minimum.

A study of $^{12}C + ^{12}C$ [13,16] and $^{16}O + ^{16}O$ [3,12] elastic scattering over a large energy range produces a total of only 4 examples of minima in $\sigma^S(\theta)$ at 90° (Figs.6) and each case indeed corresponds to a very deep minimum in the excitation function : $E_{c.m.}$ = 30 and 51 MeV for ^{12}C and $E_{c.m.}$ = 22.1 and 26.5 MeV for ^{16}O (Fig.1). In the case of α-α scattering [16] , minima in $\sigma^S(\theta)$ at 90° are more frequent since ϕ'^2 is much smaller (smaller ℓ_g) than for $^{12}C + ^{12}C$ or $^{16}O + ^{16}O$. A minimum at 90° is thus rather an exception than a rule.

The high energy $^{12}C + ^{12}C$ data were obtained and analyzed by Wieland et al. [12] over a large energy range, including the 51 MeV case mentioned above. This latter energy is about 7 times the barrier height and corresponds to a Sommerfeld parameter n = 1.95. The above authors claim that their fit requires a deep real potential ($\sim$ 500 MeV at the origin) which was obtained by a folding procedure due to Satchler and Love [17] . Their attempts to use a conventional Saxon-Woods potential were only successful up to about 60°. Between 60° and 90° the oscillatory structures were not reproduced. It is clear then that this folded potential gives a contribution to the scattering amplitude which has not been found in a conventional analysis using Saxon-Woods form factors.

Such a contribution comes from the scattering matrix $S_\ell = \eta_\ell \exp(2i\delta_\ell)$ through the non-negligible occurrence of the low partial waves. This incomplete absorption arises because the deep real potential gives a large relative velocity in the nuclear interior. The effect of these partial waves was confirmed by a calculation in which they were suppressed by strongly increasing the imaginary potential in the nuclear interior while leaving it unchanged near and outside the barrier. So long as the imaginary potential is sufficiently strong in the internal region, such a procedure is equivalent to splitting the S-matrix according to Eq.(4). In the barrier part S_B, low partial waves are absent. S_I can be attributed to that part of the flux which enters the nuclear interior and leaves again after a single or multiple reflections [9]. In Fig.7, we show for these two parts of the S-matrix the reflection coefficients η_ℓ and the deflection function :

$$\Theta_{\ell+1/2} = 2(\delta_{\ell+1} - \delta_\ell) + \Theta^C_{\ell+1/2}$$

where $\Theta^C_{\ell+1/2}$ is the Coulomb deflection function [18] defined similarly. The barrier contribution is seen to be a typical strong-absorption S-matrix [7,18]. It is totally insensitive to the nuclear interior and is also responsible for the typical

case, no oscillation can be observed, since σ/σ_R takes values between 10^{-5} to 10^{-7}. Two factors are thus decisive in the energy dependence of the elastic scattering. The first is the Coulomb repulsion, the effect of which is to push R down to smaller values when Sommerfeld parameters are larger, and the other is the absorptive nuclear field which acts preferentially on the $f^{(+)}$ component. However, it is likely that the present description is only appropriate on a limited energy range and it is not at all evident that the whole structure which is now known for the $^{16}O + ^{16}O$ [12] and $^{12}C + ^{12}C$ [13] systems has the same diffractive origin.

Two comments have to be made here. First a detailed analysis of the variation of R with h can be done. As this involves more elaborate techniques, we refer to the original paper [14] and quote the main results. More specifically, we give the results in the $^{18}O + ^{18}O$ case, as the behaviour of R is the same for the three cases studied. The ratio $|f^-/f_R|$ behaves rather simply. Near the Coulomb barrier f^- practically represents the whole amplitude, which is evidently due to the importance of the Coulomb field. It then decreases smoothly as h increases because of the absorption and/or the attractive nature of the nuclear interaction. The quantity f^+ does not behave so simply. It is convenient to divide it up according to :

$$f^+ = f_C^+ + f_N^+$$

where f_C^+ and f_N^+ refer to the Coulomb and nuclear interaction, respectively. These quantities have been plotted in the Fig.5. Near the Coulomb barrier, f_C^+ is of course dominant. It decreases with the onset of the nuclear forces, while f_N^+ starts from very small values. Near h = 1.5, the magnitude of these two terms are comparable giving rise to another type of interference and to the chaotic pattern of R. From there, the term f_N^+ dominates until it reaches a plateau. As f^- is still decreasing, the ratio R increases. This interference effect in f^+ is fairly sensitive to the imaginary part of the complex potential. For example, the energy range over which both Coulomb and nuclear terms interfere, can be increased according to the absorption, postponing the rapid rise of R.

The second comment is relative to the small oscillations found in the quantity $|f^-/f_c|^2$ in the Fig. 5. These oscillations can be shown to be present in f^-, rather than coming from the usual interference between f^+ and f^-. To understand their origin, it could be useful to split the S-matrix itself according to Eq.(4). We do not insist on this point here since a much better example of such a decomposition will be found below.

III. Angular distributions of identical systems : decomposition of the S matrix [14]

The particular interest of the elastic scattering of identical particles is that information on the phase of the amplitude is available from the interference of $f(\theta)$ with $f(\pi-\theta)$. In the case of spin-0 bosons the above amplitudes always interfere constructively at 90°. The cross section at this angle will therefore possess an extremum which can be calculated in the following way. If we write the unsymmetrised amplitudes as $|f(\theta)|\exp i\phi(\theta)$, the symmetrised cross section $\sigma^S(\theta)$ near to 90° reads :

IV. Potential resonances

In a real potential which has a pocket it may happen that a wave is trapped for a finite time giving rise to a resonance. This approach has been used to analyse the positions of bound and unbound states in light systems [18]. For states near the continuum one has however to take into account the imaginary part of the potential [20]. Using the JWKB method [9,21] it is easy to obtain the semi-classical scattering matrix $S_\ell^{sc}(E)$ which can be compared to the one obtained from optical-model codes. The agreement is excellent except when the real and/or imaginary diffusenesses are small [22].

The resonances are manifestation of the poles in the scattering matrix $S_\ell(E)$. These poles and the associated zeroes can be computed by a code due to Wolter [23] and they appear for real fixed energies at complex values of the angular momentum (Regge poles and zeroes). It is, however, much simpler to look at the behaviour of $S_\ell^{sc}(E)$ for <u>real</u> E and ℓ. Using the decomposition (4), we write symbolically :

$$S^{sc} = S_B^{sc} + S_I^{sc}$$

One can prove [21] that the poles of S^{sc} are all contained in S_I^{sc} and not in S_B^{sc}. This can be understood if one remembers that the poles eventually lead to resonances by trapping waves in the "interior" of the potential. On the other hand the zeroes of S^{sc} are due to interferences between S_B^{sc} and S_I^{sc}. Fig.(10) shows the behaviour of S_B^{sc} and S_I^{sc} for $^{16}O + ^{16}O$ at an energy E_{cm} = 16 MeV with a weak absorption (W = .5 MeV) and a medium one (W = 2 MeV). The other optical-model parameters are V_o = 17 MeV, R = R_W = 6.8 fm,

a = a_w = .49 fm. The barrier scattering matrices are almost independent of the imaginary potential. S_I^{sc}, which contains eventually many reflections in the potential, can be compared on Fig.(10 to $S_I^{(o)sc}$ calculated with a single reflection. The resonances appear for the weak-absorption case through a Bohr-Sommerfeld quantization rule [21] and their superposition is responsible for the wiggly shape of S_I^{sc}. For less weakly absorptive potentials, these Regge poles disappear, whereas Regge zeroes can again be found due to the only interference between $S_I^{sc} \approx S_I^{(o)sc}$ and S_B^{sc}. The effects of resonance are seen at backward angles in the unsymmetrized cross section. Fig.11 shows the contributions σ_I/σ_R, σ_B/σ_R for W = .5. At backward angles the cross section is entirely due to the internal part of the scattering matrix. There is an enhancement factor of about 40 compared with what would be obtained with $S_I^{(o)sc}$ alone. For strongly absorptive potentials the resonances disappear complet

One may feel, as symmetrization effects wash out large angle effects for identical ions, that the present discussion is somewhat academic. However it has some interesting physical consequences for other systems. For instance, in the $\alpha + ^{40}Ca$ case, one has an anomalous large angle scattering (ALAS), often attributed to one or several Regge poles. With the use of the above theory, one can show that ALAS is due to a coherent superposition of several waves and not to resonances [21].

In this section one has merely insisted upon the oscillations present in S_I^{sc}, or coming from the addition of S_B^{sc}

Fraunhofer diffraction oscillations observed at forward angles. As noted in Ref.[13], the conventional Saxon-Woods potential fits the cross sections up to about 60° and this is because it gives the barrier part of the above S-matrix. The folded potential however also gives the internal contribution which is responsible for the oscillations at large angles. Note that η_ℓ is actually rather small for S_I.

The appealling feature of decomposition (4) is that each of the contributions to the S-matrix is smooth and well-behaved. This is not necessarily true of the sum, in the region of their overlap ($\ell \approx 20$), due to the rapid variation of their relative phase. We might therefore expect each part of the S-matrix to give a smoothly varying contribution to the scattering amplitude which will make the origin of the interference structure in the cross section more evident.

This is done by combining the decomposition (3) and (5), i.e. each amplitude coming from the barrier or from the internal region is analysed in terms of travelling waves. They are called $f^{\pm}_{I,B}$. The moduli of $f^{\pm}$ and of f^{+}_{I} and f^{+}_{B} are shown in Fig.(8) as a function of θ. At forward angles f^{-} is almost entirely due to f^{-}_{B} and the oscillations obtained up to about 60° are the result of the usual Fraunhofer diffraction (interference of f^{-}_{B} with f^{+}_{B}). The minimum at 90° and other structure near that angle however is a result of interference of f^{+}_{I} and f^{+}_{B} which have about the same order of magnitude in this region. Thus, as previously noted, the low partial waves are absolutely essential to produce a minimum at 90°, which is sufficiently deep to persist in the symmetrised cross section.

142

The Fraunhofer diffraction is interference between two waves carrying about the same angular momentum but originating from both sides of the scattering potential. A small angular period is obtained: $\Delta\theta = \pi/\ell_g \approx 8°$ (where ℓ_g is the grazing angular momentum ≈ 23). The Fresnel pattern (which is not seen here) results from interference between Coulomb and nuclear waves arising from the same side of the nucleus with different angular momenta. This is the same situation here with f^{+}_{B} and f^{+}_{I} except that both originate from the "other" side of the nucleus (Fig.9). Thus their interference takes the form of beats with a larger period $2\pi/(\ell_g - \ell_I(\theta))$ where $\ell_I(\theta)$ is the ℓ region contributing to $f^{+}_{I}(\theta)$. A rough estimate gives $\ell_I(90°) \approx 12$. This is just the region where $\Phi_I \approx -90°$ as we would expect from a stationary phase argument. In the physical "symmetrised" cross section these beats are not clearly seen because of the additional interference with $f(\pi-\theta)$. In the case of non-symmetric systems, if the low partial waves are important, a marked change in the structure of the cross section due to these beats could be observed.

From this analysis, it should be clear that the conditions to be satisfied by the nuclear potential to reproduce such a phenomena are now rather sophisticated. It has been shown [15] that the usual continuous ambiguities are removed but some discrete ones still remain. The folded potential is thus not the only real optical-model potential which fits the data.

to S_I^{sc}, both being smooth. The former are due to the superposition of Regge pole contributions. For the latter case one can go one step further through Eq.(4) and decompose the elastic amplitude in smooth parts as it was the case for $^{12}C + ^{12}C$ (see Fig.8).

V. Conclusions and summary

The ideas developed here may appear to be somewhat unusual in the context of this Conference. However a link between various viewpoints discussed begins to appear. Feshbach has recently suggested [1] that the broad oscillations in excitation functions could be the envelope of intermediate structure observed in channels with a very light ion emitted. Experimental data [25] seem to support this picture. This situation is reminiscent of the nucleon-nucleus scattering problem where the complex potential arises from energy averaging over dense and complicated states. Though rather little is known on the origin of the ion-ion interaction (especially for its imaginary part) it is hoped that the methods reported here will help to analyze its characteristics and the physics which underlies it. For instance, the parameter R and the Regge poles are very sensitive to the imaginary part of the potential. The angular distributions of $^{12}C + ^{12}C$ at high energy require on the other hand a particular geometry for the real part, a Saxon-Woods form factor being practically excluded.

From the experimental point of view it is evident that elastic scattering data over the full angular range from energies close to the Coulomb barrier to high values of h put severe constraints on the complex potential parameters. Moreover, inelastic, transfer and fusion cross sections in the same system would greatly reduce the ambiguities on these potentials. On the theoretical side a deeper understanding, especially of the absorption, would be particularly valuable.

References

[1] H. Feshbach, J. Phys. (Paris), Colloq. 37, C5-177 (1976)

[2] J.V. Maher et al., Phys. Rev. 188, 1665 (1969)

[3] R.W. Shaw, R. Vandenbosch and M.K. Mehta, Phys. Rev. Lett. 25, 457 (1970)

[4] H. Doubre et al., Phys. Rev. C15, 693 (1977)

[5] G. Michaud and E.W. Vogt, Phys. Rev. C5, 350 (1972)
N. Cindro, Proceedings of the International School of Physics "Enrico Fermi", Course LXII, (1973), edited by M. Faraggi and R.A. Ricci, North Holland (1976) p. 273

6] R.G. Stokstad, in Proceedings of the Europhysics Study Conference on intermediate processes in Nuclear Reactions, Plitvice Lakes, (1972), edited by N. Cindro, P. Kulisic and T. Mayer-Kuckuk (Heidelberg 1973), p. 179
R.H. Siemssen, proceedings of the INS-IPCR symposium on cluster structure of nuclei and transfer reactions induced by heavy-ions, Tokyo, (1975), p. 233

7] W.E. Frahn, Ann. Phys. 24, 243 (1963)
W.E. Frahn, in Heavy-ion, high spin states and nuclear structure, IAEA, Vienna (1975) p. 157

8] J.A. Mc Intyre, S.D. Baker and K.H. Wand, Phys. Rev. 125, 584 (1962)

9] R.C. Fuller, Phys. Rev. C12, 1561 (1975)

10] D.M. Brink and N. Takigawa, Nucl. Phys. A279, 159 (1977)

[11] W.E. Frahn, Ann. Phys. 72, 524 (1972)

[12] M.L. Halbert et al., Phys. Lett. 51B, 341 (1974)

[13] R.M. Wieland, R.G. Stokstad, G.R. Satchler and L.D. Rickertsen, Phys. Rev. Lett. 37, 1458 (1976)

[14] E. Plagnol, H. Doubre and C. Marty, Phys. Lett. 67B, 377 (1977)

[15] N. Rowley, H. Doubre and C. Marty, Phys. Lett. B (under press)

[16] W. Reilly et al., Nuovo Cimento 13A, 913 (1973)

[17] G.R. Satchler and W.G. Love, Phys. Lett. 65B, 415 (1976)

[18] N. Rowley and C. Marty, Nucl. Phys. A266, 494 (1976)

[19] K.W. McVoy, Phys. Rev. C3, 1104 (1971)

[20] W.A. Friedman and C.J. Goebel, Ann. Phys. 104, 145 (1977)

[21] S.Y. Lee, N. Takigawa and C. Marty, preprint IPNO/TH 77-19 (1977)

[22] S.Y. Lee and N. Takigawa, preprint IPNO/TH 77-25 (1977)

[23] T. Tamura and H.H. Wolter, Phys. Rev. C6, 1976 (1972)

[24] H. Doubre et al., to be published

[25] T.M. Cormier et al., Phys. Rev. Lett. 38, 1940 (1977).

Table 1

General characteristics of elastic scattering excitations functions

System	Excitation function	$h=E_{c.m.}/E_B$	References
$^{40}Ca + ^{40}Ca$	no oscillations	< 2	4
$^{20}Ne + ^{20}Ne$	small and broad oscillations	$1 < h < 2$	24
$^{18}O + ^{18}O$	- idem -	$1 < h < 2$	3
$^{16}O + ^{16}O$	large and broad oscillations	$1 < h < 3$	2,12
$^{12}C + ^{12}C$	narrow structures	≈ 1	6
	broad structures	$\gtrsim 2$	13,16

Table 2

Values of the parameters of the optical-model potentials used for the calculations of Section II.
Also indicated are the values of the Coulomb barrier (E_B)

	Real Potential			Imaginary Potential			E_B	Ref.
	V (MeV)	r_o (fm)	a (fm)	V (MeV)	r_o (fm)	a (fm)	(MeV)	
$^{16}O+^{16}O$	17	1.35	0.49	$.8+.2E_{c.m.}$	1.27	0.15	10.33	2,12
$^{18}O+^{18}O$	17	1.35	0.57	$1.4+.35E_{c.m.}$	1.35	0.57	9.97	3
$^{40}Ca+^{40}Ca$	35	1.35	0.43	12.13	1.35	0.43	52.27	4

Figure Captions

Fig.1 Elastic scattering excitation functions at 90° for various systems of identical heavy ions. The arrows give the positions of the Coulomb barrier E_B.

Fig.2 Angular decomposition of the elastic amplitude into travelling waves f^+ and f^-.

Fig.3 Optical-model excitation function σ/σ_R and $R = |f^+/f^-|$ for $\theta=90°$ for $^{16}O + ^{16}O$ (dot-dashed line), $^{18}O + ^{18}O$ (dashed line) and $^{40}Ca + ^{40}Ca$ (full line) as a function of the ratio h of the incident energy (c.m.) to the Coulomb barrier (E_B).

Fig.4 Optical-model excitation functions σ/σ_R, $|f^+(\theta)/f_c(\theta)|^2$ and $|f^-(\theta)/f_c(\theta)|^2$, ($\theta_{c.m.} = 90°$) for $^{16}O + ^{16}O$ as a function of the ratio h of the incident energy (c.m.) to the Coulomb barrier (E_B).

Fig.5 The different amplitudes f^-, f_N^+, f_c^+ divided by the Coulomb one f_c are given in moduli for $^{18}O + ^{18}O$, as a function of the ratio h of the incident energy (c.m.) to the Coulomb barrier (E_B). Note also the behaviour of $|f^+/f^-|$.

Fig.6 Angular distributions for $^{12}C + ^{12}C$ and $^{16}O + ^{16}O$ elastic scattering. Note the relative minima at 90° for $E_{c.m.}$=30 and 51 MeV in $^{12}C + ^{12}C$ and for $E_{c.m.}$ = 22.5 and 26.5 in $^{16}O + ^{16}O$.

Fig.7 Decomposition of the S-matrix into barrier and internal contributions : a) and c) show the respective reflection coefficients (note the exaggerated scale of η_I) and b) shows the corresponding deflection functions (as defined in the text) along with that for pure Coulomb scattering.

Fig.8 The non-symmetrised scattering amplitude is split into f^- and $f^+_{I,B}$. At forward angles f^- is essentially f^-_B and at backward angles f^-_I. Up to about 60°, f^-_B and f^+_B give the usual Fraunhofer diffraction but around 90° one obtains beating between f^+_B and f^+_I (see f^+). The internal contribution is fairly evenly spread over all angles $-\pi \lesssim \theta \lesssim 0$ (see fig.7) giving an essentially constant $f^+_I(\theta)$.

Fig.9 The different kinds of interference phenomena are shown :
a) Fresnel : interference between the Coulomb f^-_C and nuclear part f^-_N of the amplitude f^-
b) Fraunhofer : interference between f^+ and f^-
c) Beating as observed in Sect.III between f^+_B and f^+_I.

Fig.10 The amplitudes of semiclassical S matrices for ^{16}O-^{16}O scattering at E_{cm} = 16 MeV are compared for weak absorption (W_0= 0.5 MeV) and medium absorption (W_0 = 2 MeV). The parameters of the two potentials are given in Section IV.
In the figure, $|S^{sc}_B|$, $|S^{(o)sc}_I|$, $|S^{sc}_I|$ and $|S^{sc}|$ are the amplitudes of barrier wave, internal wave without multiple reflection, internal wave with multiple reflection and total semiclassical S matrices respectively.

Fig.11 The unsymmetrised semiclassical cross section (thick solid line) of ^{16}O-^{16}O scattering at E_{cm} = 16 MeV with weak absorption is decomposed into the internal wave cross section (dashed line) σ_I/σ_R and barrier wave cross section (thin solid line) σ_B/σ_R. The parameters of the potential used in this calculation are given in Sect. IV.

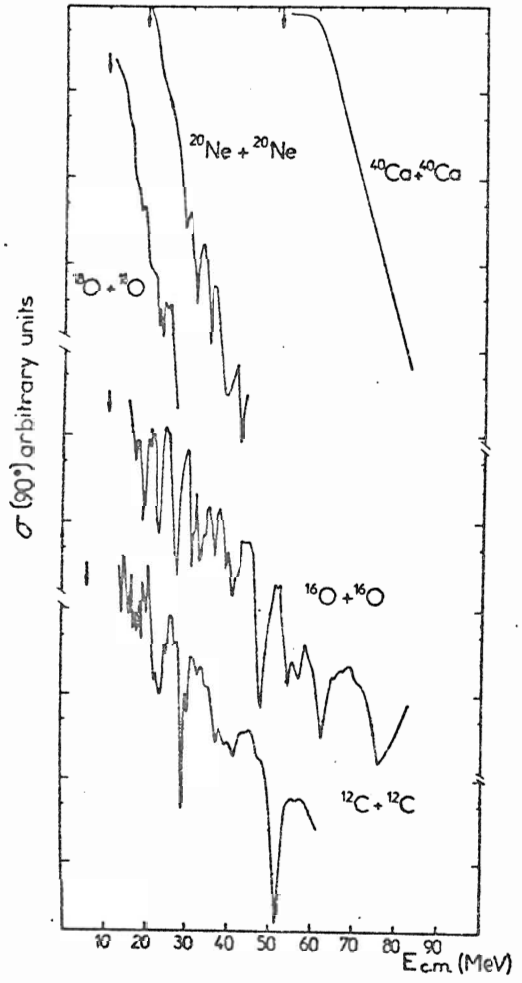
$^{20}Ne + ^{20}Ne$
$^{40}Ca + ^{40}Ca$
$^{18}O + ^{18}O$
$^{16}O + ^{16}O$
$^{12}C + ^{12}C$
σ (90°) arbitrary units
10 20 30 40 50 60 70 80 90
$E_{c.m.}$ (MeV)

Fig. 1

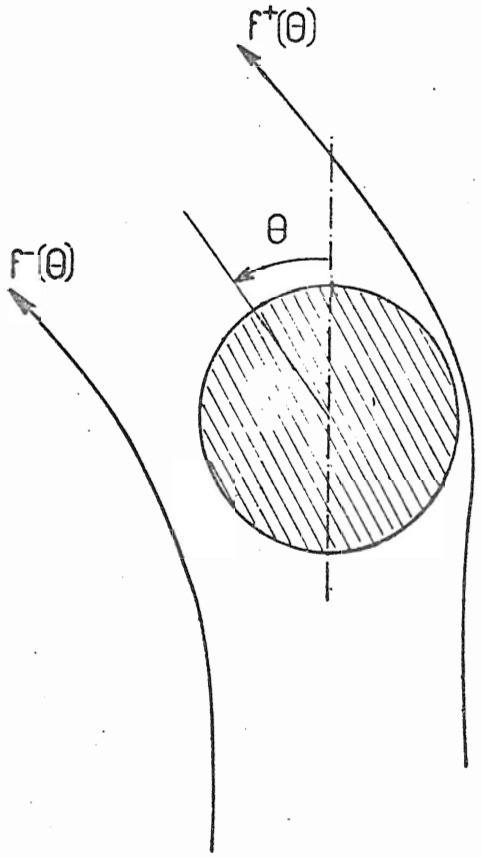
$f^+(\theta)$
θ
$f^-(\theta)$

Fig. 2

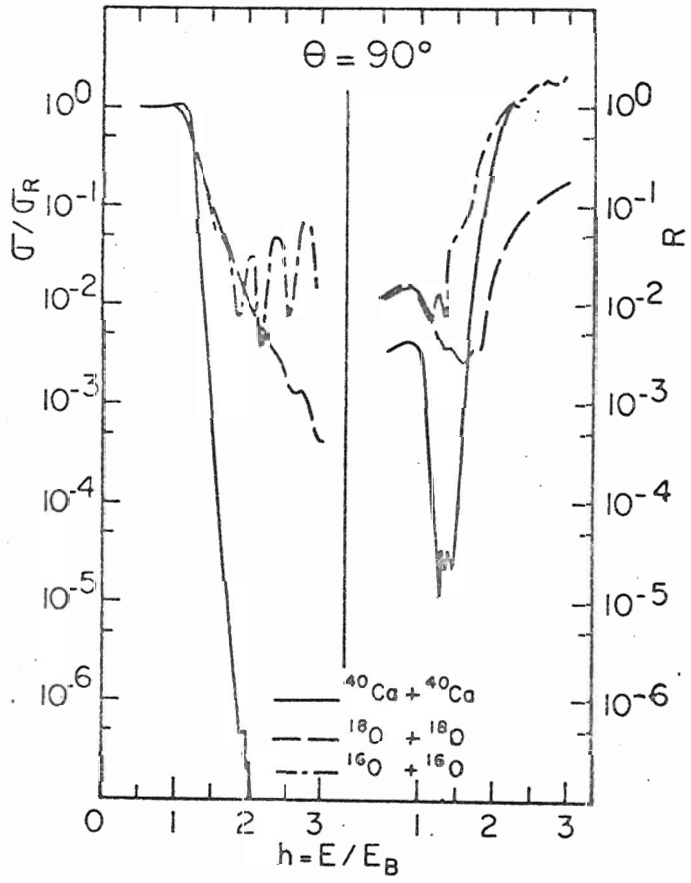
θ = 90°
σ/σR
R
h = E/EB
40Ca + 40Ca
18O + 18O
16O + 16O

Fig..3

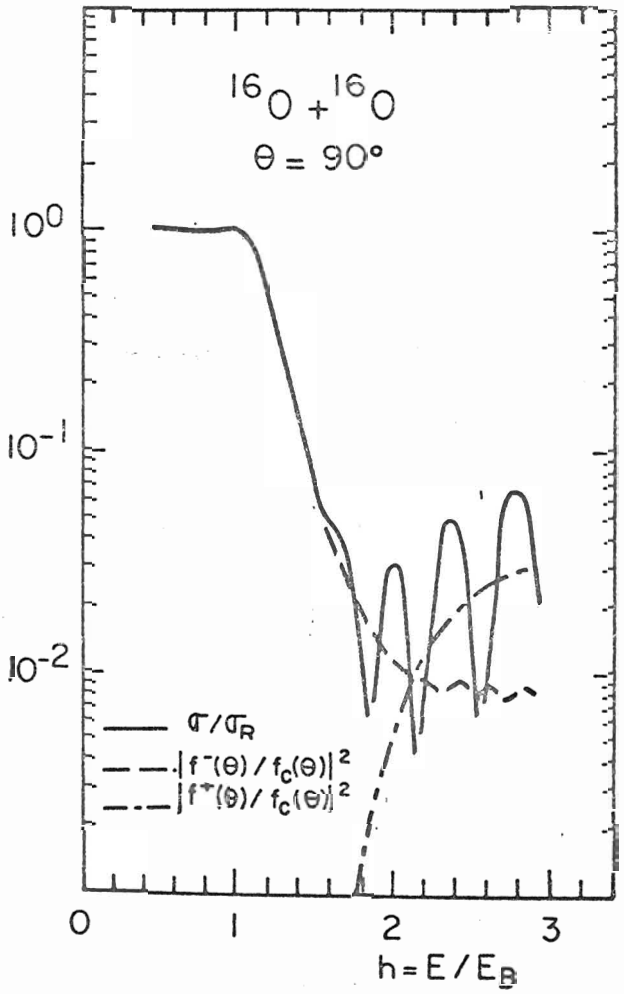
16O + 16O
θ = 90°
σ/σR
|f⁻(θ) / fc(θ)|²
|f⁺(θ)/ fc(θ)|²
h = E/EB

Fig. 4

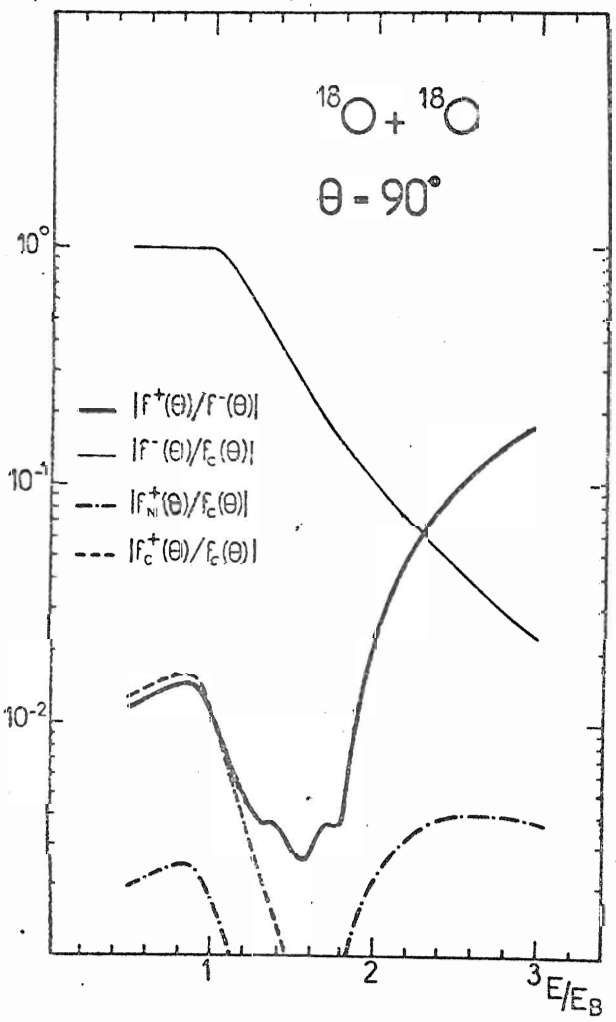
$^{18}O + ^{18}O$
θ = 90°
10^0
10^{-1}
10^{-2}
$|f^+(\theta)/f^-(\theta)|$
$|f^-(\theta)/f_c(\theta)|$
$|f^+_{Ni}(\theta)/f_c(\theta)|$
$|f^+_c(\theta)/f_c(\theta)|$
1
2
3
E/E_B

Fig. 5

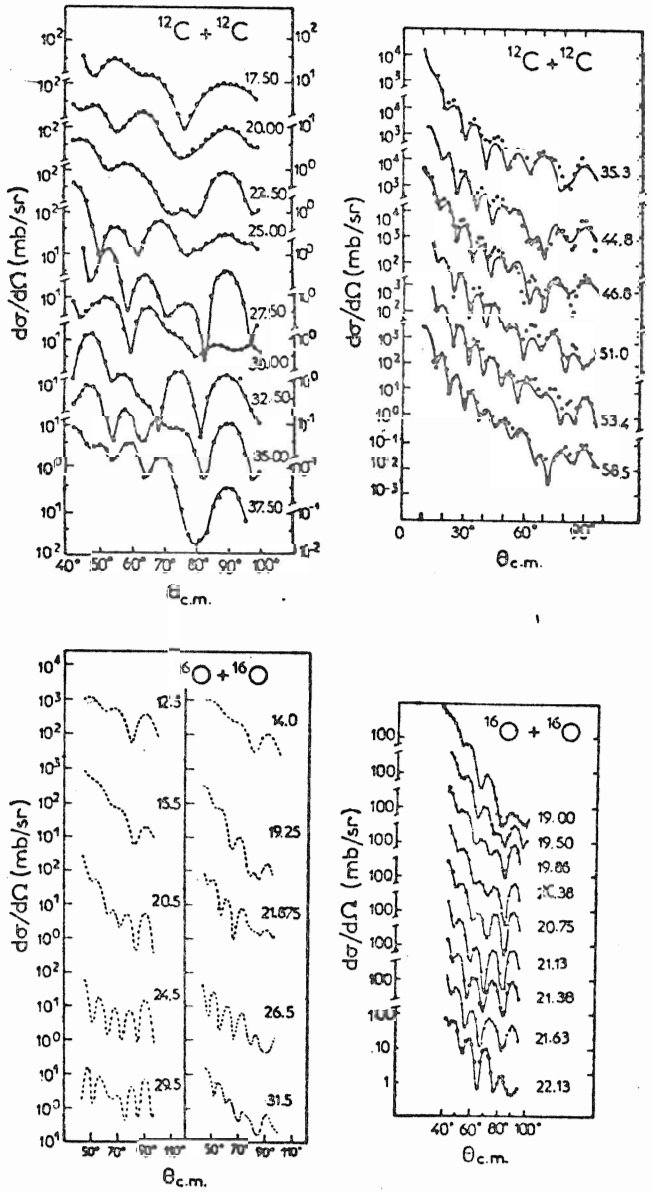
$^{12}C + ^{12}C$
17.50
20.00
22.50
25.00
27.50
30.00
32.50
35.00
37.50
$d\sigma/d\Omega$ (mb/sr)
$\theta_{c.m.}$
$^{12}C + ^{12}C$
35.3
44.8
46.8
51.0
53.4
58.5
$d\sigma/d\Omega$ (mb/sr)
$\theta_{c.m.}$
$^{16}O + ^{16}O$
12.5
14.0
15.5
19.25
20.5
21.675
24.5
26.5
29.5
31.5
$d\sigma/d\Omega$ (mb/sr)
$\theta_{c.m.}$
$^{16}O + ^{16}O$
19.00
19.50
19.86
20.38
20.75
21.13
21.38
21.63
22.13
$d\sigma/d\Omega$ (mb/sr)
$\theta_{c.m.}$

Fig. 6

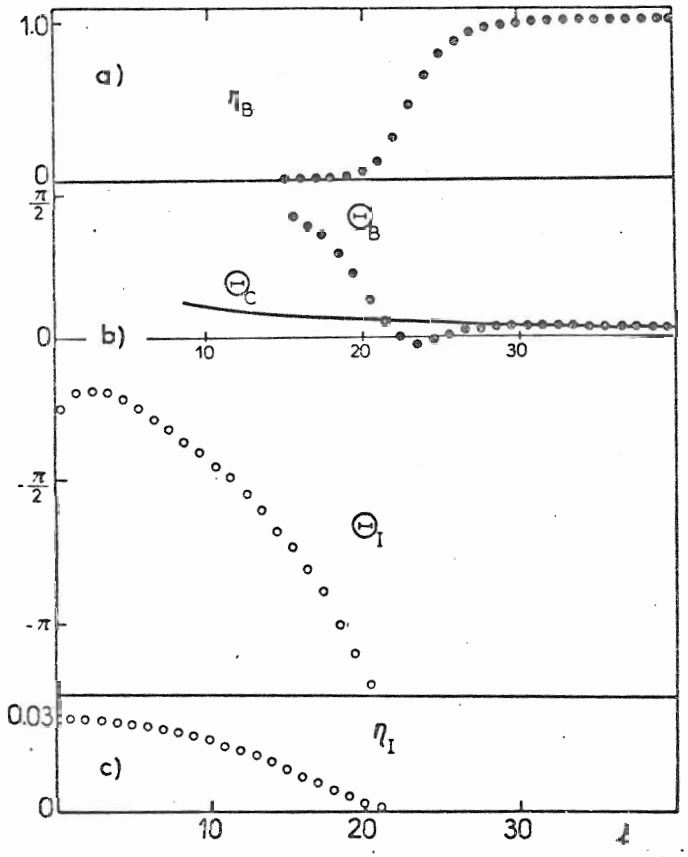
a)
η_B
1.0
0
$\frac{\pi}{2}$
Θ_B
Θ_C
b)
10
20
30
0
$-\frac{\pi}{2}$
Θ_I
$-\pi$
0.03
η_I
c)
0
10
20
30
l

Fig. 7.

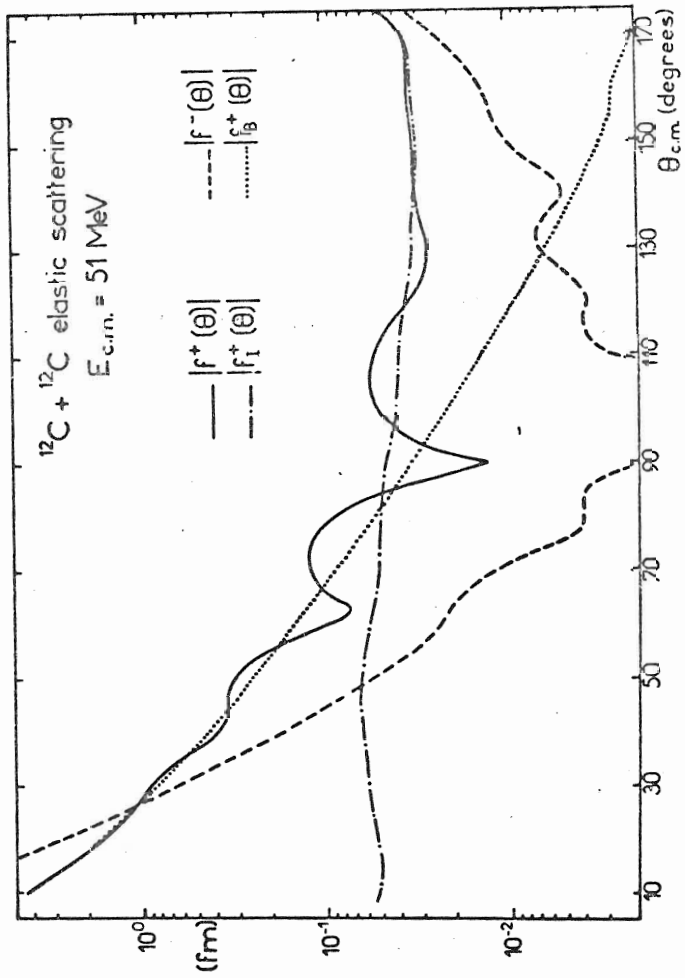
$^{12}C + ^{12}C$ elastic scattering
$E_{c.m.} = 51$ MeV
$|f^+(\theta)|$
$|f^-(\theta)|$
$|f_I^+(\theta)|$
$|f_B^+(\theta)|$
10^0
10^{-1}
10^{-2}
(fm)
10
30
50
70
90
110
130
150
170
$\theta_{c.m.}$ (degrees)

Fig. 8

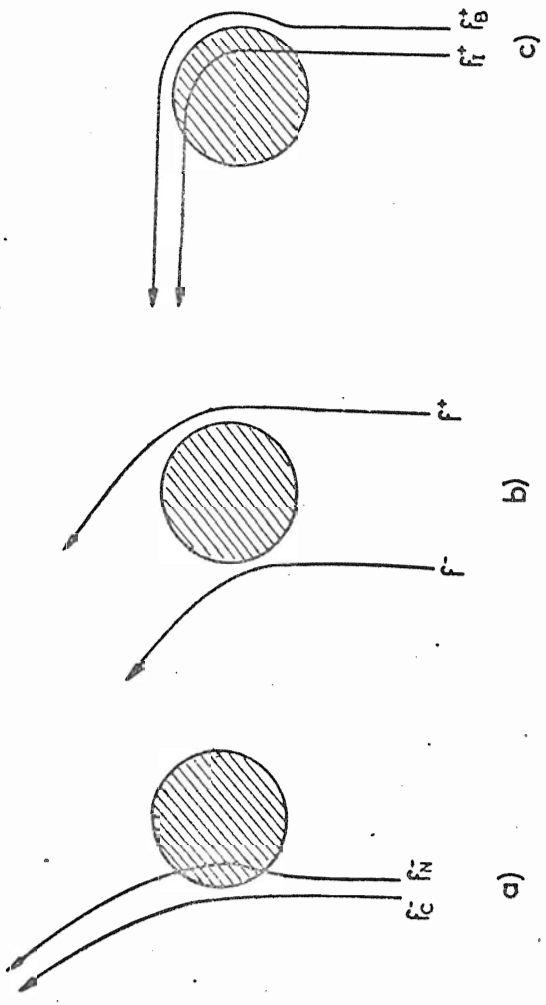

Fig. 9

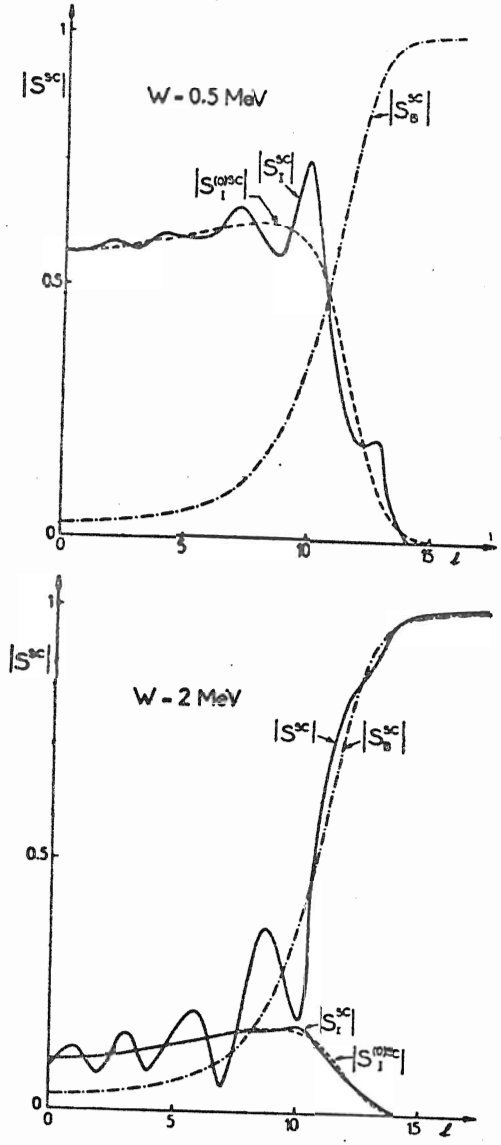

Fig. 10

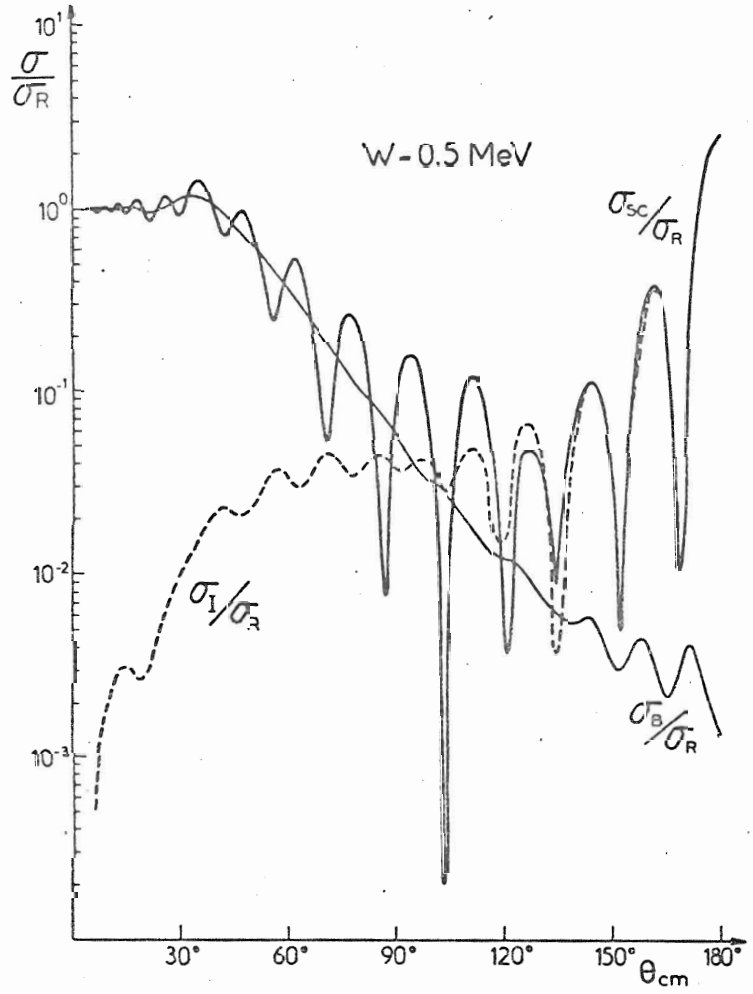
W - 0.5 MeV
$\frac{\sigma}{\sigma_R}$
10^1
10^0
10^{-1}
10^{-2}
10^{-3}
σ_{sc}/σ_R
σ_I/σ_R
σ_B/σ_R
30°
60°
90°
120°
150°
180°
θ_{cm}

Fig. 11